

Electronic Thesis and Dissertation Repository

6-9-2022 10:00 AM

Characterization of disease-causing HARS mutations

Yi Qiu, *The University of Western Ontario*

Supervisor: Heinemann, Ilka, *The University of Western Ontario*

A thesis submitted in partial fulfillment of the requirements for the Master of Science degree in Biochemistry

© Yi Qiu 2022

Follow this and additional works at: <https://ir.lib.uwo.ca/etd>

Recommended Citation

Qiu, Yi, "Characterization of disease-causing HARS mutations" (2022). *Electronic Thesis and Dissertation Repository*. 8627.

<https://ir.lib.uwo.ca/etd/8627>

This Dissertation/Thesis is brought to you for free and open access by Scholarship@Western. It has been accepted for inclusion in Electronic Thesis and Dissertation Repository by an authorized administrator of Scholarship@Western. For more information, please contact wlsadmin@uwo.ca.

Abstract

Aminoacyl-tRNA synthetases ligate amino acids to their cognate tRNAs during protein synthesis. Mutations in the catalytic domain of histidyl-tRNA synthetase (HARS) lead to an incurable neurodegenerative disease Charcot Marie Tooth Disease Type 2W (CMT2W), with the molecular basis of many disease-causing mutations unknown. I generated a yeast model for CMT2W-causing HARS mutations V133F, V155G, Y330C, and S356N. All human HARS variants complemented genomic deletion of yeast ortholog histidyl tRNA synthetase 1 (HTS1) but with reduced growth. HARS V155G and S356N lead to global insoluble protein accumulation, with their growth defect and perturbed proteome rescued by histidine supplementation. HARS V133F and Y330C decreased HARS abundance and histidine supplementation further reduced viability, indicating histidine toxicity. As histidine is in clinical trials for treating patients with HARS mutations, our data will inform treatment options for CMT patients, where histidine supplementation may either have a toxic or compensating effect depending on the nature of the causative HARS variant.

Keywords

histidyl-tRNA synthetase (HARS), neurodegeneration, Charcot Marie Tooth Disease, CMT2W, proteome, protein synthesis, transfer RNA (tRNA)

Summary for Lay Audience

Histidyl tRNA synthetase (HARS) is an enzyme that ligates the amino acid histidine to tRNAs, which is a molecule that brings amino acids into the cell's protein-making machinery to make proteins. Mutations in the human HARS gene cause two hereditary diseases named Usher Syndrome type 3B (USH3B) or Charcot Marie Tooth 2W (CMT2W) disease. In USH3B, patients develop blindness, deafness, and hallucination during fevers. CMT2W is a disease that affects the peripheral nerves, leading to motor and sensory defects and weaker muscles. It is unclear what changes these mutations cause on the cellular and molecular level to lead to disease. This study aimed to study mutations V133F, V155G, Y330C, and S356N in HARS that lead to CMT2W. I generated a yeast model where I replaced the yeast version of HARS gene with the human HARS gene. Yeast is a powerful model system for human disease as it shares many similar cellular processes with humans, yet it is also a simple eukaryotic organism to manipulate. I found that yeast with mutant HARS grew slower compared to normal HARS. Mutants V155G and S356N caused problems in protein production throughout the cell, leading to insoluble protein accumulation, which could mean that proteins are not being made properly, and therefore not being folded properly. Supplementing these two mutants with extra histidine allowed them to grow better, and restored proper protein synthesis. On the other hand, mutants V133F and Y330C lead to less expression of the HARS protein itself. Giving these two mutants extra histidine made their growth defect even worse. Currently there is a clinical trial for oral histidine supplements to treat USH3B. This study is important in showing that we need to be cautious when giving extra histidine to treat patients with CMT2W as it could make the patients worse. This study also proposes the molecular mechanisms of how mutations in HARS lead to growth defects in yeast.

Co-Authorship Statement

Yeast dissection was performed by Dr. Christopher Brandl and Andrew Petropavlovskiy (Fig. 11A,B). The first yeast model for USH3B with mutation Y454S was generated by Rosan Kenana. All remaining experiments relating to V133F, V155G, Y330C and S356N mutants were carried out by Yi Qiu. HARS protein purification was completed by Aruun Beharry (Fig. 20A). Thermal shift assay for hsHARS and Y330C were carried out by Aruun Beharry (Fig. 20B,E), and the remaining mutants were performed by Yi Qiu. The high/low histidine sedimentation assays (Fig. 24) and amino acid stress growth curves (Fig. 25) were performed with the help of undergraduate student Sunidhi Syal.

Plasmids were kind gifts from Dr. Martin Duennwald and Dr. Christopher Francklyn. Yeast strains were kind gifts from Dr. Martin Duennwald and Dr. Christopher Brandl. PKG1 antibody was a kind gift from Dr. Martin Duennwald. Amino acids were kind gifts from Dr. David Litchfield.

Acknowledgments

I would like to give my warmest thanks to my supervisor Dr. Ilka Heinemann. She has played an inspiring role in my journey from an undergraduate to a graduate student. She is always supportive, enthusiastic, and necessarily critical to help me achieve the most that I can. Words are not enough to express my sincere gratitude for how she has shaped my research career. She has made a lasting impact in my life, and I will always look up to her as I advance to my next chapter in scientific research. I would like to extend my gratitude to Dr. Patrick O'Donoghue, who played a critical role in the success of my work. His valuable input and optimistic encouragements make him a mentor who I will always appreciate and respect with deepest sincerity.

My graduate student life could not have been fulfilled without the students from the Heinemann and O'Donoghue labs. They have always shown me kindness and support, and I'm honored to be their colleague in the lab and friend outside the lab.

I would like to thank my committee members Dr. Murray Junop and Dr. Patrick Lajoie who provided me with critical feedback and suggestions to push my research forward. Additionally, I appreciate the kindness of the Duennwald lab, Brandl lab, and Litchfield Lab for generously providing materials for my work.

Lastly, I would like to thank my family and friends who continue to show me unconditional love to guide me through the toughest experiences and happiest moments in my present and future journeys in life.

Table of Contents

Abstract.....	ii
Summary for Lay Audience	iii
Co-Authorship Statement	iv
Acknowledgments	v
Table of Contents	vi
List of Tables.....	x
List of Figures.....	xi
List of Abbreviations	xiii
List of Appendices.....	xvii
Chapter 1	1
1 Introduction.....	1
1.1 The Central Dogma	1
1.1.1 Protein Translation	2
1.2 Aminoacyl-tRNA Synthetases.....	5
1.2.1 ARS Disease-Causing Mechanisms	7
1.2.2 ARS and Neurobiological Diseases.....	8
1.3 Human Histidyl tRNA Synthetase.....	10
1.3.1 HARS Active Site.....	12
1.3.2 HARS-tRNA Recognition	13
1.3.3 Human disease-causing HARS Mutations	14
1.3.4 HARS Mutations of Interest.....	16
1.4 Charcot Marie Tooth Peripheral Neuropathy	18
1.5 Yeast as Model Organism	20
1.5.1 Yeast Deletion Strains	21

1.5.2	Yeast Cellular Stress.....	22
1.6	Rationale, Experimental Goals and Hypothesis	23
Chapter 2	25
2	Materials and Methods	25
2.1	Materials	25
2.1.1	Plasmids and primers.....	25
2.1.2	<i>E. coli</i> strain, media, and growth conditions	25
2.1.3	Yeast strain, media, and growth conditions.....	25
2.1.4	Antibodies.....	26
2.2	Methods	27
2.2.1	Yeast sporulation and dissection	27
2.2.2	QuikChange Site directed mutagenesis	27
2.2.3	<i>E. coli</i> transformation	28
2.2.4	Yeast transformation	28
2.2.5	Plasmid shuffling.....	29
2.2.6	Yeast Growth Analysis.....	29
2.2.6.1	Spotting assays.....	29
2.2.6.2	Growth curves	30
2.2.6.3	Fluorescent microscopy	30
2.2.7	Yeast sedimentation assay	30
2.2.8	Protein analysis.....	31
2.2.8.1	SDS-PAGE.....	31
2.2.8.2	Western blot	32
2.2.9	HARS <i>in vitro</i> studies.....	32
2.2.9.1	HARS purification	32
2.2.10	Thermal shift assay.....	33

2.2.11 Statistical analysis	34
Chapter 3	35
3 Results.....	35
3.1 Generation of a yeast model for HARS deficiency	35
3.2 Dose-dependence of HARS complementation	41
3.3 Mutations in the HARS active site cause global growth defects.....	42
3.4 HARS V155G and S356N induce protein aggregation in yeast.....	45
3.5 V133F and Y330C lead to reduced HARS abundance in yeast	48
3.6 Mutants V133F, V155G, and Y454S lead to reduced HARS protein stability	51
3.7 Histidine supplementation rescues HARS V155G and S356N growth defects and prevents accumulation of insoluble proteins	56
3.8 Growth phenotype characterization under supplementation with all 20 amino acids	63
3.9 Growth phenotype characterization under chemical stress	68
Chapter 4	71
4 Discussion.....	71
4.1 HARS V133F and Y330C are loss-of-function mutations.....	72
4.2 HARS V155G and S356N disease variants de-regulate protein synthesis.....	74
4.3 Rescuing HARS deficient V155G and S356N with histidine	75
4.4 HARS Y454S associated with USH3B is rescued by histidine <i>in vitro</i>	76
4.5 Chemical stress shows no synthetic toxicity	77
4.6 CMT-HARS mutants are more sensitive to certain amino acid stress	78
Chapter 5	80
5 Conclusions.....	80
5.1 Significance	80
5.2 Future work	80
References	82

Appendices	91
Curriculum Vitae	101

List of Tables

Table 1. Neurological diseases caused by ARS mutations.....	9
Table 2. Summary of all HARS mutations previously studied.	15
Table 3. Major known stressors of <i>S. cerevisiae</i> and their stress-inducing mechanisms	22
Table 4. Doubling time of yeast grown in high histidine and low histidine conditions.....	58
Table 5. Summary of effect of amino acid stress on CMT-HARS mutants.....	79

List of Figures

Figure 1. The central dogma.....	2
Figure 2. Transfer RNA structure	4
Figure 3. Simplified schematic representation of transcription and translation.....	4
Figure 4. Aminoacylation occurs in two steps.	6
Figure 5. Aminoacylation of tRNA by ARSs and mistranslation.	8
Figure 6. Structure of human HARS.	11
Figure 7. Thg1 action on tRNA ^{His}	13
Figure 8. HARS mutations of interest	17
Figure 9. Mating cycle of budding yeast.....	21
Figure 10. Workflow for the generation of HARS mutant model system in <i>S. cerevisiae</i>	37
Figure 11. Generation of yeast model.	38
Figure 12. Complementation of CMT-HARS mutants.	39
Figure 13. Fluorescence microscopy of mutant HARS yeast model in vivo.	40
Figure 14. HARS complementation is dose-dependent.	41
Figure 15. Spotting assay for growth phenotype analysis.....	43
Figure 16. Growth curves for growth phenotype analysis.	44
Figure 17. CMT-HARS mutants lead to global protein aggregation.	46
Figure 18. Sedimentation assay for Y454S mutant.....	47

Figure 19. Quantification of HARS expression	50
Figure 20. HARS thermal shift assay and melting temperature curves.	53
Figure 21. Recombinant proteins mutants V133F and V155G lead to reduced protein stability, which can be rescued by substrate supplementation.	55
Figure 22. Histidine supplementation rescues V155G and S356N mutants' growth deficiency and protein aggregation.	59
Figure 23. Growth curves of Y454S with temperature and histidine treatment.....	61
Figure 24. Sedimentation assay gels after histidine treatment..	62
Figure 25. Doubling time of HARS variants supplemented with all 20 amino acids.	64
Figure 26. Heat map visualization of fold change of doubling times from amino acids supplementation.....	67
Figure 27. Chemical stress on hsHARS and CMT-HARS.....	70
Figure 28. CMT2W associated mutations have different phenotypes	77

List of Abbreviations

5-foa	5-Fluoroorotic Acid
AARS	Alanyl-tRNA synthetase
AIMPs	ARS-Interacting Multifunctional Proteins
Amp	Ampicillin
AMP	Adenosine Monophosphate
ANOVA	Analysis of variance
ARS	Aminoacyl-tRNA synthetases
ATF4	Activating transcription factor 4
ATP	Adenosine triphosphate
AZC	L-azetidine-2-carboxylic acid
CMT	Charcot Marie Tooth
CMT1	Charcot Marie Tooth type 1
CMT2	Charcot Marie Tooth type 2
CMT2W	Charcot Marie Tooth type 2W
CMT3	Charcot Marie Tooth type 3
CMT4	Charcot Marie Tooth type 4
CMTX	Charcot Marie Tooth X-linked
DARS	Aspartyl-tRNA synthetase
DMSO	Dimethyl Sulphoxide
DNA	Deoxyribose nucleic acid
DSF	Differential scanning fluorimetry
DTT	Dithiothreitol
EDTA	Ethylenediaminetetraacetic acid

eIF2 α	Eukaryotic initiation factor 2 α
EPRS	Glutamyl-prolyl-tRNA synthetase
ER	Endoplasmic reticulum
EtOH	Ethanol
FARS	Phenylalanyl-tRNA synthetase
G418	Geneticin
GARS	Glycyl-tRNA synthetase
GCN2	General control nonderepressible 2
GFP	Green fluorescent protein
GRIDHH	Growth retardation, intellectual developmental disorder, hypotonia and hepatopathy
H ₂ O ₂	Hydrogen peroxide
HARS	Mammalian Histidyl-tRNA synthetase
HLD	Hypomyelinating leukodystrophy
HMN5A	Neuropathy distal hereditary motor 5A
hsHARS	Home sapien HARS
HTS1	Histidyl tRNA synthetase 1
HU	Hydroxyurea
IARS	Isoleucyl-tRNA synthetase
IgG	Immunoglobulin G
ISR	Integrated stress response
KARS	Lysyl-tRNA synthetase
LB	Lysogeny Broth
Leu	Leucine
MARS	Methionyl-tRNA synthetase

MOPS	3-(N-Morpholino)propane sulfonic acid
mRNA	Messenger RNA
MSC	Multisynthetase complex
MSCCA	Microcephaly, progressive with seizures and cerebral and cerebellar atrophy
NCV	Nerve conduction velocity
NEDMAS	Neurodevelopmental disorder with microcephaly, ataxia and seizures
NEM	N-Ethylmaleimide
Ni-NTA	Nickel-Nitrilotriacetic acid
OD	Optical density
PBS-T	Phosphate-buffered saline - tween
PC12	Pheochromocytoma cells
PCR	Polymerase Chain Reaction
PDB	Protein Data Bank
PEG	Polyethylene Glycol
PERK	Protein kinase RNA-like endoplasmic reticulum kinase
PMSF	Phenylmethylsulfonyl fluoride
PNS	Peripheral nervous system
Ppi	Pyrophosphate
PVDF	Polyvinylidene Fluoride
QARS	Glutaminyl-tRNA synthetase
RARS	Arginyl-tRNA synthetase
RNA	Ribonucleic acid
RNase P	Ribonuclease P

RPM	Rotations per minute
SAC	Substrate assisted catalysis
SARS	Seryl-tRNA synthetase
SD	Synthetic defined
SDS	Sodium Dodecyl Sulphate
SDS-PAGE	Sodium Dodecyl Sulphate–Polyacrylamide Gel Electrophoresis
SUMEB	SDS-Urea-MOPS-EDTA-bromophenol blue
TAE	Tris-acetate-EDTA
TE	Tris-EDTA
Thg1	tRNA ^{His} guanylyltransferase
T _M	Melting temperature
tRNA	Transfer RNA
tRNA ^{His} _{Micro}	tRNA ^{His} Microhelix
Ura	Uracil
USH3B	Usher Syndrome Type IIIB
VARS	Valyl-tRNA synthetase
WES	Whole Exome Sequencing
YARS	Tyrosyl-tRNA synthetase
YFP	Yellow fluorescence protein
YNB	Yeast nitrogen base
YPD	Yeast Extract Peptone Dextrose

List of Appendices

Appendix 1. Plasmid used in this study.....	91
Appendix 2. Primers used in this study.	92
Appendix 3. Melting temperatures (T_M) for wildtype hsHARS with and without substrate addition as determined by differential scanning fluorimetry.....	94
Appendix 4. Melting temperatures (T_M) for HARS Y330C with and without substrate addition as determined by differential scanning fluorimetry.....	95
Appendix 5. Melting temperatures (T_M) for HARS Y454S with and without substrate addition as determined by differential scanning fluorimetry.....	96
Appendix 6. Melting temperatures (T_M) for HARS V133F with and without substrate addition as determined by differential scanning fluorimetry.....	97
Appendix 7. Melting temperatures (T_M) for HARS V155G with and without substrate addition as determined by differential scanning fluorimetry.....	98
Appendix 8. Doubling time (min) \pm <i>standard deviation</i> of yeast strains grown in the presence of amino acid supplementation.....	99
Appendix 9. Doubling time (min) \pm <i>standard deviation</i> of yeast strains grown in the presence of chemical stressors.....	100

Chapter 1

1 Introduction

1.1 The Central Dogma

The central dogma of molecular biology explains the flow of genetic information within a biological system. It was first coined by Francis Crick that “the central dogma of molecular biology deals with the detailed residue-by-residue transfer of sequential information” (1). There are three major components of the central dogma: DNA, RNA, and protein. DNA (deoxyribose nucleic acid) consists of a chain of the four different nucleotides adenine, cytosine, guanine, and thymine that are connected through a phospho-deoxyribose backbone. The phospho-ribose backbone of RNA (ribonucleic acid) strings the same nucleotides as DNA except for the replacement of thymine for uracil. Proteins are complex molecules made up of up to 20-22 different amino acids connected via peptide bonds.

The blueprint of an organism is stored in its DNA, which is transmitted from parent to progeny. As summarized in Figure 1, double stranded DNA can be replicated to preserve its information and pass it on to the two progeny cells during cell division. DNA can also be transcribed into RNA, a single stranded less stable intermediate form of information storage. Finally, during translation, the information encoded in RNA is converted into the amino acid sequence of proteins. Francis Crick initially postulated three scenarios. First, general transfers (solid line) refer to the scenarios outlined above: the classical transfer of information from DNA to DNA, DNA to RNA, and RNA to protein. Then, special transfers (dashed lines) are the possible or probable transfers of information from RNA to DNA, RNA to RNA, and DNA to protein. The final group is unknown transfer, including the impossible transfer of information from protein to protein, or protein to DNA (1). Each of the three components of the central dogma are made up of monomeric units, therefore their sequences dictate the information that is faithfully passed on to the next step. Each polymeric sequence is used as a template for the synthesis of the next polymeric sequence.

The central dogma therefore explains how conglomerated genetic information can be transferred into the formation of a functional biological system.

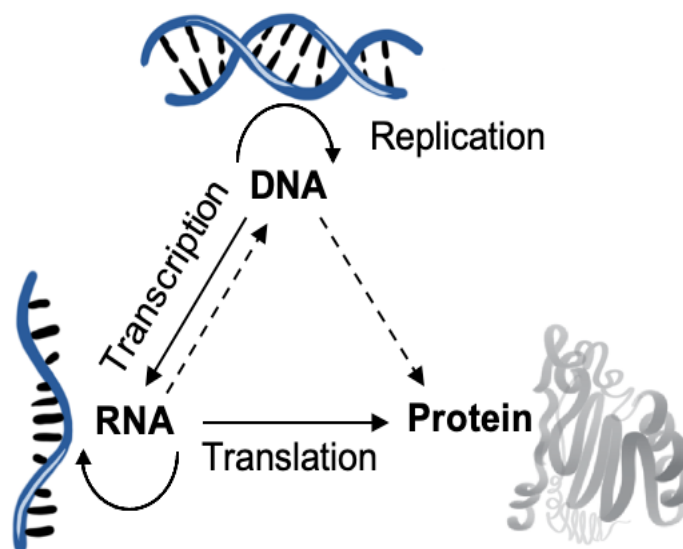


Figure 1. The central dogma. Transfer of information between RNA, DNA, and protein as originally postulated (1). Replication is of DNA. Transcription is the transfer of information from DNA to RNA, while translation is the transfer of information from RNA to protein. Solid lines represent general transfers. Dashed lines represent probable transfers.

1.1.1 Protein Translation

In eukaryotes, DNA is transcribed into RNA in the nucleus, and RNA is translated into proteins in the cytoplasm. This process is summarized in Figure 3. During DNA transcription, RNA polymerase binds to the promoter region of DNA, leading to the separation of the DNA double strands. DNA reads one of the single stranded templates one base at a time and builds a polymeric chain of RNA molecules that is complementary to the DNA. Nucleotide polymerization always occurs in the 5' to 3' direction. Transcription is terminated once a terminator sequence is transcribed. This RNA sequence is then processed through a series of splicing and modification events to create the final messenger RNA (mRNA). This mRNA will then exit the nucleus and become the information for the making of proteins, or translation (2).

In the process of translation, mRNA is “read” based on the genetic code that dictates the correspondence between RNA sequence and amino acids. Three ribonucleic acid molecules or “bases” constitute a codon that specifies for a particular amino acid. Humans have 20 standard proteinogenic amino acids encoded by 61 different codon sequences, with 3 codons serving as stop codons. The translation process takes place within the ribosome of the cell. Ribosomes recognize the 5’ end of the mRNA and reads towards the 3’ end. The process of translation relies crucially on a specialized RNA molecule called transfer RNA (tRNA). tRNA molecules fold into a distinctive secondary structure consisting of three hairpin loops, and tertiary structure resembling a L-shape (Figure 2). One arm of the tRNA molecule is called the anticodon loop, and contains a 3 base sequence called the anticodon, that is complementary to a triplet codon of the mRNA. Another arm of the tRNA, the acceptor stem, attaches to a specific amino acid through the help of an enzyme called aminoacyl-tRNA synthetase, a process discussed in detail later. When an amino acid-carrying tRNA binds to the ribosome, it can base pair with its corresponding codon in the mRNA, and that amino acid is incorporated as part of the amino acid chain that constitutes the protein. Initiation of translation starts with the first amino acid methionine. Elongation of translation occurs when subsequent amino acids are incorporated according to the codon sequence encoded in the mRNA. As ribosomes travel towards the 3’ end of the mRNA, the amino acid sequence is elongated by the formation of a peptide bond between amino acids, resulting in a polypeptide chain. Termination of translation occurs when any one of the three mRNA codon sequences UAA, UAG, and UGA is encountered by the tRNA, since no tRNA molecules contain anticodon sequences for these codons, but is recognized by so-called release factors. This final polypeptide chain will exit the ribosome and is processed into a functional protein after undergoing various folding and modification events (3). Events of transcription and translation are summarized in Figure 3.

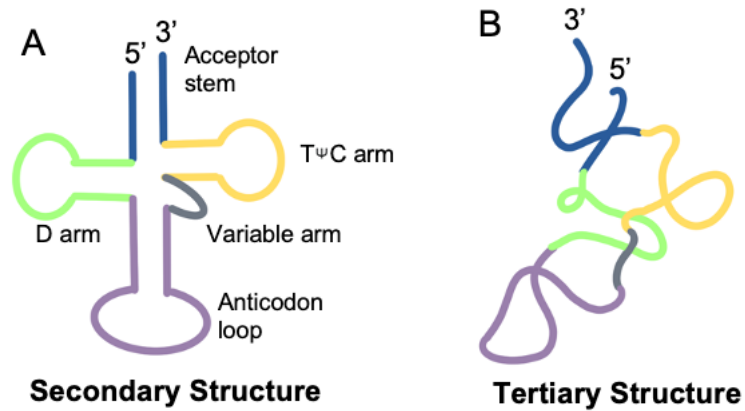


Figure 2. Transfer RNA structure. Secondary (A) and tertiary (B) structure of tRNA showing the anticodon loop (purple), variable arm (grey), TΨC arm (yellow), D arm (green) and acceptor stem (blue).

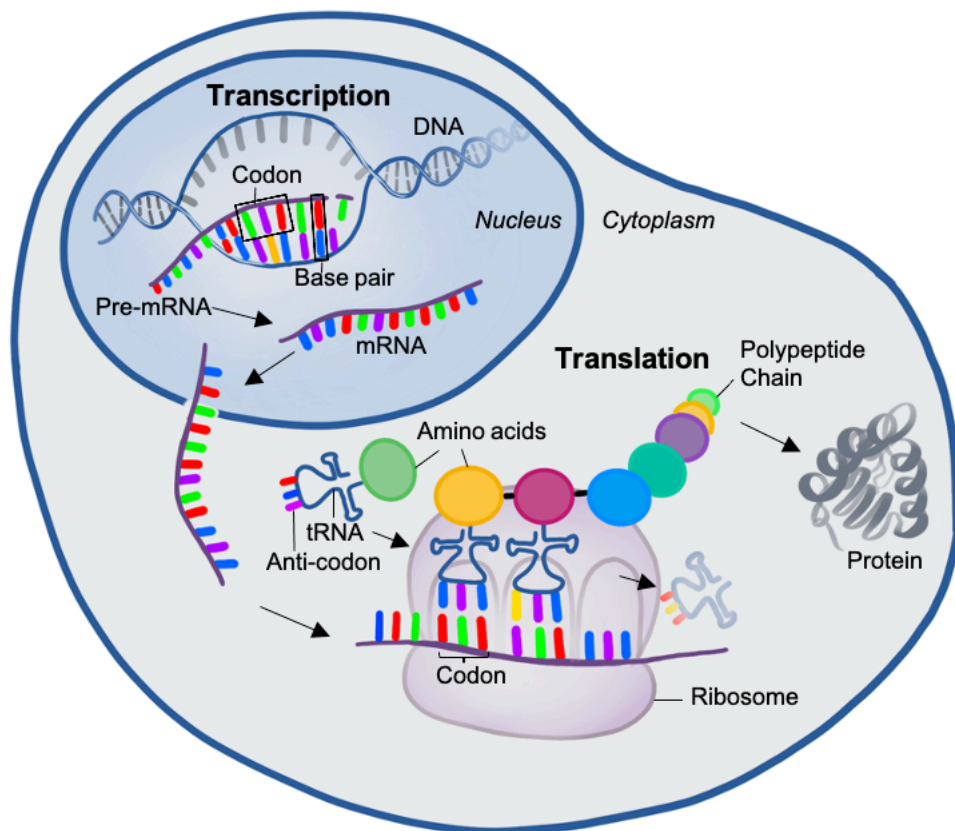


Figure 3. Simplified schematic representation of transcription and translation. Within the nucleic acid depictions, blue represents guanine, red represented cytosine, green represents thymine, purple represents adenine, and yellow represents uracil.

1.2 Aminoacyl-tRNA Synthetases

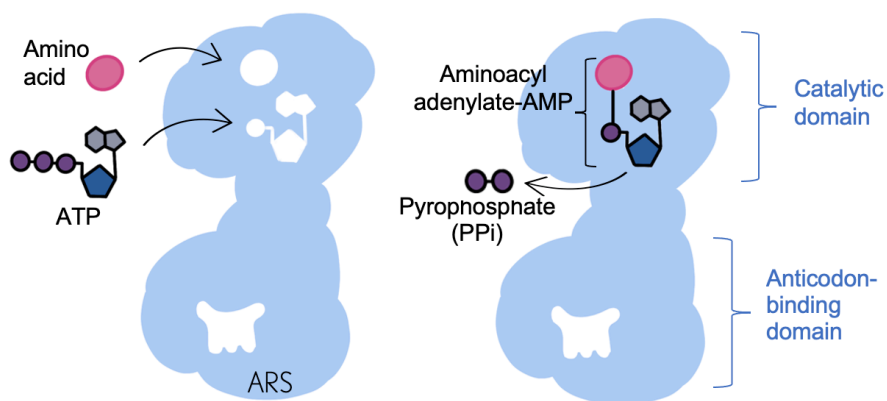
Aminoacyl tRNA synthetases (ARS) are responsible for charging amino acids onto tRNAs in the process of protein translation. Cytoplasmic ARSs belong to a family of 19 enzymes, one for each of the 20 human proteinogenic amino acids with the exception for the bifunctional glutamyl-prolyl-tRNA synthetase (for amino acids glutamine and proline). The abbreviation XARS is designated for each ARS protein, where X represents the single-letter amino acid code of the cognate amino acid that pairs with the tRNA (4,5). Separate genes encode for mitochondrial ARSs. The exceptions are glycyl-tRNA synthetase (GARS) (6) and lysyl-tRNA synthetase (KARS) (7), for which the mitochondrial and cytoplasmic versions are encoded by the same gene and altered by differing translational start sites or mRNA splicing. ARSs are divided into two major classes, namely class I and class II. Class I synthetases are usually monomeric with α -helices connecting a five-stranded β sheet, whereas class II synthetases are usually dimeric or multimeric with α -helices connecting a seven-stranded β sheet. Within each class, subclasses a, b, and c are further divided according to their tendencies in recognizing chemically related amino acids (5).

ARSs are responsible for ligating amino acids to their corresponding tRNAs. This process occurs with high fidelity in two stages as shown in Figure 4. In the first stage, the correct amino acid is activated by hydrolyzing adenosine triphosphate (ATP) to form aminoacyl adenylate-AMP, with inorganic pyrophosphate (PPi) released. In the second stage, the appropriate tRNA is recruited to the ARS, and the amino acid is transferred to the 3' end of the tRNA at the acceptor stem, forming an aminoacyl-ester bond (4). The tRNA is now aminoacylated or “charged” and enters the ribosome for protein synthesis.

The above two-staged reaction takes place in the catalytic domain of the ARS. Most ARSs encode an anticodon binding domain for the recognition of the tRNA anticodon loop. Additionally, some ARSs contain a WHEP domain, which is responsible for protein-protein interactions between synthetases as well as high-affinity interactions with the tRNA (8). The protein-protein interactions can be observed in certain cytoplasmic ARSs when forming a large 11-subunit multisynthetase complex (MSC) composed of 8 ARSs and 3 ARS-Interacting Multifunctional Proteins (AIMPs), which increases protein synthesis

efficiency and enhances other non-canonical functions (9). ARSs distinguish their cognate tRNA from a large pool of similar tRNAs by the presence of identity element nucleotides (10). For most ARSs, an anticodon-binding domain directly reads one or more bases of the anticodon, physically linking the amino acid to its codon assignment. Identity elements are also found throughout the tRNA body, including the variable arm. Indeed, ARSs for serine and alanine do not recognize the anticodon at all, while ARSs for histidine has a critical identity element outside of the canonical tRNA body. Some ARSs have additional proofreading capabilities carried out in their editing domain, which is responsible for cleaving incorrectly paired aminoacyl-tRNA molecules to prevent misaminoacylation (5).

Stage 1: Amino acid activation



Stage 2: Transfer of the aminoacyl group to tRNA

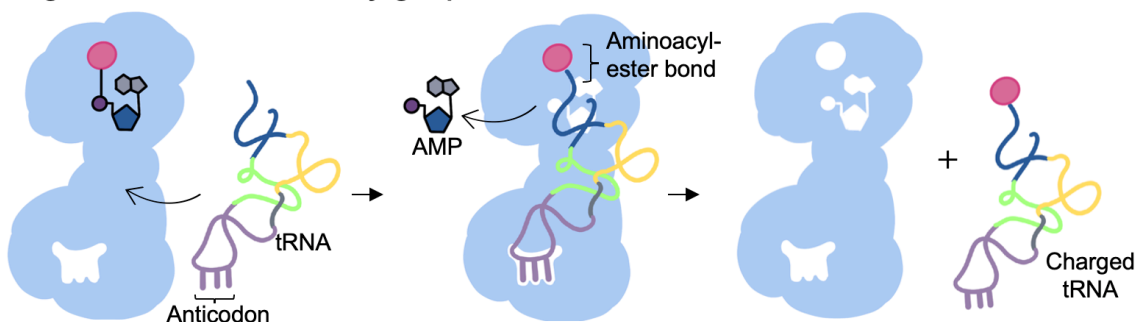


Figure 4. Aminoacylation occurs in two steps. In step 1, the amino acid is activated with ATP to form aminoacyl adenylate-AMP. In step 2, the aminoacyl group is transferred to the tRNA. White spaces within the ARSs represent binding pockets for amino acids, ATP and tRNA anticodon.

1.2.1 ARS Disease-Causing Mechanisms

Many different mutations in an ARS can lead to disease phenotypes, most of which can be summarized as loss-of-function and gain-of-function mechanisms. Loss-of-function describes mutations leading to decreased or elimination of the original activity of the ARS. Examples of loss-of-function include mutations in signal peptides resulting in failure of enzyme localization, mutations of residues resulting in improper folding or dimerization of ARS, as well as mutations impairing ATP, tRNA or amino acid binding (11). These mutations will lead to a decrease or elimination of the catalytic activity of the ARS, which can lead to reduced translational fidelity and impaired cell growth. Gain-of-function describes mutations leading to increased enzyme activity or erroneous enzyme activity. The primary gain of function mutation in ARS is due to aminoacylation defects allowing for the ligation of the non-cognate amino acid to a tRNA, which results in mis-aminoacylation and potentially mistranslation (5). In mistranslation, mutated residues in ARSs can lead to ARSs' recognition of an incorrect tRNA or charging of an incorrect amino acid onto the tRNA (Figure 5). As a result, a misacylated tRNA is produced, and the mRNA message is translated into a faulty protein as the codon-amino acid pairing is impaired. Mistranslation can lead to overall protein misfolding, aggregation and an impaired proteome (12). In addition, functions beyond aminoacylation have been identified in several ARSs such as glycyl-tRNA synthetase (GARS) (13), tyrosyl-tRNA synthetase (YARS) (14), methionyl-tRNA synthetase (MARS) (15) and histidyl-tRNA synthetase (HARS) (16). It is possible that mutations in ARSs can contribute to disease-phenotypes through the impairment of these non-canonical pathways.

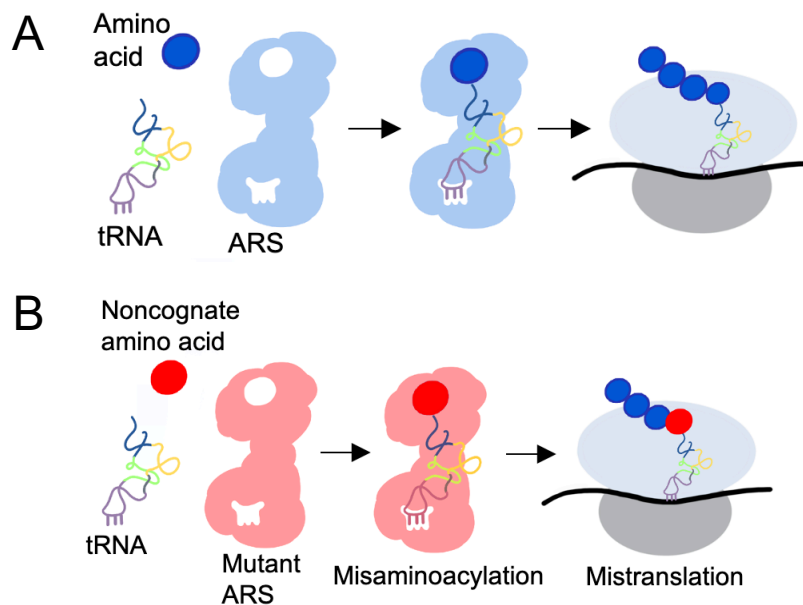


Figure 5. Aminoacylation of tRNA by ARSs and mistranslation. (A) Wild-type ARSs (blue) charge cognate amino acids onto tRNAs for protein translation. **(B)** Mutations in ARSs (red) can for example lead to charging of non-cognate amino acids into tRNAs, leading to mistranslation.

1.2.2 ARS and Neurobiological Diseases

Mutations in ARSs correlate with many pathological human genetic diseases. Notably, many cytoplasmic ARSs lead to neurological diseases involving the central and peripheral nervous system (Table 1) (5). The mechanisms of how many variants of ARSs cause neuropathies and why disease is specific to the nervous system is not fully elucidated and is not generalizable. For example, since ARSs are responsible for proper protein translation, it is possible that the long protein-rich axons of the peripheral nervous system are particularly sensitive to defective protein translation (17). Other possible explanations include neuromuscular junction defects causing synaptic maturation abnormalities such as that seen in GARS (18). Neuronal cells may be particularly vulnerable to defects in proteostasis and may act distinctly towards protein quality control mechanisms. Accumulation in protein translation errors of the proteinaceous myelin sheath may overwhelm the protein folding/degradation systems. Neuronal cells may also be significantly sensitive to timely transport, targeting and recycling of proteins (19).

However, these potential explanations still need to be verified through further studies of mutant ARSs using model systems to provide insight for disease mechanism.

Table 1. Neurological diseases caused by ARS mutations. All currently known defects in ARSs that lead to neurological diseases are summarized. Table adapted from Kwon et al., (2019).

<i>ARS</i>	<i>Neurological disease</i>
<i>Alanyl-tRNA synthetase (AARS)</i>	Charcot Marie Tooth (CMT) Distal hereditary motor neuropathy (a variant of CMT) Early infantile epileptic encephalopathy
<i>Aspartyl-tRNA synthetase (DARS)</i>	Hypomyelination with brainstem and spinal cord involvement and leg spasticity
<i>Glutamyl-prolyl-tRNA synthetase (EPRS)</i>	Hypomyelinating leukodystrophy (HLD)
<i>Phenylalanyl-tRNA synthetase (FARS)</i>	Hypotonia
<i>Glycyl-tRNA synthetase (GARS)</i>	Charcot Marie Tooth (CMT) Neuropathy distal hereditary motor 5A (HMN5A)
<i>Histidyl-tRNA synthetase (HARS)</i>	Charcot Marie Tooth (CMT) Usher syndrome 3B (USH3B)
<i>Isoleucyl-tRNA synthetase (IARS)</i>	Growth retardation, intellectual developmental disorder, hypotonia and hepatopathy (GRIDHH)
<i>Lysyl-tRNA synthetase (KARS)</i>	Deafness, autosomal recessive 89 Charcot Marie Tooth (CMT)
<i>Methionyl-tRNA synthetase (MARS)</i>	Charcot Marie Tooth (CMT)
<i>Glutaminyl-tRNA synthetase (QARS)</i>	Microcephaly, progressive with seizures and cerebral and cerebellar atrophy (MSCCA)
<i>Arginyl-tRNA synthetase (RARS)</i>	Hypomyelinating leukodystrophy (HLD)
<i>Seryl-tRNA synthetase (SARS)</i>	Neurodevelopmental disorder with microcephaly, ataxia and seizures (NEDMAS)
<i>Valyl-tRNA synthetase (VARs)</i>	Progressive microcephaly
<i>Tyrosyl-tRNA synthetase (YARS)</i>	Charcot Marie Tooth (CMT)

1.3 Human Histidyl tRNA Synthetase

Histidyl tRNA synthetase (HARS) is a class II ARS responsible for the ligation of amino acid histidine onto its corresponding tRNA. Human *HARS* gene is situated on chromosome 5, and codes for a 509 amino acid long polypeptide with a molecular mass of 57.4 kDa (20). While HARS typically refers to cytoplasmic HARS, there is also mitochondrial HARS encoded by the *HARS2* gene located on the same chromosome. Mitochondrial HARS contains an N-terminal mitochondrial targeting signal, and therefore functions inside the mitochondria and its mutations lead to different disease phenotypes compared to cytoplasmic HARS. Human HARS is dimeric and contains a WHEP-TRS domain, a catalytic domain, and a tRNA binding domain, characteristic of class II ARSs (Figure 6). The WHEP-TRS domain (shown in pink) consists of a helix-turn helix motif. The catalytic domain (shown in blue) is made up of 7-stranded antiparallel β -sheet and features 3 motifs: motif 3 binds to ATP, and motif 2 couples ATP to histidine and transfers the amino acid to the tRNA (21). The anticodon-binding domain (shown in green) consists of both α helices and β sheets (22). No crystal structure data is available for human HARS in complex with tRNA^{His}, but structure data is available for bacterial HARS in complex with the tRNA and histidine. Figure 6 was obtained by aligning human HARS (PDB code: 6O76, (23)) and *Thermus thermophilus* HARS (PDB code: 4RDX, (24)), showing human HARS monomer in complex of *T. thermophilus* tRNA^{His}.

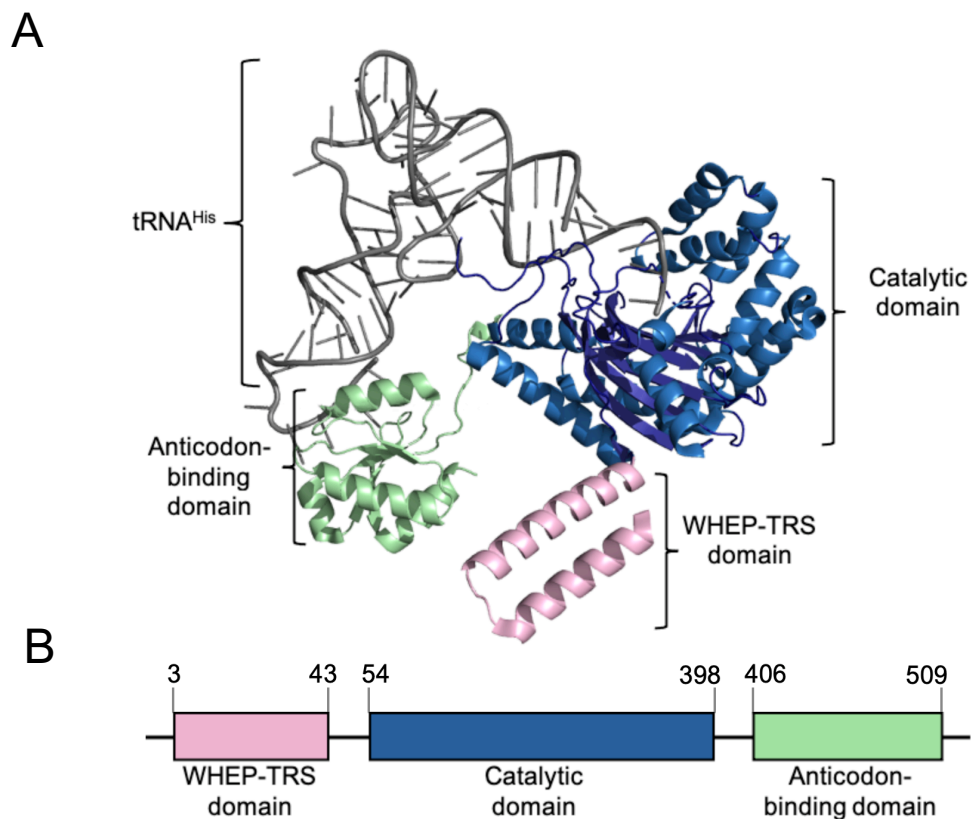


Figure 6. Structure of human HARS. (A) Monomer of human HARS (PDB code: 6O76) in complex with *T. thermophilus* tRNA^{His} (PDB code: 4RDX) with the catalytic domain (blue), anticodon-binding domain (green) and WHEP-TRS domain (pink), in complex with tRNA^{His}. Figure generated with PyMOL (Schrodinger, LLC). (B) HARS gene domains. Numbers represent the location of amino acids at the beginning and end of each domain in human HARS.

1.3.1 HARS Active Site

HARS catalysis for histidine binding is through an induced-fit model (25). Histidine binding in the active site initiates conformational changes in the histidine binding pocket, which is formed by a highly conserved HisA loop that extends over a part of the active site, and a glycine-rich β -strand (26). Within the binding pocket of human HARS, histidine forms hydrogen bonds with eight amino acid residues.

ATP bound in the active site of HARS forms a “fishhook” conformation uniquely conserved across class II ARSs. Similarly, residues involved in ATP binding are mostly conserved across most members of the class II family. In *Escherichia coli* HARS, ATP-binding specificity is accomplished by the π -stacking interactions between the adenine ring of ATP and Phe125. Four arginine residues mediate the interaction with the triphosphate of ATP. When HARS is in complex with adenylyate-AMP after catalysis, two of the arginine loose contacts and adopt different conformations (27,28).

Coordinated metal ions are necessary for HARS to carry out catalysis. Two magnesium ions coordinate with the α and β phosphates of ATP during catalysis forming aminoacyl adenylyate-AMP, and the departing inorganic pyrophosphate leaving group (29).

After the formation of histidyl-adenylate, aminoacylation is carried out by HARS, forming an aminoacyl ester in the 3'OH of tRNA^{His}. Substrate assisted catalysis (SAC) describes the transfer of the aminoacyl-adenylate intermediate to tRNA^{His}. Glu83 of HARS forms an electrostatic interaction with the α -amino group of the histidyl-adenylate to neutralize the charge. During SAC, a proton is abstracted from the 3'OH of the A67 ribose on tRNA^{His}. Then the A67 oxygen facilitates a nucleophilic attack on the carboxyl carbon of the histidyl-adenylate, thus releasing AMP, forming aminoacylated His-tRNA^{His} (30).

1.3.2 HARS-tRNA Recognition

Typically, specific amino acid side chains in ARSs recognize identity elements of cognate tRNA molecules in the anticodon regions. HARS is one of the few ARSs that do not recognize the anticodon in the tRNA as major identity element. tRNA^{His} has an unique additional nucleotide at the 5' end that is absent in all other tRNAs, the G⁻¹ residue. Human HARS recognizes G⁻¹ even when the anticodon is mutated (24,31). This residue is not encoded in the genome, therefore is missing in the eukaryotic pre-tRNA^{His}. Ribonuclease P (RNase P) processes the 5'-end of pre-tRNA^{His} by cleaving at position +1. The unique G⁻¹ residue in eukaryotes is added post-transcriptionally by tRNA^{His} guanylyltransferase (Thg1), through its 3' to 5' RNA polymerization function (32) (Figure 7). Although HARS does not recognize the tRNA^{His} anticodon, the Thg1 enzyme uses the tRNA^{His} anti-codon as its key recognition site to append the G₋₁ residue. G⁻¹ pairs with C₇₃ at the top of the acceptor stem of tRNA^{His} in bacteria and archaea canonically, but mis-pairs with A₇₃ in eukaryotes (32). A tRNA^{His} lacking the G⁻¹ residue is not a competent substrate for HARS (33).

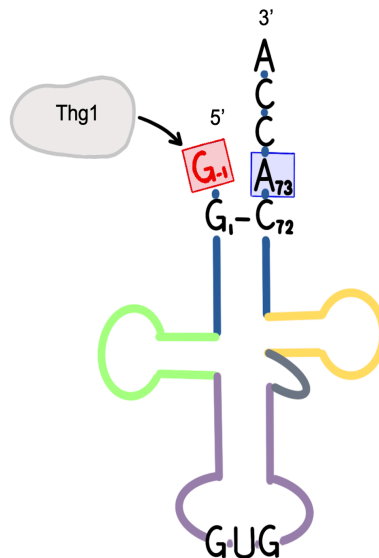


Figure 7. Thg1 action on tRNA^{His}. tRNA^{His} with GUG anticodon shown. Thg1 inserts a guanylyl residue at position -1 on the 5' end of the tRNA. This G⁻¹ residue mismatches with A₇₃ near the 3' end.

1.3.3 Human disease-causing HARS Mutations

Aminoacylation and tRNA recognition functions have been studied intensely in bacterial HARS (34-38). Some studies have investigated the functions of human HARS and the effects of its mutations. Notably, autosomal dominant mutations in the catalytic domain of HARS have been associated with Charcot Marie Tooth Type 2W (CMT2W) (OMIM #616625) (23,39-42), while mutations in the HARS anticodon-binding domain were associated with Usher Syndrome Type IIIB (USH3B) (OMIM #614504), a disease of progressive hearing and vision loss (43). Although there currently is no cure for CMT, histidine supplementation has been explored as a treatment option for USH3B patients with a clinical trial currently in its final phase (Clinicaltrials.gov NCT02924935). A summary of all known studies on human HARS mutations to date is outlined in Table 2.

Table 2. Summary of all HARS mutations previously studied.

<i>Publication</i>	<i>Mutations of interest</i>	<i>Major Study Outcome</i>
<i>Mutations in mitochondrial histidyl tRNA synthetase HARS2 cause ovarian dysgenesis and sensorineural hearing loss of Perrault syndrome (Pierce et al., 2011)(44)</i>	L200V, V368L (mitochondrial HARS)	Aberrant mitochondrial translation and Perrault disease are caused by a decline in HARS2 activity caused by these inherited mutations.
<i>A loss-of-function variant in the human histidyl-tRNA synthetase (HARS) gene is neurotoxic in vivo (Vester et al., 2013) (39)</i>	R137Q, G205D, V238A, K376R, P505S,	HARS has been reported to be the fifth ARS locus related to axonal peripheral neuropathy. The implications for detecting ARS alleles in human populations and determining if they play a role in neurodegenerative phenotypes are discussed.
<i>Loss of function mutations in HARS cause a spectrum of inherited peripheral neuropathies (Safka Brozkova et al., 2015)(40)</i>	T132I, T132S, P134H, D175E, D364Y	Expands the genetic and clinical scope of aminoacyl-tRNA synthetase-related human disease by demonstrating the function of HARS mutations in peripheral neuropathy.
<i>The Usher Syndrome Type IIIB Histidyl-tRNA Synthetase Mutation Confers Temperature Sensitivity (Abbott et al., 2017)(43)</i>	Y454S	The thermal sensitivity associated with the Y454S mutation represents a biochemical basis for understanding USH3B.
<i>Substrate interaction defects in histidyl-tRNA synthetase linked to dominant axonal peripheral neuropathy (Abbott et al., 2018)(41)</i>	V155G, Y330C, S356N	The first biochemical investigation of CMT-related HARS mutations shows how the loss of the primary aminoacylation feature can lead to disease pathology.
<i>Peripheral neuropathy and cognitive impairment associated with a novel monoallelic HARS variant (Royer-Bertrand et al., 2019)(42)</i>	V133F	First time that this HARS variant has been linked to a cognitive deficit as well as peripheral neuropathy.
<i>CMT disease severity correlates with mutation-induced open conformation of histidyl-tRNA synthetase, not aminoacylation loss, in patient cells (Blocquel et al., 2019)(23)</i>	T132I, P134H, D175E, D364Y	HARS-linked CMT disease arises from open conformation-induced mechanisms distinct from loss of aminoacylation.
<i>Neuropathy-associated histidyl-tRNA synthetase variants attenuate protein synthesis in vitro and disrupt axon outgrowth in developing zebrafish (Mullen et al., 2021)(45)</i>	V155G, Y330C, R137Q	Expression of CMT-HARS1 mutations led to attenuation of protein synthesis and increased phosphorylation of eIF2 α in PC12 cells and was accompanied by impaired neurite and axon outgrowth in rat pheochromocytoma cells and zebrafish model.

1.3.4 HARS Mutations of Interest

My investigation will focus on missense mutations V133F (c.397G>T, p.Val133Phe), V155G (c.454T>G, p.Val155Gly), Y330C (c.989A>G, p.Tyr330Cys), and S356N (c.1067G>A, p.Ser356Asn) of human HARS identified in patients with CMT2W phenotypes (41,42). All mutations are autosomal dominant and localize to the amino acid binding pocket of the enzyme in the catalytic domain (Figure 8).

V133F

Monoallelic HARS variant V133F is a relatively novel mutation first identified in a 49-year-old male of Spanish origin through Whole Exome Sequencing (WES). This patient had late onset of symptoms starting at age 40, including leg weakness, difficulty in walking, progressive motor incoordination, and mild to moderate impairment of multiple cognitive functions. No neurological conditions were found in his family (42).

V155G

HARS variant V155G was first identified in 5 individuals in a three-generation family of Persian-Jewish origin with peripheral neuropathy. The inheritance pattern was autosomal dominant with male-to-male transmission. Most were around 20 for the age of onset. All were present with motor dysfunction, while two elders have severe weakness requiring cane or wheelchair use (41).

Y330C

HARS variant Y330C was first identified in 2 individuals from a two-generation pedigree of mother and son. Both patients had onset of peripheral neuropathy during childhood. Both show distal motor deficits, hammer toes, and pes cavus. The mother requires use of a wheelchair while the son has difficulty walking without aid (41).

S356N

HARS variant S356N was first identified in a family of asymptomatic mother and affected daughter with peripheral neuropathy. The onset of symptoms for the daughter

was age 10, where she has progressive difficulties in walking, ankle weakness, and a hand tremor. WES confirmed this variant was inherited from the asymptomatic mother, suggesting the variant might have less penetrance or is non-pathogenic (41).

In addition, data for yeast model of mutation Y454S (c.1361A>C) generated by previous graduate student Rosan Kenana will also be included to provide a more comprehensive characterization of HARS deficiency. This single missense mutation is inherited in an autosomal recessive fashion, first identified in an Old Order Amish family in Ontario, Canada (46). Patients present with Usher syndrome type IIB (USH3B), a disease characterized by progressive hearing and vision loss in the first two decades of life, and rapid clinical deterioration during fevers (46).

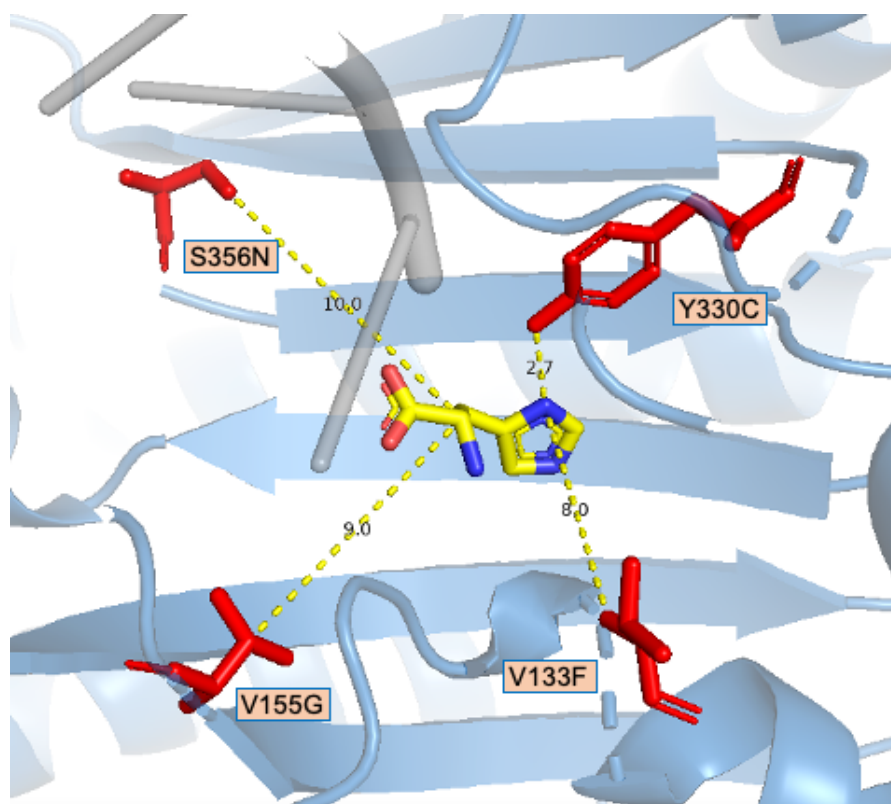


Figure 8. HARS mutations of interest. Monomer of human HARS (PDB code: 6O76) in complex with *T. thermophilus* tRNA^{His} (PDB code: 4RDX). Figure outlines a close-up view of the HARS active site in the catalytic domain with CMT2W associated mutations depicted as red sticks. Histidine is depicted in yellow. Dashed lines measure the distance in angstrom of V155G/S356N to the alpha carbon of histidine, and V133F/Y330C to the R-group of histidine. Figure generated with PyMOL (Schrodinger, LLC).

1.4 Charcot Marie Tooth Peripheral Neuropathy

Charcot Marie Tooth (CMT) is a heterogeneous genetic disorder that leads to progressive chronic neuropathy affecting the motor and sensory nerves. It is the most common inherited neurological disease with a prevalence of 1 in 2500 people. Patterns of genetic inheritance for CMT include autosomal dominant, autosomal recessive and X-linked. However, a portion of mutations arise *de novo* (47). The onset of disease phenotype is around the first or second decade of life (48). There is currently no cure for CMT, only ways to cope with the disabling symptoms of the disease (49). There are 4 types of CMT with an additional X-linked classification. Type 1 and type 2 are the two main types distinguished using electrophysiological studies. CMT1 is the most common demyelination type characterized by slower median or ulnar nerve conduction velocity (NCV), which measures how fast an electrical impulse moves through the nerves. CMT2 is the less common axonal type characterized by normal NCV but reduced muscle action potential, which is the first step in a chain of events leading to muscle contraction. CMT3 is a more rare and severe type also known as Dejerine-Sottas syndrome causing severe muscle and sensory difficulties in infancy or early childhood. CMT4 is another rare and severe type where it is inherited in an autosomal recessive pattern. Finally, CMTX is a variation of CMT1 and CMT2 with an X-linked inheritance pattern, therefore affecting males much more severely than females (50). Based on the underlying genes responsible for the disease, subtypes within CMT classifications can be made. Despite the distinct types, there are classical clinical features of CMT shared amongst all types. There is typically weakness, and disappearance of muscle stretch reflex beginning distally from the feet and ascending the body. Bone deformities such as high-arched feet and hammer toes can arise (51). Additionally, loss of sensory to pain, temperature or vibration in the legs often occur (52).

5 different ARSs have been associated with CMT peripheral neuropathy, namely YARS (53), AARS (54), MARS (55), GARS (56), and HARS (40). HARS is associated with CMT2W, which is an autosomal dominant axonal-form subtype of CMT. Most patients present with gait difficulties, foot deformities, and distal sensory impairments (40). In reflection of the disease-causing mechanism of ARS described above, experimental evidence has proven that both loss-of-function and gain-of-function of different ARSs can

lead to CMT phenotypes, and both mechanisms may not be mutually exclusive. In HARS mutations previously investigated, research shows that HARS-linked CMT disease may be caused by either loss of aminoacylation (41), or a relaxed conformation-driven mechanism (23). Furthermore, a system-wide knock-down of HARS lead to cell cycle arrest and apoptosis of neuronal progenitor cells in zebrafish (57). This further extends the link between HARS and neurological disease phenotypes. However, further research into the molecular details of CMT-ARS pathogenesis is required for the development of effect drug treatment for this irreversible class of illness.

1.5 Yeast as Model Organism

Yeast are eukaryotic, single-celled microorganisms, and a powerful tool in research and the food industry. Yeast is a general term that encompasses many phylogenetic divisions. The most commonly manipulated yeast species is *Saccharomyces cerevisiae* or “Baker’s/budding yeast”, which is also one of the best characterized eukaryotic organisms (58). For over ten thousand years, *S. cerevisiae* has been used for brewing and baking (59). In 1996, the first complete eukaryote genome sequencing was performed on *S. cerevisiae* through a worldwide collaboration (60). It was also clear that yeast encode very similar proteins as mammals. This prompted the explosion of scientific endeavors that use *S. cerevisiae* as a model system to study mammalian molecular systems and human diseases (61). In the laboratory setting, many characteristics of *S. cerevisiae* budding yeast make them great model organisms. The natural life and mating cycle of budding yeast shown in Figure 9 allow them to exist stably as either diploid or haploid forms. A haploid yeast cell can be one of two mating types: a or α (alpha). These two types of cells undergo mitosis through budding off of the mother cell and generation of daughter cells. Both cells release pheromones, initiating the formation of nodules called shmoo that allow subsequent mating. Haploid yeast cells of one mating type mate with the other mating type, producing stable diploid cells. Diploid cells can also go through mitotic division through budding. During stress or nutrient depletion, diploid cells can undergo meiosis/sporulation to produce two haploid “a” spores and two haploid “ α ” spores (62). Since yeast cells are visible under the microscope, dissection of the haploid cells can be accomplished. Yeast cells also divide rapidly compared to other animal models. All of these characteristics make yeast suitable model organisms in molecular and system biology research.

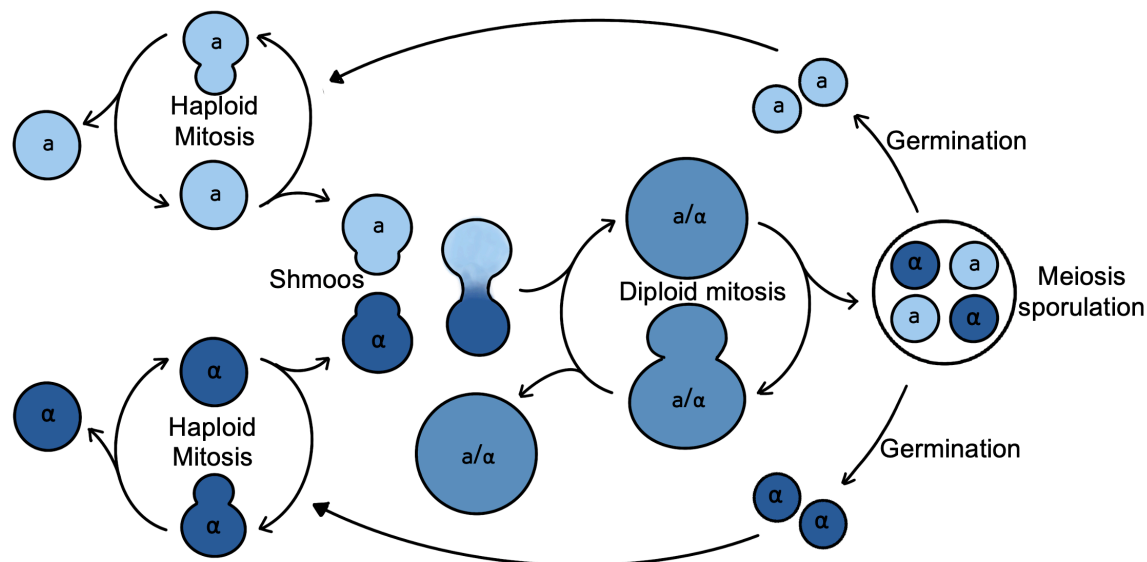


Figure 9. Mating cycle of budding yeast. Yeast type a is in light blue. Yeast type α is in dark blue. Diploid yeast is in medium blue.

1.5.1 Yeast Deletion Strains

Yeast deletion strains have been widely used to model for various human diseases. The *Saccharomyces Genome Deletion Project* is a project initiated by researchers from Stanford University to generate a nearly complete set of possible yeast deletion strains. The overall goal is to assign function to the open reading frame through phenotypic analysis of the deletion yeast mutants. From this, we can demonstrate which genes are essential for growth under different environments. More than 20,000 deletion strains are available to date, which constitutes 90% of the yeast genome. Because *S. cerevisiae* exist stably in both haploid and diploid forms, four different mutant collections can be generated: haploid of mating type a, haploid of mating type α , homozygous diploids, and heterozygous diploids (63).

We can take advantage of the yeast deletion strains to perform complementation assays using human genes as an experimental platform to test the functionality of human genetic mutations (64). As mentioned previously, many human genes have yeast homologs. The use of a haploid yeast deletion strain for a specific gene, along with transformation of a

maintenance vector that carries the mutated human version of the deleted yeast gene, may be able to complement or rescue the yeast. As such, phenotypic studies of this human gene mutation in a yeast model system will provide insight into the functional mechanism of how this genetic variant leads to human disease.

1.5.2 Yeast Cellular Stress

To further manipulate the yeast model organism to aid and supplement the study of yeast complementation, cellular stressors are often applied. The response of mutants to stress provide insight on their disease-causing mechanisms. Major stressors of *S. cerevisiae* and their stress-inducing mechanisms are outlined in Table 3.

Table 3. Major known stressors of *S. cerevisiae* and their stress-inducing mechanisms.

<i>Stressor</i>	<i>Effect of stressor</i>	<i>Mechanism of stress-induction</i>
<i>L-azetidine-2-carboxylic acid (AZC)</i>	Mistranslation	AZC competes with its analog proline, causing misincorporation of AZC instead of proline, leading to defective protein and proteotoxic stress (65).
<i>Ethanol (EtOH)</i>	Growth and viability defect	Main target of ethanol damage in the plasma membrane. Ethanol has a drastic effect on membrane fluidity, amino acid permeability and glucoses uptake. The yeast cellular response towards excessive ethanol involves heat shock proteins and trehalose production (66) as factors that aid in suppressing protein aggregation during ethanol stress (67).
<i>Hydrogen peroxide (H₂O₂)</i>	Proteome stress	Hydrogen peroxide is a reactive oxygen species that can damage a variety of cellular components causing oxidation of proteins and DNA lesions (68).
<i>Hydroxyurea (HU)</i>	DNA replication arrest	Hydroxyurea is a potent inhibitor of the enzyme ribonucleotide reductase, which catalyzes the formation of deoxyribonucleotides from ribonucleotides. Hydroxyurea therefore leads to cell stress inhibiting DNA synthesis (69).

1.6 Rationale, Experimental Goals and Hypothesis

My investigation will focus on missense mutations V133F, V155G, Y330C, and S356N of human HARS identified in patients with CMT2W phenotypes (41,42). All mutations are autosomal dominant and localize to the amino acid binding pocket of the enzyme in the catalytic domain (Figure 8). No organismal models have been established to study the V133F variant. This mutation was recently linked to cognitive impairment in addition to peripheral neuropathy, which was not previously seen in CMT2W type neuropathies caused by other identified HARS mutations (42). Previous attempts to study V155G, Y330C and S356N variants in a yeast model showed that these mutant variants of HARS failed to complement the deletion of yeast HARS homolog HTS1 (41). Therefore, detailed phenotypic characterization of these HARS variants in yeast is lacking.

I hypothesize that mutations in the active site of HARS cause a reduction of amino acid specificity, which leads to a gain-of-function mutation, where mutant aminoacylates tRNA^{His} non-specifically with other amino acids. This gain of function mutation will lead to mistranslation, which can be observed by the accumulation of mutated and misfolded proteins, and reduction in cellular viability. I hypothesize that these variants in human HARS will lead to growth defects in a yeast model of CMT2W through a gain-of-function mechanism with defective protein folding and loss of specificity in aminoacylation. My aims for my investigations are detailed below:

Aim 1: I will generate a yeast model for CMT2W disease by replacing yeast HARS homolog HTS1 with human wildtype and mutant V133F, V155G, Y330C, and S356N HARS (collectively referred to as CMT-HARS).

Aim 2: I will perform a phenotypic characterization of these CMT-HARS disease models by measuring growth deficiencies under different temperature and chemical stress as summarized in Table 3. This will provide insight into the effects of CMT-HARS on the yeast proteome and cellular viability.

Aim 3: I will analyze biochemical processes related to mistranslation and protein misfolding as the first steps into deciphering whether these disease variants are loss-of-function or gain-of-function.

Through this investigation, I will gain a better understanding of the mechanistic basis of CMT-HARS pathology. The results will refine the molecular and cellular basis of CMT2W syndrome, which can be subsequently confirmed using patient samples. The data will also inform future treatment approaches.

Chapter 2

2 Materials and Methods

2.1 Materials

2.1.1 Plasmids and primers

HARS homolog in yeast (*HTS1*) was expressed from the pBY011 vector that was obtained from the DNASU plasmid repository in an *E. coli* DH5 α stock (70). Wild-type *Homo sapiens* HARS (hsHARS) in pCAG/FLAG/RFC/A plasmid backbone was a kind gift from Dr. Christopher S. Francklyn. All constructs were created through the standard procedures of Gateway cloning following the protocol developed by Invitrogen (71). p426-ccdB-GPD (URA3 plasmid) and p425-ccdB-GPD (LEU2 plasmid) are yeast episomal plasmids that stably propagate, which we used to express HARS as a HARS-Yellow Fluorescent Protein fusion (HARS-YFP). Site-directed mutagenesis primers were designed to generate the V133F, V155G, Y330C, and S356N mutations in HARS on the LEU2 plasmids as described by manufacturer's instructions (72). All plasmids are listed in Appendix 1. All primers are listed in Appendix 2.

2.1.2 *E. coli* strain, media, and growth conditions

Competent DH5a and TOP10 *E. coli* strains were used for transformation. *E. coli* strains were cultured on either liquid media or agar plates (15 g/L) containing 10 g/L NaCl, 10 g/L tryptone, and 5 g/L yeast extract or 25 g/L Lysogeny Broth (LB) miller (BioShop, LBL407). 100 mg/mL ampicillin was added based on the plasmids' selected antibiotic resistance.

2.1.3 Yeast strain, media, and growth conditions

The *S. cerevisiae* Δ *hts1* heterozygous deletion strain was obtained from the *Saccharomyces* Genome Deletion Project (73), where one allele for *hts1* was replaced with a KanMX gene, leading to Geneticin (G418) resistance. All haploid *S. cerevisiae* yeast strains were BY4742 with genotype MATa his3 Δ 1 leu2 Δ 0 lys2 Δ 0 ura3 Δ 0, which were derived from the S288C strain. Cells were grown on YPD (10 g/L yeast extract, 20 g/L peptone, and 20

g/L Dextrose or 50 g/L of YPD Broth) or selective synthetic defined (SD) liquid media (6.7 g/L yeast nitrogen base (YNB), 2% glucose, 60 mg/L L-isoleucine, 20 mg/L L-arginine, 40 mg/L L-lysine, 60 mg/L L-phenylalanine, 10 mg/L L-threonine, 10 mg/L L-methionine and 10 mg/L adenine hemisulfate salt), supplemented with 20 g/L agar for growth on solid media. SD media was supplemented with amino acids as adequate for the selectivity marker or the plasmid at 40 mg/L L-tryptophan, 20 mg/L L-histidine-monohydrate, 60 mg/L L-leucine or 20 mg/L uracil. SD Leu(-) media lacked the addition of L-leucine, SD Ura(-) media lacked the additional of L-uracil, while SD Leu(-) Ura(-) lacks the addition of both leucine and uracil. 5-foa media prepared with final concentrations of 6.7 g/L YNB, 2% glucose, 25 mg/L adenine 100 mg/L L-isoleucine, 100 mg/L L-lysine, 50 mg/L Tryptophan, 100 mg/L histidine, 50 mg/L L-methionine, 50 mg/L uracil, and 0.1% 5- Fluoroorotic acid (5-foa) in either liquid media or agar plates (24 g/L). For histidine assays, cells were grown with adjusted histidine concentrations for low histidine (2 mg/L) or high histidine (200 mg/L) at 30 °C or 40 °C as indicated. For amino acid stress assays, final concentration of 200 mg/L of L-alanine, L-arginine, L-asparagine, L-aspartic acid, L-cysteine, L-glutamine, L-glutamic acid, L-glycine, L-isoleucine, L-leucine, L-lysine, L-methionine, L-phenylalanine, L-proline, L-serine, L-threonine, L-tryptophan, L-tyrosine, and L-valine were added separately in additional to the standard SD Leu(-) media. Final concentration for chemical stressors are AZC (0.5mM), ethanol (4%), H₂O₂ (100µM), and hydroxyurea (200mM).

2.1.4 Antibodies

Primary antibody for HARS was anti-GFP (Abcam, ab32146) prepared in a 1:10,000 dilution in blocking solution (5% skimmed milk powder in Phosphate Buffered Saline (PBS) (137 mM NaCl, 2.7 mM KCl, 10mM Na₂HPO₄, 1.8 mM KH₂PO₄) with 0.01 % (v/v) Tween (PBS-T)). Secondary antibody was IRDye® 800CW Goat anti-Rabbit IgG (Li-Cor, 926-32211) was prepared in a 1:20,000 dilution using washing solution (0.5% skimmed milk in PBS-T). Loading control antibody used was anti-PGK1 (Invitrogen, PA5-28612) in 1:5,000 dilution in blocking solution. For purified HARS experiments, anti-6xHis primary antibody (ab18184) was used in 1:1,000 dilution.

2.2 Methods

2.2.1 Yeast sporulation and dissection

Yeast sporulation was carried out by Rosan Kenana and dissection was carried out by Dr. Christopher Brandl and Andrew Petropavlovskiy. To allow the sporulation of diploid *Δhts1* yeast strains, cells were first grown in YPD liquid culture at 30°C overnight without shaking. Cells were washed twice with 5 mL of water and resuspended in 3 mL of 1% potassium acetate. Cultures were incubated at 25°C for 3-5 days while shaking at 220 rpm. Once sporulated and tetrads were visible under the microscope, 300 μL of sterile water was added to 30 μL of culture, then treated with 10 μL lyticase (5 μg/mL) for 11 minutes at room temperature to digest the membrane encapsulating the four tetrad spores and incubated. 30 μL of sporulated cultures were transferred to a YP-dissection plate. The plate was then tilted to create a horizontal line of the cell media. The haploid spores were then dissected as previously described (74) and grown at 25°C for three days until spore colonies appeared.

2.2.2 QuikChange Site directed mutagenesis

QuikChange Site-directed mutagenesis (Agilent) was used to generate mutations c.397G>T (V133F), c.454T>G (V155G), c.989A>G (Y330C), and c.1067G>A (S356N) separately in the HARS gene in the pRS-425 (p425) plasmid. Mutagenesis was performed according to manufacturer's instructions (72) using primers listed in Appendix 2. The final PCR reaction parameters were as follows: The parental plasmid was amplified in an initial reaction with 2 minutes of denaturation at 94 °C followed by 29 cycles of denaturation at 94 °C for 40 seconds, primer annealing at 55 °C for 40 seconds, and DNA synthesis at 72 °C for 10 minutes. The reaction was then held at 4 °C. For each mutant, the two 25 μL reaction volumes were then combined and heated to 95 °C then slowly cooled to 37 °C, allowing annealing of PCR products. DNA sequencing was carried out at the London Regional Genomics Centre (LRGC, London, ON).

2.2.3 *E. coli* transformation

E. coli transformation was performed to replicate and amplify prepared plasmids. 40 μL of competent DH5 α or TOP10 cells stored in $-80\text{ }^{\circ}\text{C}$ were thawed on ice, then mixed in with 1-5 μL (0.1~0.5 μg) of plasmid DNAs by gently flicking the tubes. Cells were allowed to sit for 20 mins on ice, underwent heat shock at $42\text{ }^{\circ}\text{C}$ for 90 seconds, followed by two minutes on ice. One mL of preheated LB media was added to the cells before allowing the cells to recover at $37\text{ }^{\circ}\text{C}$ in a rotator incubator for at least one hour. Following recovery, 100 μL of transformed cells were plated on an LB/Ampicillin agar plate, the remaining culture was centrifuged at 10,000 $\times g$ for two minutes. The supernatant was aspirated, the cells were resuspended in 100 μL of LB media and plated on an LB/Ampicillin agar plate. Plates were flipped and incubated overnight in a stationary $37\text{ }^{\circ}\text{C}$ incubator. Next day, single colonies were collected, inoculated in LB/Ampicillin liquid, and cultured overnight at $37\text{ }^{\circ}\text{C}$ in a shaking incubator at 150 rpm. Glycerol stocks were made by adding 350 μL of 80% glycerol to 650 μL cultures and were kept at $-80\text{ }^{\circ}\text{C}$. Plasmids were miniprepmed using the remaining cultures and purified using the Qiagen Plasmid Miniprep Kit according to manufacturer's instructions. DNA sequencing was carried out at the London Regional genomics Centre (LRGC, London, ON).

2.2.4 Yeast transformation

Yeast transformations were performed according to standard PEG/lithium acetate method protocol (75). Single colonies were inoculated in 3 mL SD Leu(-) media, then incubated overnight at $30\text{ }^{\circ}\text{C}$ while shaking at 300 rpm. Media was added up to 30 mL the next morning and allowed to incubate/shake for 3-4 extra hours until cells reach the log phase (an OD600 of 0.4 to 0.5). Culture was centrifuged at 2000 $\times g$ for 5 minutes; the supernatant was discarded as the cells were washed twice with 2 mL of sterile water before resuspended in 2 mL of 100 mM Li-Acetate in TE buffer (1M Tris-Cl (pH 8.0), 0.5M EDTA (pH 8.0), ddH₂O) and incubated at the same shaking setting for 30 minutes. Plasmids for transformation were prepared during incubation time by mixing 250 μL transformation buffer (40% PEG, 100 mM Li-Acetate, 1X TE), 12 μL salmon sperm DNA (denatured at $99\text{ }^{\circ}\text{C}$ for 10 minutes), 2 μL (0.3~0.5 μg) plasmid DNA, and 13 μL

DMSO. After incubation, the culture was centrifuged at 2000 x g for 5 minutes, and pellet was resuspended with 100 μ L transformation buffer. The cultures were incubated at 30 °C for 30 minutes with 1,500 rpm shaking, followed by a 20-minute heat shock at 42 °C shaking at 500 rpm. Cells were kept on ice for 10 minutes before they were centrifuged for 1 minute at 2,000 xg. Pellet was resuspended in 100 μ L TE buffer, plated onto selective agar plates and incubated at 30 °C for 2-3 days.

2.2.5 Plasmid shuffling

Growing cells harbouring a URA3 expressing plasmid (p426) on 5-Fluoroorotic Acid (5foa)-containing plates obligates the cells to eliminate p426 in order to maintain survival (76). Following the transformation of LEU2 plasmids into the haploid Δ *hts1*-HARS-p426 strain, the dual-plasmid transformants were grown on SD Leu(-) Ura(-) plates for 2 days at 30 °C. Single colonies were streaked on 5-foa agar plates for 3-5 days at 30 °C. Viable strains harboring LEU2 plasmids only were selected and streaked on SD Leu(-), SD Ura(-) and SD Leu(-) Ura(-) plates for the verification of the plasmid shuffling. Strains that only grew on SD Leu(-) plates proceeded to further experiments.

2.2.6 Yeast Growth Analysis

2.2.6.1 Spotting assays

Single colonies were inoculated in 3 mL selective SD media and cultured overnight at 30 °C and 300 rpm. 3 biological replicates were performed for each yeast strain. OD600 were normalized to 1 the next morning to final volume of 200 μ L. Cultures were serially diluted to yield dilutions 1:1, 1:4, 1:4², 1:4³ and 1:4⁴. A multichannel or a 48-pin replicator (V&P Scientific, NC0540875) was used to spot 3-5 μ L of on selective SD plates, with each row representing a dilution. Spotted plates were incubated in 30 °C or 40 °C for temperature stress for 2-5 days. Plates were imaged daily to monitor the growth of the yeast colonies using the Gel Doc XR+ (Biorad). Quantification of spot plates was performed using Image J to measure the mean grey values of spots following previously established protocol (77).

2.2.6.2 Growth curves

Growth curve assays were performed to monitor growth of the strains over 24 hours. Single colonies were inoculated in 3 mL selective SD media and cultured overnight at 30 °C and 300 rpm. 3 biological replicates were performed for each yeast strain. OD600 was measured using the Synergy-H1 plate reader (BioTek), then normalized to OD600=0.1 in using selective SD growth media (with or without chemical stressors). For each biological replicate, 3 replicates of 300 µL culture was transferred into 3 adjacent wells of a 96-well plate. OD600 readings of the plates were done in the Synergy-H1 over 24 hours in 30 °C or 40 °C, with 10 min OD600 read intervals, and shaking for 10 seconds prior to each read. Doubling time in minutes is calculated by finding the slope of the exponential phase of the growth curves, and calculating the $\log(2)/\text{slope}$ value.

2.2.6.3 Fluorescent microscopy

To monitor the fluorescence of YFP tagged to HARS, cultured inoculated overnight were centrifuged at 2,000 xg for 5 minutes. 1 µL of the cell pellet was placed on a microscope glass slide and pressed with a cover slip. The cells were imaged using the EVOS® FL Auto Imaging System (ThermoFisher Scientific) at 40X magnification.

2.2.7 Yeast sedimentation assay

The sedimentation assay was adapted from Shiber et al. (78) to fractionate yeast cell lysate whole lysate, supernatant and pellet, followed by running the samples on an SDS gel. Single colonies were inoculated in 3 mL SD Leu(-) media and cultured overnight at 30 °C and 300 rpm. 3 biological replicates were performed for each yeast strain. OD600 were normalized to 1. Cultures were centrifuged at 2000 xg for 2 minutes and cells were washed once with 200 µL sterile water, then resuspended in 200 µL of complete lysis buffer (100 mM Tris, pH 7.5, 200 mM NaCl, 1 mM EDTA, 1mM DTT, 5% glycerol, 0.5% TritonX-100, 50 mM NEM, 2mM PMSF, and 1X protease inhibitor tablet (Roche, Cat. No. 04 693 159 001). A 1:1 volume (200 µL) of acid-washed glass beads (425-600 µm, Sigma) was added as cultures rested on ice for 2 minutes. Cultures were disrupted using the Genie Disrupter (Scientific Industries) to allow rapid pulsing of the beads and thus allowing cells to be lysed. Cells were pulsed with 30-second bursts at and 30-second

intervals on ice for a total of 6 repetitions. Then the bottom of Eppendorf tubes was pierced with a 16-gauge needle to allow elution of only the lysate and not the glass beads under pulsed centrifugation. The lysate was resuspended and 80 μ L of volume was taken to represent the whole lysate portion. The remaining lysate was centrifuged at 500 \times g for 15 min at 4 $^{\circ}$ C. 80 μ L of the supernatant was taken to represent the soluble portion. The remaining supernatant from the lysate was aspirated off, and the leftover pellet represented the insoluble portion. 80 μ L of SUMEB buffer (8M Urea, 1% SDS, 10 mM MOPS, 10 mM EDTA, and 0.01% bromophenol blue) was added to the whole lysate and soluble samples, while 80 μ L of lysis buffer (without protease inhibitors) and 80 μ L of SUMEB buffer was added to the insoluble sample. The samples were then boiled at 95 $^{\circ}$ C for 5 min and stored at -20 $^{\circ}$ C or separated by SDS-PAGE.

2.2.8 Protein analysis

2.2.8.1 SDS-PAGE

Sodium dodecyl-sulfate polyacrylamide gel electrophoresis SDS-PAGE gel recipe was adapted from Sambrook and Russell (79). SDS gels were prepared with 15% separating gel and 5% stacking gel. Samples were boiled at 95 $^{\circ}$ C for 5 minutes prior to loading. 15 μ L of samples were loaded to the gel along with 5 μ L of pre-stained protein ladder (FroggaBio). The gel was run at 90 volts until the samples crossed the separating-stacking line, then ran at 120 volts until the loading dye front reached the bottom of the gel or there is a clear separation of the ladder. Following the electrophoresis, the gel was stained in 25 mL of Coomassie Blue stain (30% ethanol, 10% acetic acid and 0.25% Coomassie Brilliant Blue G-250) for an hour, then de-stained in SDS-gel de-staining solution (30% ethanol and 10% acetic acid) for 1 hour, both by shaking gently at room temperature. Gels were further detained using distilled water overnight until there is clear visualization of the lanes. Gels were imaged using the Gel Doc XR+ (Biorad).

2.2.8.2 Western blot

All SDS gels were ran according to the SDS-PAGE procedures. Proteins were transferred from the gel onto a PVDF membrane (BioRad) using the Bio-Rad Trans-Blot Turbo machine following the manufacturer's protocol. The membrane was blocked using blocking solution (5% skimmed milk powder in Phosphate Buffered Saline (PBS) (137 mM NaCl, 2.7 mM KCl, 10mM Na₂HPO₄, 1.8 mM KH₂PO₄) with 0.01 % (v/v) Tween (PBS-T)) with gentle shaking for 1 hour at room temperature. The membrane was then incubated in primary antibody (in blocking solution) overnight with gentle shaking at 4 °C. The following morning, the membrane was washed with washing solution (0.5% skimmed milk in PBS-T), 3 times of 10-minute intervals. The membrane was incubated with the secondary antibody (in washing solution) for 1 hour with shaking at room temperature, followed by washing with PBS-T 3 times in 5-minute intervals. Membranes were incubated in PBS. Protein bands were visualized using the Odyssey Classic (Li-Cor).

2.2.9 HARS *in vitro* studies

2.2.9.1 HARS purification

The hsHARS gene was integrated into a pDest527 destination vector using Gateway Cloning to yield a 6x-His tag expression construct. QuickChange site-directed mutagenesis methods were used to introduce point mutations to create V133F, V155G, Y330C, S356N, and Y454S HARS variants. HARS proteins were purified following HisPur Ni-NTA column (Thermo Scientific) purification protocol according to manufacturer instructions. Plasmids encoding hsHARS variants were transformed into *E. coli* BL21, inoculated into 10 mL precultures and transferred to 1 L cultures of LB grown at 37 °C to an OD₆₀₀ of 0.6. Protein expression was then induced with 400 mM isopropyl β-D-1-thiogalactopyranoside (IPTG) and cultures were grown overnight at 18 °C with 150 rpm shaking. Cells were harvested and resuspended in Buffer A (50 mM Tris-HCl pH 8.0, 300 mM NaCl, 20 mM MgCl₂) supplemented with 20 mM imidazole, 1 mM phenylmethylsulphonyl fluoride (PMSF), 0.1 mg/mL lysozyme, and 50 μL/g of protease inhibitor mixture. Cells were lysed by sonication (750W sonicator for 5 cycles, 30 seconds pulse, 30s pause at 60% amplitude). Cell lysate was centrifuged at 60,000 xg for 1 hour at 4 °C. The cell free extract was loaded

onto a HisPur Ni-NTA column (Thermo Scientific) pre-equilibrated with 10 column volumes of Wash Buffer (Buffer A + 20 mM imidazole). The column was then washed three times with 10 column volumes of Wash Buffer. A stepwise elution was performed with 2 mL each of the following buffers: Elution Buffer 1 (Buffer A + 100 mM imidazole), Elution Buffer 2 (Buffer A + 300 mM imidazole), and Elution Buffer 3 (Buffer A + 500 mM imidazole). A 40 μ L of the lysate, cell-free extract, pellet, flow-through, wash, and each elution fraction was combined with 20 μ L of 3X SDS-dye (3% (w/v) SDS, 188 mM Tris-HCl, pH 6.8, 0.01% (w/v) bromophenol blue, 15% (v/v) β -mercaptoethanol, 30% (v/v) glycerol, water) and boiled for 5 minutes at 95 $^{\circ}$ C before SDS-PAGE analysis. Fractions containing HARS were combined and dialyzed at 4 $^{\circ}$ C into Buffer A using dialysis tubing with a 15 kDa molecular weight cut-off. Protein concentration was determined by measuring A_{280} and samples were stored at -80 $^{\circ}$ C.

2.2.10 Thermal shift assay

Differential scanning fluorimetry (DSF) or thermal shift assay was performed as described previously (27). HARS protein samples were prepared on ice with a final concentration of 1 μ M in a 96-well 0.1 mL microplate with 8X Protein Thermal ShiftTM Dye and Protein Thermal ShiftTM Buffer (ThermoFisher) to a final volume of 20 μ L. tRNA^{His_{Micro}} was used as tRNA (5'-GGCCAUCCUGCGGGUGGCACCA-3') that was previously shown to be a suitable HARS substrate (80). Proteins were incubated with either 2 μ M, 1 μ M, or 0.5 μ M of tRNA^{His_{Micro}}. Samples were also incubated with 1 mM histidine or 500 μ M ATP either on their own, in combination, or with 2 μ M tRNA^{His_{Micro}}. Plates were sealed and protein unfolding was monitored with a QuantStudioTM 3 Real-Time PCR System (ThermoFisher). Samples were heated from 25 $^{\circ}$ C to 96 $^{\circ}$ C at 1 $^{\circ}$ C per minute and fluorescence intensity was measured every 0.017 $^{\circ}$ C. Initial analysis was performed in the Protein Thermal Shift software (ThermoFisher) and the data was fit to the Boltzmann equation to estimate the melting temperature (T_M). Subsequent statistical analysis was performed through GraphPad Prism 9.1.0.

2.2.11 Statistical analysis

All statistical significance was obtained by running unpaired t-tests to compare the means and standard deviations between the control data set and the experiment data set or a one-way ANOVA test for multiple comparisons. Significance levels are indicated using asterisks (**** $p < 0.0001$, *** $p < 0.001$, ** $p < 0.01$, * $p < 0.05$, ns = statistically non-significant).

Chapter 3

3 Results

To investigate the biochemical and cellular effects of HARS deficiency in cells, our lab generated a *Saccharomyces cerevisiae* yeast model system, replacing endogenous yeast HTS1 with human HARS variants expressed *in trans*. The generation of the first yeast model was performed by a previous graduate student Rosan Kenana to study HARS mutation Y454S that leads to USH3B syndrome. This model was subsequently used by me as the basis for the generation of CMT2W disease model in yeast, and all work relating to mutants V133F, V155G, Y330C, and S356N was performed by me. In my results I will include the data for the Y454S mutant along with the data for V133F, V155G, Y330C, and S356N mutants in order to provide a more comprehensive story of the impact of HARS deficiency. From this point forward, wildtype HARS will be referred to as hsHARS.

3.1 Generation of a yeast model for HARS deficiency

Interestingly, previous attempts to generate a model system for CMT-HARS variants were not successful in yeast (41). Our lab's approach is outlined in Figure 10. Yeast *hts1* is an essential gene, therefore its deletion would be lethal to yeast. We generated a Δ *hts1* (HTS1 deletion) haploid yeast strain for which its survival is only maintained by the successful complementation of human HARS. To do this, we first obtained a diploid *hts1* heterozygous deletion strain from the yeast haploid deletion collection that has one *hts1* allele and the other *hts1* allele deleted and replaced by the *KanMX* gene (73). Human wild-type HARS (hsHARS) fused to YFP was cloned into the p426-ccdB-GDP (URA3) yeast episomal plasmid and transformed into the parental diploid deletion strain. These transformed yeast cells were allowed to sporulate until yeast haploid tetrads were visible under the microscope (Fig. 11A). We expect half of the haploid spores to carry the *hts1* allele the other half to be the *hts1* knockouts with the *KanMX* gene as replacement. The haploid spores were then dissected onto YP-dissection plates, forming 5 spore colonies (I-V) that looked visibly smaller than the diploid colonies (Fig. 11B).

To select for the presence of the HARS plasmid, haploid cells were patched on SD Ura(-) plates (Fig. 11C). To select for the haploids that have *hts1* replaced by the *KanMX* gene, the same haploids were patched on geneticin (G418) plates (Fig. 11D). Only the haploid colonies that grew on both SD Ura(-) and G418 plates were proceeded with as these are the Δ *hts1* haploids with survival maintained by HARS.

We performed further verification to confirm that colonies I-V were indeed haploid Δ *hts1* strains. First, spot plate analysis was performed for haploid colonies I-V and their parental diploid strain bearing the same HARS plasmid. There was slower growth for colonies I-V compared to the corresponding diploid Δ *hts1* strain (Fig. 11E). Slower growth was due to differences in ploidy and absence of chromosomal *hts1* expression. Then we allowed colonies I-V to mate with Mat a and Mat α tester strains that are lysine auxotrophs. It was expected that haploid colonies I-V were uracil auxotrophs and therefore would not be able to survive on YNB minimal plates lacking any amino acids, unless they mate with a tester strain to allow the auxotrophies to be compensated. Haploid yeast cells of one mating type only mate with the other mating type to produce stable diploid cells. The haploids from colonies I-V mated only with Mat a and not the α tester strains, suggesting that they were initially α haploids (Fig. 11F). Finally, haploid colonies I-V were patched on 5foa plates to select against yeast carrying a URA3 plasmid. 5foa is converted to a toxic metabolite by a URA3-encoded gene, forcing yeast to kick out the URA3 plasmid to maintain survival. Haploids from colonies I-V failed to survive when patched on a 5foa plate as they lose the URA3 plasmid encoding human HARS and do not have endogenous *hts1* allele to maintain survival (Fig. 11G). A diploid strain was able to survive as they express endogenous HTS1 regardless of the loss of URA3 plasmid due to 5foa (Fig. 11G). Thus, we confirmed that we have generated a haploid Δ *hts1* yeast model that is complemented by hsHARS to maintain survival.

Mutant HARS variants were then introduced into the haploid deletion background by plasmid shuffling. The wild-type or mutant hsHARS variants (V133F, V155G, Y330C, and S356N, point mutations) encoded in a p425-ccdB-GDP (LEU2) plasmid were transformed into the haploid Δ *hts1* strain containing the p426-HARS maintenance vector, and successful transformation was selected for on SD media lacking Uracil and Leucine

(SD Ura(-) Leu(-)). These strains were grown on 5foa media toxic to URA3⁺ cells (Fig. 12A), and successful plasmid shuffling was selected for on SD Leu(-) media for LEU2⁺ (Fig. 12D). No growth on SD Ura(-) (Fig. 12B) or SD Ura(-) Leu(-) plates (Fig. 12C) verified successful plasmid shuffling, as well as the complementation of mutant HARS for the deletion of yeast HTS1. YFP fluorescence in cells confirmed successful HARS-YFP expression and showed no visual difference between the yeast strains (Fig. 13). Thus, we successfully generated a model system to study HARS deficiency caused by 5 different HARS mutations in a $\Delta hts1$ yeast background.

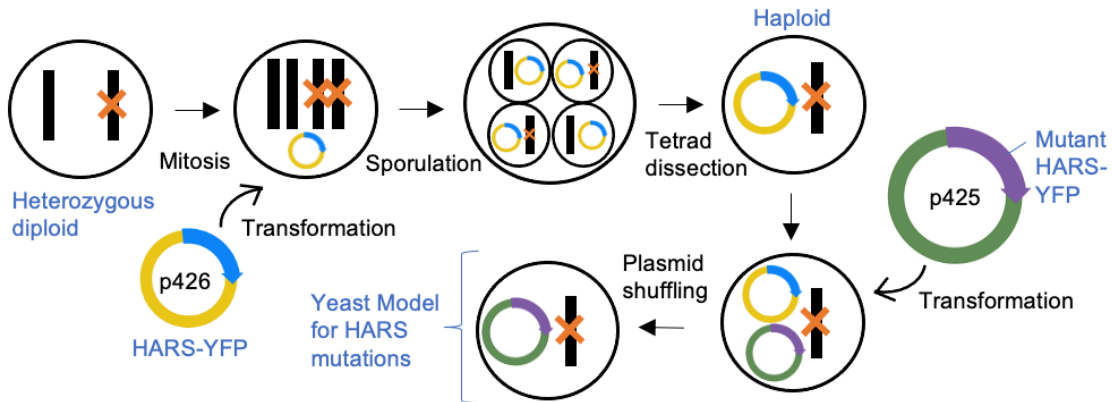


Figure 10. Workflow for the generation of HARS mutant model system in *S. cerevisiae*. p426 (URA3) plasmids carrying HARS-YFP is transformed into heterozygous diploids with only one functional *hts1* allele. Yeast sporulation and dissection yields haploid yeast colonies with no genomic *hts1* allele and are dependent on complementation by human HARS. Transformation of p425 LEU2 plasmids carrying wildtype HARS-YFP gene or HARS-YFP with point mutations (V133F, V155G, Y330C, Y356N, Y454S) yields dual plasmid haploids. The URA3 plasmid is subsequently eliminated, generating the yeast model for HARS deficiency.

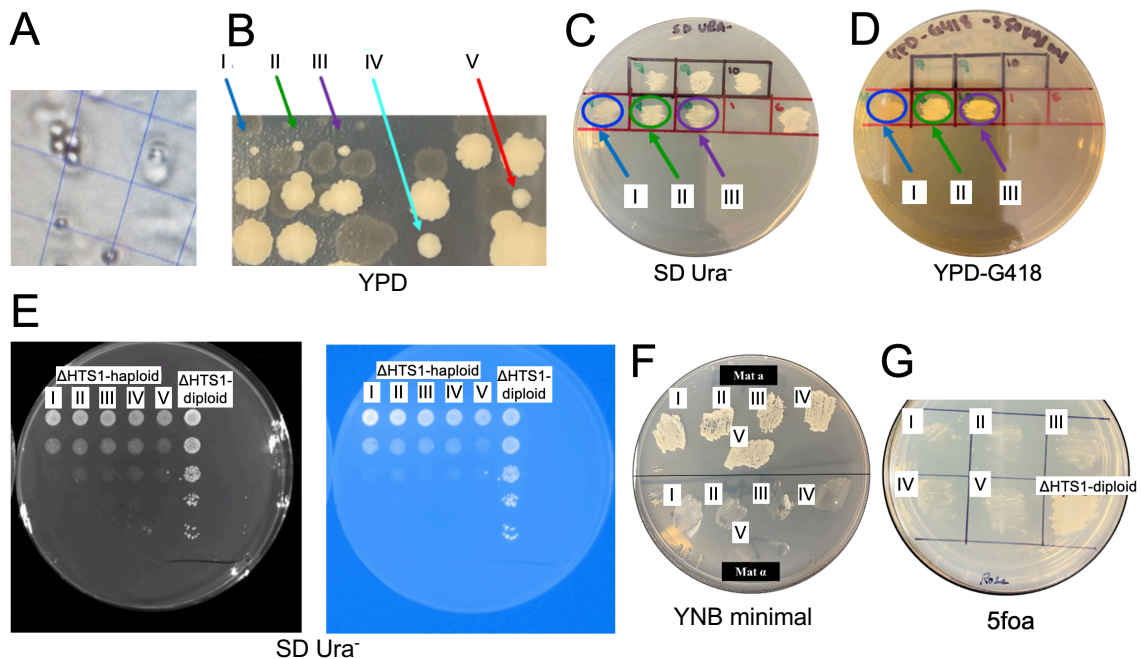


Figure 11. Generation of yeast model. (A) Visible yeast tetrads from sporulation plates under the light microscope. (B) Dissection of tetrads showed smaller colonies (I-V) which were suspected to be the *hts1* knockout haploids. Smaller sized colonies were then patched on (C) SD Ura(-) to check for the expression of p426 plasmid and (D) YPD-G418 plates to verify the knockout of the *hts1* allele. Five colonies labelled I to V survived on both plates and were selected for further experiments. Here, we show only colonies I-III on SD Ura(-) and YPD-G418 plates. (E) Spotting plates of post-dissection Δ *hts1* haploid selected colonies in comparison to a corresponding diploid (BY4743 strain). Colonies I to V grew slower than their parental diploid strain bearing the same HARS-plasmid. Plates imaged using the Gel Doc XR+ (Biorad) under normal light and UV light. (F) Mating of strains I to V with Mat a or Mat α tester strains. Colonies I to V mated only with Mat a tester strain (BY4741) and not Mat α (BY4742) suggesting that they were initially α haploids. (G) Counter selection for URA3-expressing plasmids on 5foa plates. Colonies I to V were patched on a 5foa-containing plate along with the parental Δ *hts1* diploid strain expressing the same HARS plasmid (Y454S-HARS-YFP-p426) as a positive control. Colonies I-V failed to survive; thus, they were dependent on the introduced HARS-bearing plasmids for their survival.

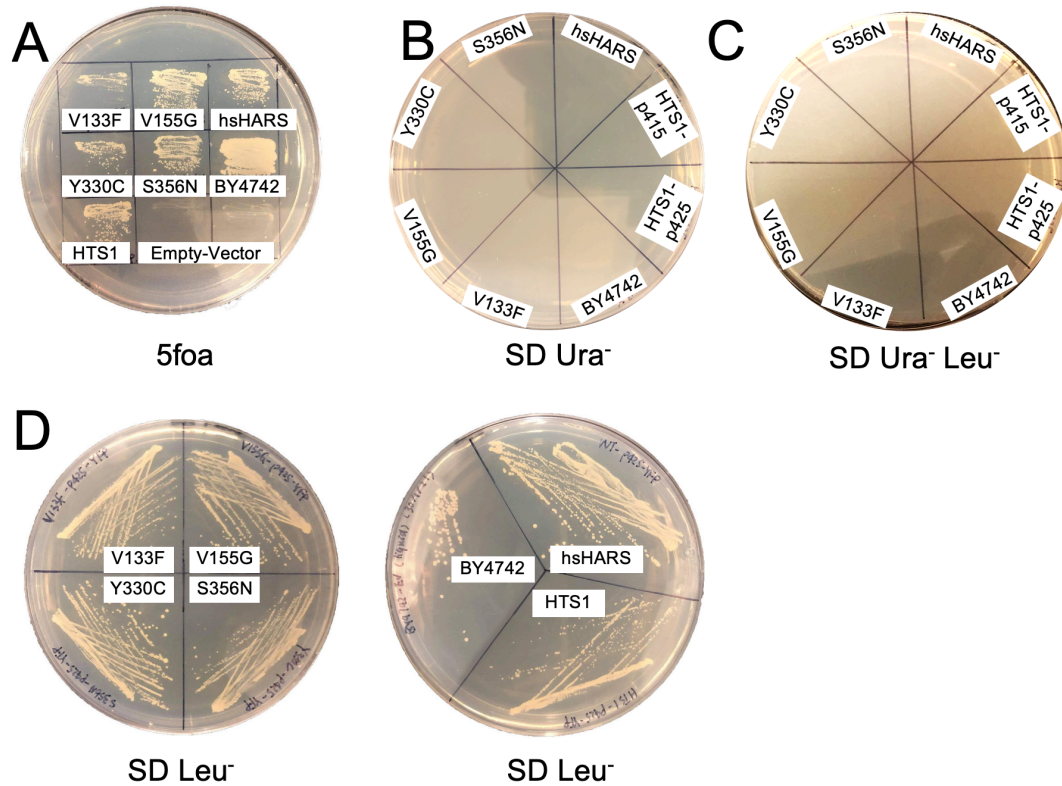


Figure 12. Complementation of CMT-HARS mutants. (A) Plasmid shuffling. Haploid yeast strains with both URA3-resistant plasmid carrying hsHARS and LEU2-resistant plasmid carrying HTS1, hsHARS, or CMT-HARS were patched on 5foa plate for plasmid shuffling to kick out the URA3 plasmid. BY4742, haploid control yeast strain. HTS1, yeast homolog of human HARS. Empty vector, negative control. Yeast complementation negative control (B) SD Ura⁻ and (C) SD Ura⁻ Leu⁻ plates. After plasmid shuffling, no growth on these negative control plates demonstrates that only the LEU2 plasmid remains. (D) Successful selection of Yeast disease models. Colonies after plasmid shuffling were streaked on SD Leu⁻ and incubated at 30 °C for 4 days, showing successful complementation of haploid yeast *hts1* deletion cells.

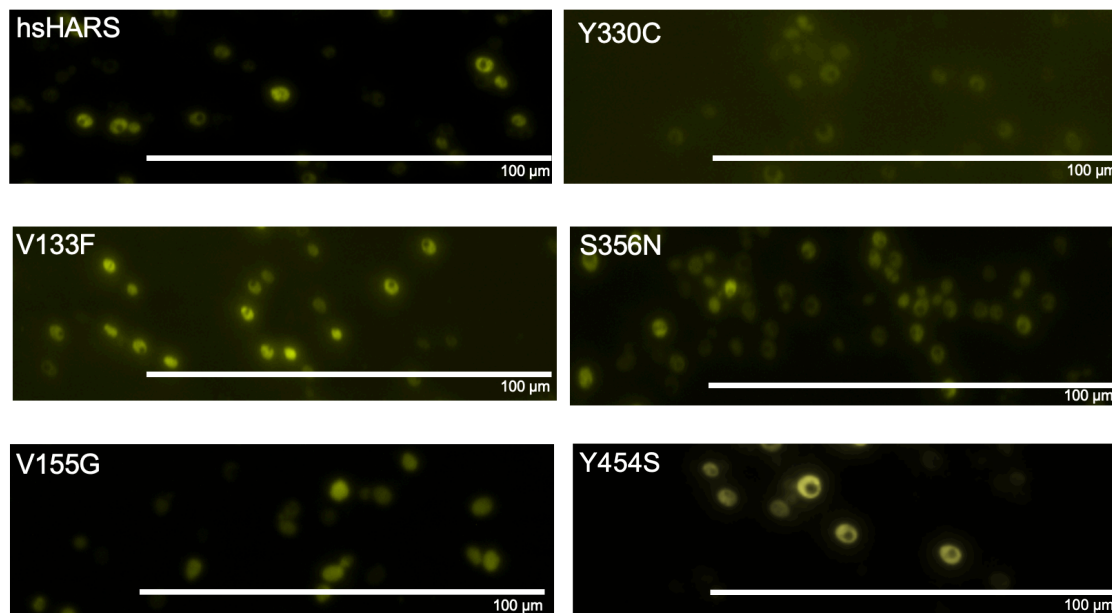


Figure 13. Fluorescence microscopy of mutant HARS yeast model *in vivo*. Wildtype (hsHARS), V133F, V155G, Y330C, S356N, and Y454S-HARS expressing strains were imaged under the EVOS M5000 microscope (Thermo Fisher) enabling visualization of HARS-YFP expression at 40X magnification.

3.2 Dose-dependence of HARS complementation

To determine the impact of HARS expression level on cell growth, we investigated whether high or low copy number were able to complement our yeast HTS1 deletion strain. p425 is a high copy number episomal (2 micron) plasmid that allows 50+ copies of the plasmid to stably propagate per cell. p415 is a low copy number centromeric plasmid that replicates similarly to independent chromosomes and are thus typically found as single copies. Both yeast HTS1 and wild-type hsHARS in low or high copy numbers complement the yeast deletion strain (Fig 14A). High doses of yeast HTS1 are increasingly toxic to yeast cells, whereas wild-type hsHARS is tolerated at high and low expression levels (Fig. 14B). The data show a dose-dependent phenotype for HTS1 complementation, suggesting that over-activity of histidyl-tRNA synthetase creates proteotoxic stress in cells. Interestingly, our attempts to complement the deletion strain with any of the mutant hsHARS alleles using a low copy centromeric plasmid failed in agreement with previous studies (41). These data show that high levels of mutant human HARS are necessary and sufficient to sustain translation in a yeast HTS1 deletion strain.

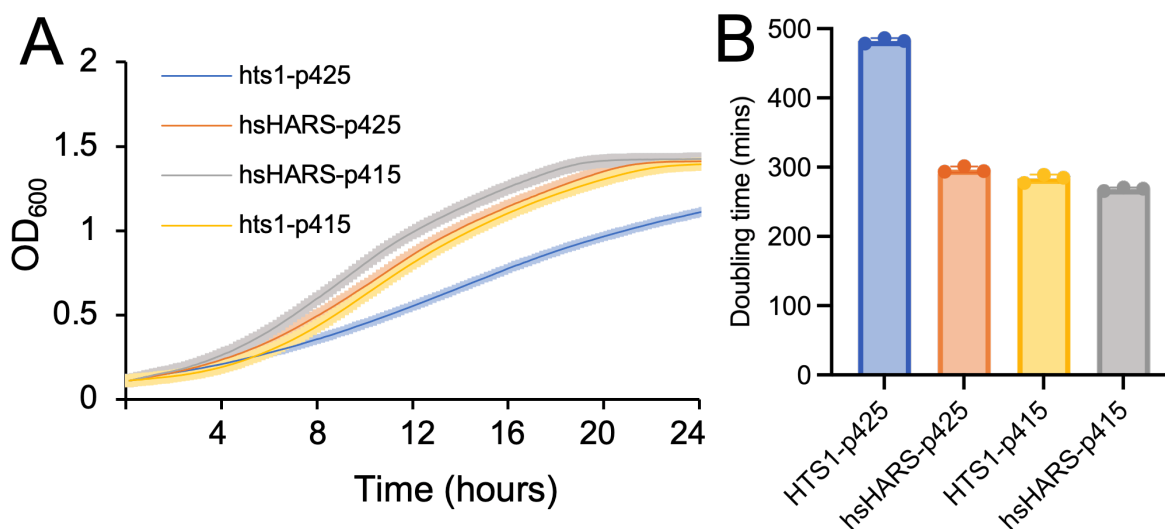


Figure 14. HARS complementation is dose-dependent. (A) Growth curve and (B) doubling time of control strains hsHARS and HTS1 in low (p415) and high (p425) copy number plasmids. Yeast cultures were grown in SD Leu(-) media in 96 well plates for 24 hours with 10-min read intervals with 3 biological replicates and 3 technical replicates each. One standard deviation represented by error bars.

3.3 Mutations in the HARS active site cause global growth defects

To investigate the growth phenotype of the HARS yeast model, we performed spotting assays (Fig. 15A) and growth curve analysis at 30 °C (Fig. 16A), as well as at 40 °C to induce heat stress (Fig 16C) as patients with Y454S mutation is known to experience clinical deterioration during fevers. At 30 °C, cells expressing the CMT2W associated mutants (V133F, V155G, Y330C, and S356N) displayed significantly decreased growth and increased doubling times on solid and in liquid media compared to wild-type hsHARS, while the Y454S mutant sustained wild-type-like growth (Fig. 15B, 16B). Thus, all CMT-HARS mutants lead to growth impairments in the yeast model at 30 °C indicating dysfunctional HARS. Under heat stress, there was no significant difference in doubling time between the V155G, Y330C and S356N mutants compared to hsHARS. However, the V133F growth impairment was exacerbated at 40 °C (Fig. 16D). Surprisingly, the Y454S mutant did not show a significant growth phenotype at 40 °C (Fig 16D), even though fever significantly escalates the disease phenotype of USH3B patients (46). These data show that HARS CMT2W associated mutants are functional in yeast but cause a significant growth defect, making yeast a suitable model organism for further characterization.

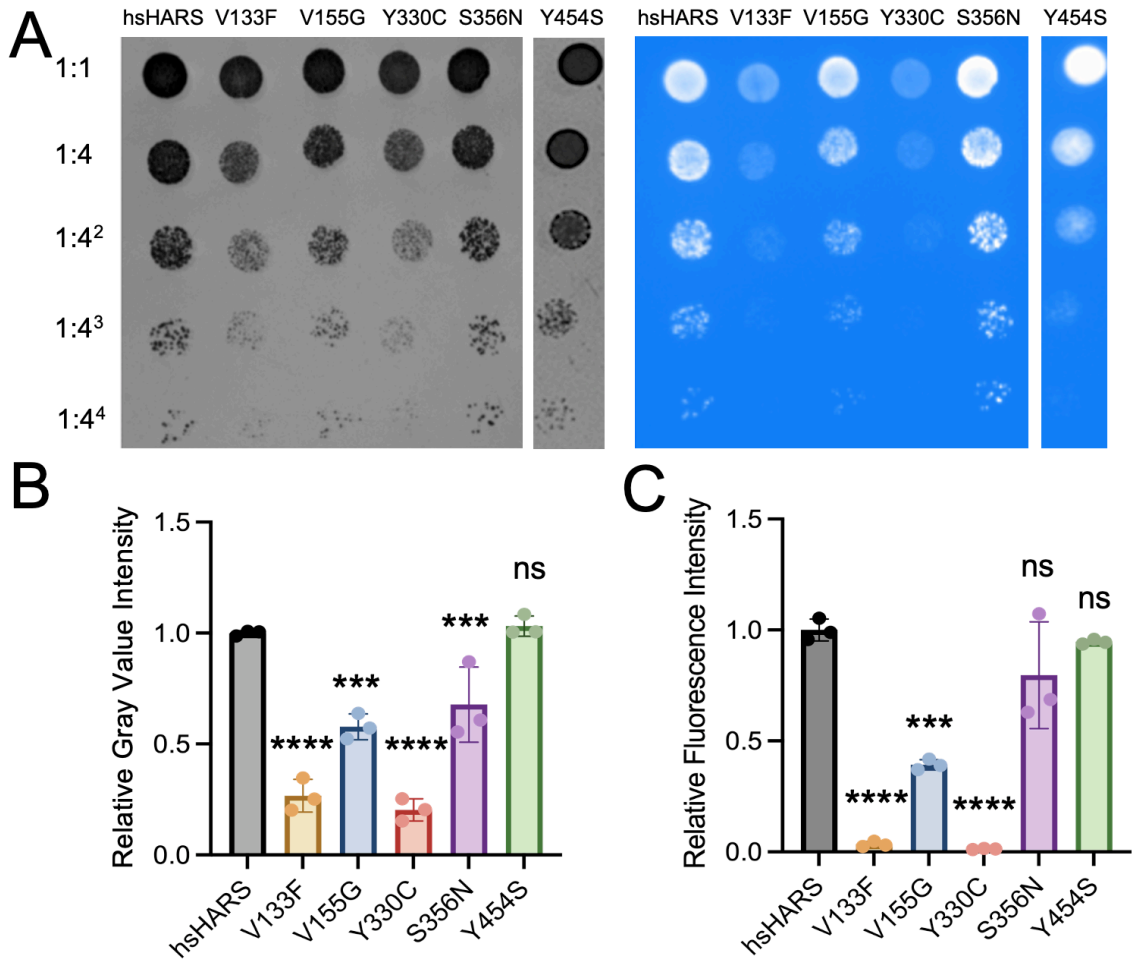


Figure 15. Spotting assay for growth phenotype analysis. (A) Spotting assay at 30 °C. Yeast strains were grown at 30 °C in SD Leu(-) media, normalized to OD600 = 1, and serially diluted 1:1, 1:4, 1:4², 1:4³, and 1:4⁴. 3 replicates of plates were incubated in 30 °C for 4 days. Spot plates were imaged using the Gel Doc XR+ (Biorad) under normal light (left) and UV light (right) to verify the expression of YFP fused to HARS. V133F and Y330C mutants grew slower and showed less fluorescence than hsHARS, V155G and S356N mutants. Quantification of spotting assay at 30 °C for (B) mean gray spot intensity and (C) fluorescence spot intensity. Spots were quantified using ImageJ as described (50). (****p<0.0001, ***p<0.001, ns = statistically non-significant).

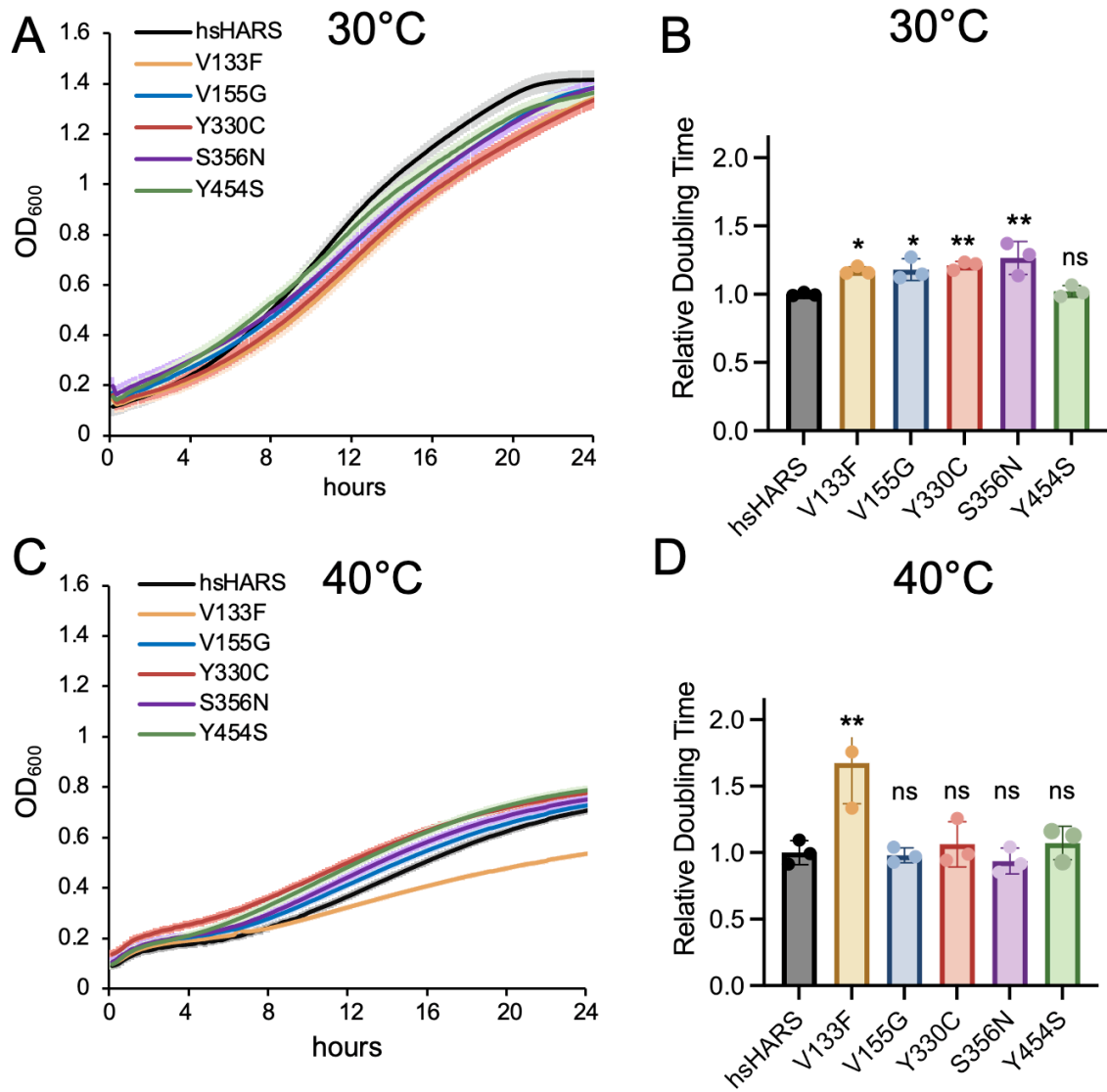


Figure 16. Growth curves for growth phenotype analysis. Growth curve at (A) 30 °C and (C) 40 °C. Yeast cultures were inoculated overnight in SD Leu(-) media until OD₆₀₀=1, then incubated in Synergy-H1 plate reader (BioTek) for 24 hours with 10-min read intervals using 3 biological replicates and 3 technical replicates per biological. One standard deviation of each data point represented by lighter-colored error bars. Doubling time in (B) 30 °C and (D) 40 °C. The doubling time was obtained from growth curves in A and B. (**p<0.01, *p<0.05, ns = statistically non-significant).

3.4 HARS V155G and S356N induce protein aggregation in yeast

Mis-folded proteins aggregate and accumulate in cells (81). To investigate whether the HARS mutations lead to protein misfolding and accumulation in the insoluble protein fraction in yeast, we performed a sedimentation assay. The ratio of soluble to insoluble protein levels in cells expressing wild-type human HARS or mutant HARS was determined (Fig. 17A,C-F, 18A). Interestingly, hsHARS V155G and S356N, but not V133F and Y330C, caused a significant increase in the insoluble protein fraction compared to wild-type hsHARS, indicating the accumulation of unfolded or misfolded proteins (Fig. 17B). In cells expressing mutant hsHARS, we observed an increase in the fraction of insoluble proteins compared to cells expressing wild-type hsHARS by 1.8-fold for V155G and 1.5-fold for S356N (Fig. 17B). The changes in protein solubility were evident across the proteome and not restricted to particular protein bands on the SDS-PAGE (Fig 17A,C-F), indicating HARS alleles V155G and S356N lead to global protein misfolding in cells. For the Y454S variant, the assay was performed with cell growths at 30 °C and 40 °C to look for potential changes in protein synthesis due to HARS instability at 40°C mimicking fever stress in USH3B patients. However we found no evidence of increased insoluble proteins in Y454S-expressing cells compared to cells expressing wild-type hsHARS (Fig 18C).

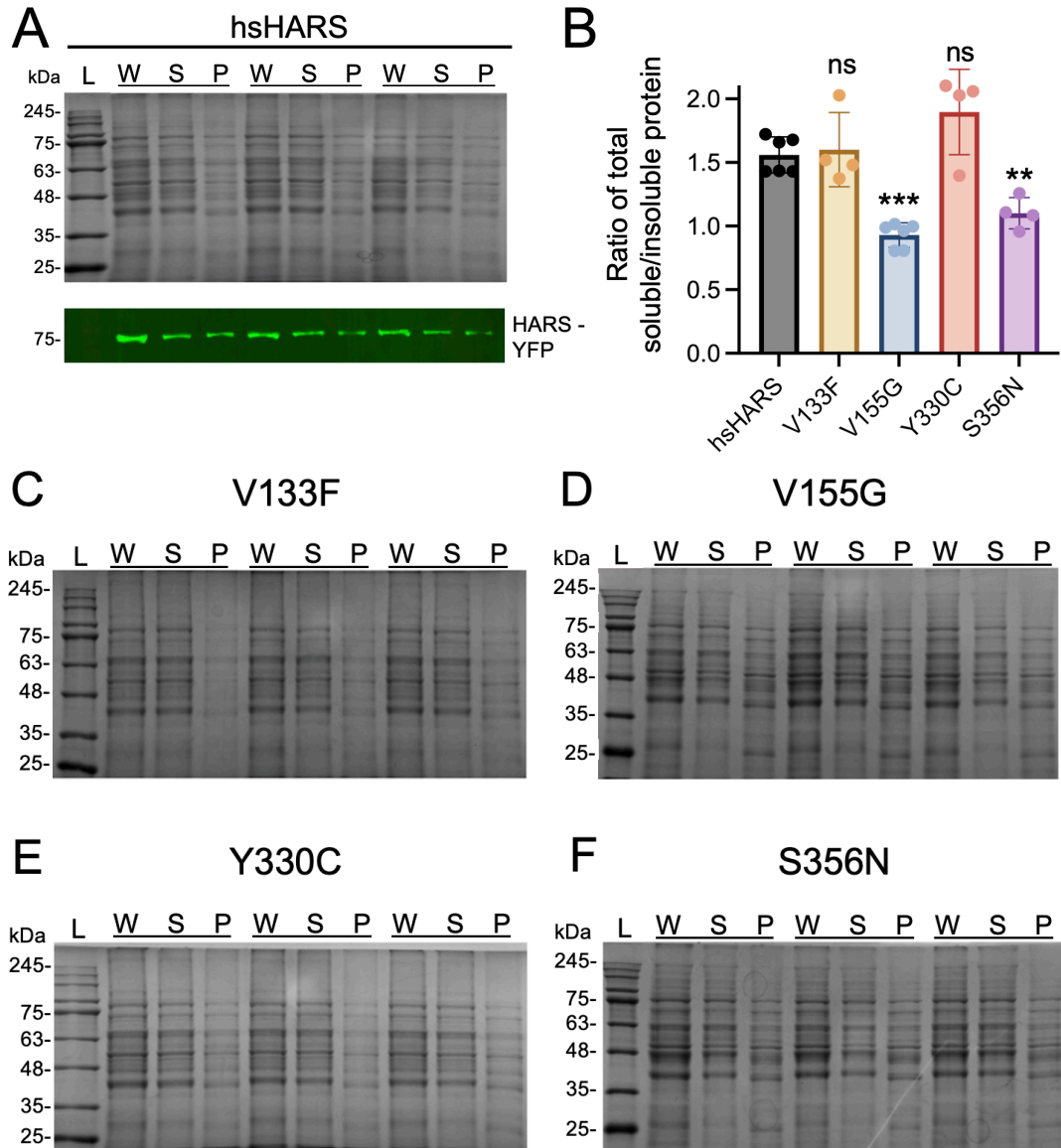


Figure 17. CMT-HARS mutants lead to global protein aggregation. Sedimentation assay SDS gels of (A) hsHARS, (C) V133F, (D) V155G, (E) Y330C, and (F) S356N. First lane is the protein ladder (FroggaBio) with labelled molecular weights. Equal volumes of whole lysate (W), soluble fraction (S) and insoluble fraction (P) extracted from different yeast variants in the sedimentation assay was loaded on to 15% SDS gel in 3 replicates. Gels imaged using the Gel Doc XR+ (Biorad). Gels were quantified using ImageJ. (B) Ratio of soluble to insoluble total protein fraction for CMT mutants. A lower ratio represents a higher proportion of insoluble fraction compared to soluble fraction.

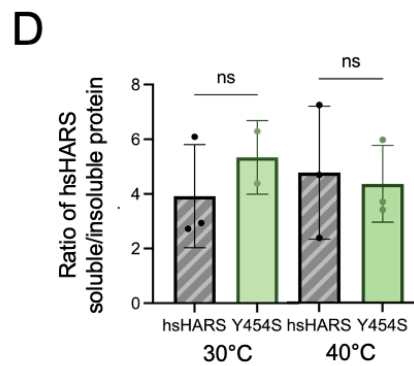
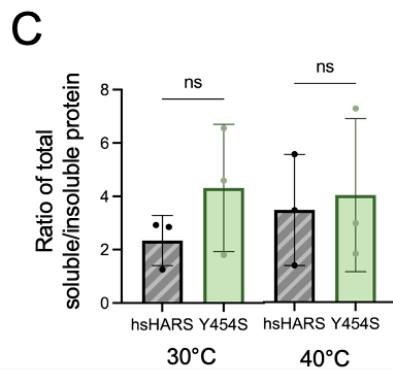
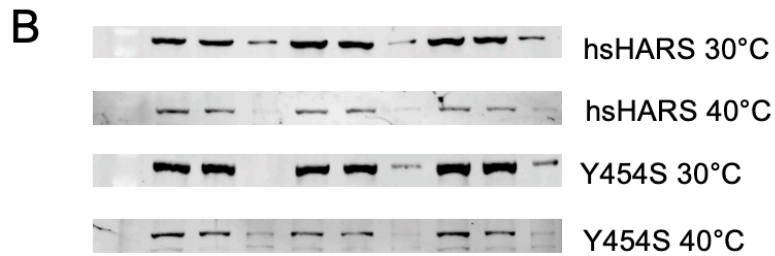
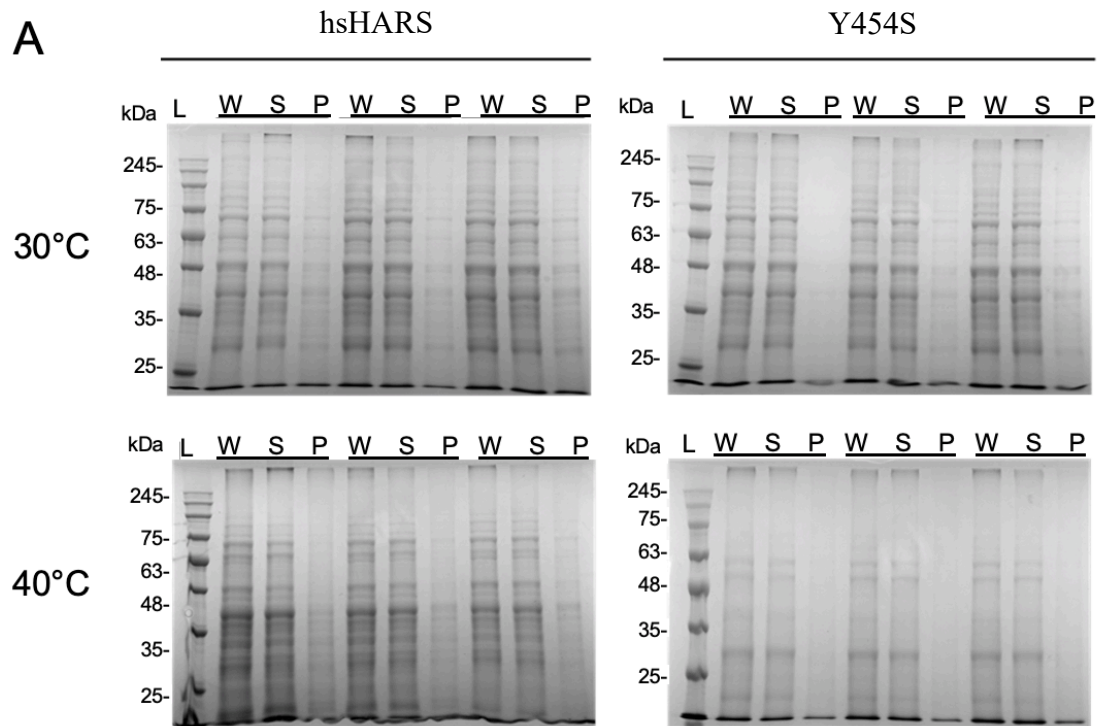


Figure 18. Sedimentation assay for Y454S mutant. (A) Sedimentation assay gels for hsHARS and Y454S mutant. First lane is the protein ladder (FroggaBio) with labelled molecular weights. Equal volumes of whole lysate (W), soluble fraction (S) and insoluble fraction (P) extracted from different yeast variants in the sedimentation assay was loaded on to 15% SDS gel in 3 replicates. Gels imaged using the Gel Doc XR+ (Biorad). Gels were quantified using ImageJ. (B) Western Blots for HARS. Western Blot of sedimentation assay gels performed using primary anti-GFP rabbit monoclonal (ab32146) in 1:10,000 dilution, and secondary antibody used was IRDye® 800CW Goat anti-Rabbit IgG (926-32211) in 1:10,000 dilution. Blots were imaged using the Li- Cor Odyssey imaging system and quantified using ImageJ. (C) Ratio of soluble to insoluble total protein fraction for CMT mutants. (D) Ratio of soluble to insoluble hsHARS-blotting fraction for Y454S mutant.

3.5 V133F and Y330C lead to reduced HARS abundance in yeast

A previous study showed that the USH3B mutant Y454S leads to reduced recombinant protein stability (43). We therefore investigated whether expression of mutant proteins in yeast leads to an increase of HARS proteins in the insoluble protein fraction. We first tested overall HARS abundance by western blotting whole cell lysates (Fig. 19A). The V133F and Y330C mutations lead to significantly reduced abundance of HARS in the whole lysate by 1.3-fold compared to hsHARS (Fig. 19B). The V155G and S356N variants were produced to a similar level as wild-type hsHARS. Since the HARS genes are each expressed from the same promoter on identical plasmids, wild-type and mutant HARS gene expression itself should not be affected by the mutations, but defects in HARS protein stability may lead to degradation of mutant HARS proteins.

To more accurately quantify HARS abundance in cells, we measured YFP fluorescence from the YFP-HARS fusion protein in living cells on spot plates (Fig. 15A). YFP fluorescence intensity was significantly reduced for V133F (29-fold), V155G (2.5-fold), and Y330C (76-fold) (Fig 15C). Since several mutants displayed a reduced growth phenotype, we next calculated the ratio of fluorescence to gray value spot intensity to determine the level of HARS expression per cell (Fig. 19C). After accounting for differences in cell growth, we found that all mutants except for S356N displayed a

significant reduction of fluorescence/spot intensity compared to hsHARS. V133F and Y330C mutants led to 10-fold reduction in fluorescence per cell, whereas V155G (1.5-fold) showed more modest reductions in abundance in live cells (Fig. 19C). A reduction in fluorescence can indicate either reduced protein abundance, or indicate misfolded, non-fluorescent proteins (82).

To test whether HARS aggregation is responsible for the observed decrease in HARS-YFP fluorescence, we blotted for HARS in the total, soluble and insoluble protein fraction (Fig. 19E). Interestingly, insoluble HARS does not significantly aggregate in the mutants compared to wild-type hsHARS expressing cells, as the ratio of HARS in the soluble and insoluble fraction remains unchanged in all mutants (Fig. 19D). For Y454S, which was previously shown to be temperature sensitive, we tested accumulation of insoluble HARS at both 30 °C and 40 °C, but no increase in HARS in the insoluble fraction was observed (Fig. 18D). Together, these data show that the V133F and Y330C mutants lead to significant 10-fold reduction in HARS-YFP fluorescence in live cells, accompanied with a 1.25-fold HARS reduced protein abundance as measured by western blotting (Fig. 19B,C), indicating HARS V133F and Y330C protein misfolding in yeast, leading to subsequent degradation. For V155G, the 1.5-fold reduced fluorescence/gray value was not accompanied with a significant change in protein abundance, and S356N shows minor (1.2-fold) increased fluorescence/gray value accompanied with no change in HARS abundance (Fig. 19B,C), indicating that HARS misfolding and degradation alone are not major contributors to the observed growth phenotype.

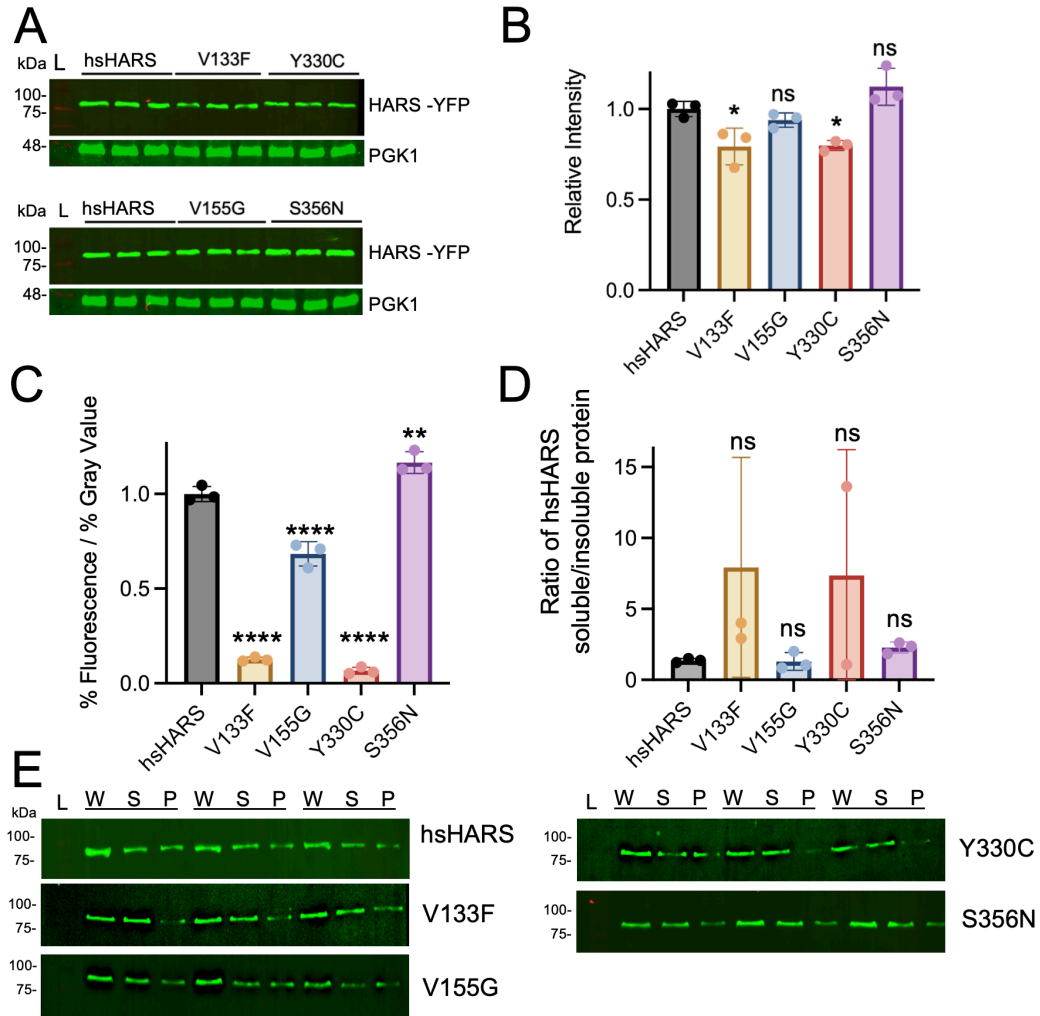


Figure 19. Quantification of HARS expression. (A) Western blot and (B) quantification of blots for HARS in whole cell lysates. Equal volume of whole cell lysate extracted from each yeast strain was loaded and blotted for HARS. Blots were imaged using the Li- Cor Odyssey 9120 imaging system. Western blot bands for HARS were quantified using ImageJ. (C) Ratio of %Fluorescence over %Gray value spot intensities. This ratio measures the expression of functional fluorescence-producing HARS-YFP fusion protein, relative to the amount of growth for each mutant. %Gray value is the relative intensity of spots between mutants and hsHARS in the spotting assay calculated in Fig. 15B. %Fluorescence is the YFP quantification from Fig. 15C. (D) Ratio of soluble to insoluble hsHARS-blotted fraction for CMT mutants. Western Blot of sedimentation assay gels using an anti-GFP antibody were imaged using the Li- Cor Odyssey imaging system and quantified using ImageJ. (**** $p < 0.0001$, *** $p < 0.001$, ** $p < 0.01$, * $p < 0.05$, ns = statistically non-significant). (E) Western Blots for HARS. Western Blot of sedimentation assay gels performed using primary anti-GFP rabbit monoclonal (ab32146) in 1:10,000 dilution, and secondary antibody used was IRDye® 800CW Goat anti-Rabbit IgG (926-32211) in 1:10000 dilution. Blots were imaged using the Li- Cor Odyssey imaging system and quantified using ImageJ.

3.6 Mutants V133F, V155G, and Y454S lead to reduced HARS protein stability

To investigate the stability of mutant HARS proteins, we constructed and purified His-tagged hsHARS and variants from *E. coli* (Fig. 20A). Purified proteins were analyzed by differential scanning fluorimetry to measure protein stability and protein-ligand interactions. To quantify protein stability, the melting temperature (T_M) was determined from the melting curves of hsHARS and mutant HARS variants (Fig. 20B-F). We were unable to purify sufficient amounts of the S356N mutant, because the protein precipitated quickly and complicated the reproducibility of the experiments. We show that the melting temperature of Y454S is reduced from 62 °C (hsHARS) to 54 °C for the mutant protein. Similarly, we found a significant reduction in T_M for mutants V133F to 52 °C and V155G to 60 °C, demonstrating reduced protein stability. No significant change in stability was observed for the HARS Y330C protein (Figs. 20G).

We next tested whether addition of the HARS substrate tRNA^{His}_{Micro} at 2 μ M, 1 μ M, 0.5 μ M, ATP at 500 μ M or histidine at 1mM, or a combination of substrates, could restore HARS stability. The tRNA^{His} Microhelix (tRNA^{His}_{Micro}) was previously shown as a suitable substrate for eukaryotic HARS (80,83,84). For wild-type hsHARS and HARS Y330C, tRNA, ATP or histidine supplementation had no effect on the T_M of the protein compared to apo form (Fig. 21AD, Appendix 3,4), indicating that substrate binding is not normally required for HARS protein stabilization. In the Y454S mutant, substrate supplementation led to a significant increase in T_M to a maximum of 59 °C for ATP in combination with histidine (43) (Fig. 21E, Appendix 5), but did not quite rescue stability to wild-type levels (62 °C) as described previously (43). The addition of tRNA or ATP alone or in combination slightly increased stability (54 °C), while histidine supplementation drastically restored thermal stability (58 °C), which was further increased when ATP was added to a T_M = 59 °C.

Interestingly, substrate supplementation restored thermal stability for both V133F (Fig. 21B, Appendix 6) and V155G (Fig. 21C, Appendix 7) to wild-type levels. For V133F, thermal stability was initially most drastically reduced by 11 °C compared to wild-type HARS with a T_M = 52 °C. The addition of tRNA slightly but significantly increased

thermal stability at lower tRNA concentrations, but at a high tRNA concentration restored thermal stability to above wild-type levels ($T_M=68$ °C), indicating that tRNA binding can rescue the mutant HARS thermal lability. Similarly, high ATP concentrations increased the thermal stability of HARS V133F to wild-type levels (to $T_M=62$ °C), while histidine addition had no effect on V133F. Thermal stability of V155F was reduced compared to wild-type (reduced by 3 °C), and all substrate supplementations restored wild-type like levels of protein stability (Fig 21C, Appendix 7). The thermal shift assay demonstrates that mutants V133F and Y454S are significantly less thermodynamically stable than hsHARS, and V155G is only slightly reduced and easily restored in stability. Y454S protein instability can be rescued directly by histidine supplementation, whereas V133F protein stability was rescued by high tRNA or ATP concentrations.

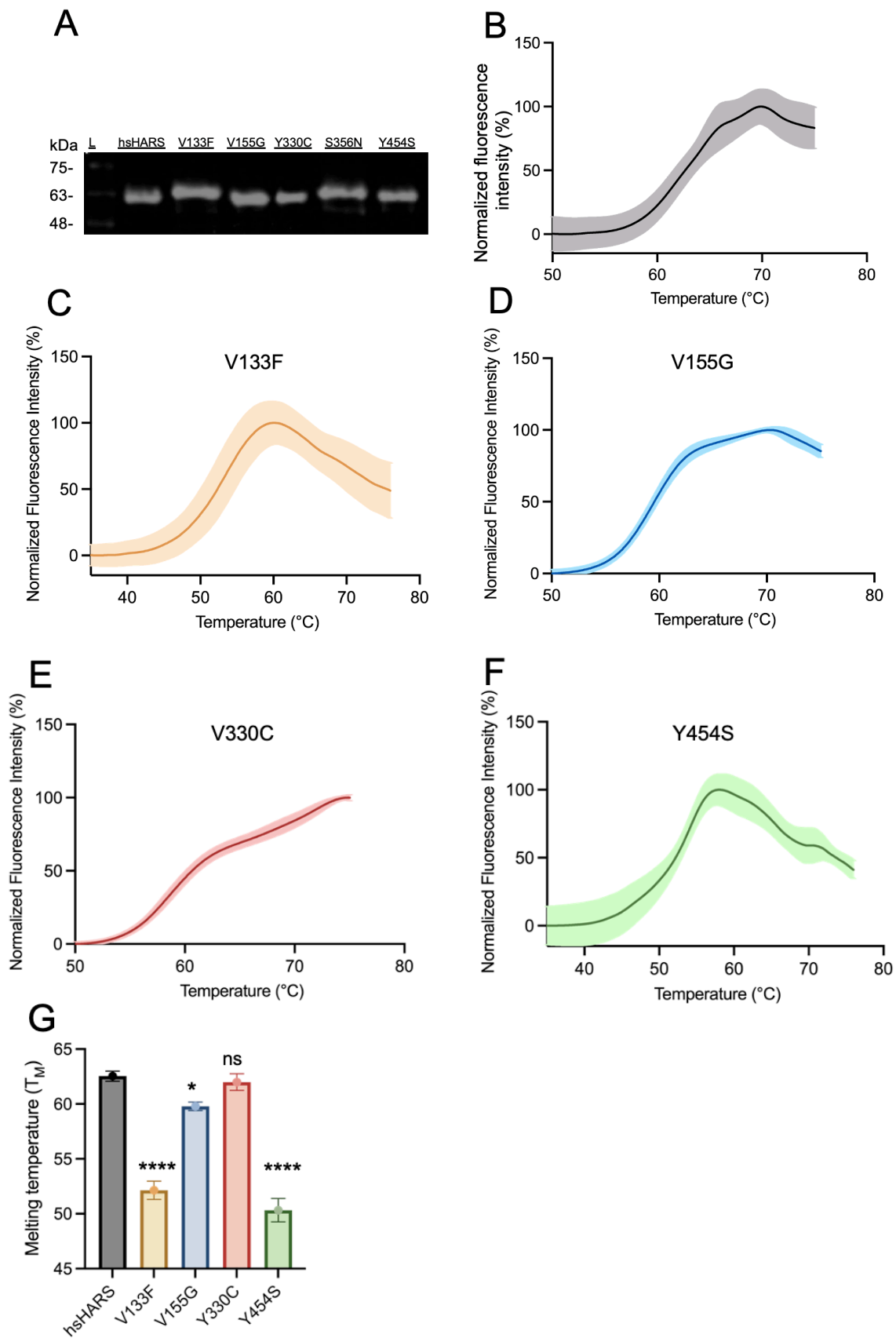


Figure 20. HARS thermal shift assay and melting temperature curves. (A) Western blot of wildtype (hsHARS) and mutant HARS proteins. HARS protein were purified from *E. coli* using Ni²⁺ affinity chromatography. Purified hsHARS, V133F, V155G, Y330C, S356N and Y454S HARS were separated by SDS-PAGE and transferred to PVDF membrane. Proteins were blotted using anti-6xHis primary antibodies. First lane is the protein ladder (L) with labelled molecular weights. Expected mass of 6x-His tagged HARS is 58 kDa. Melting curve of (B) hsHARS, (C) V133F, (D) V155G, (E) Y330C, and (F) Y454S. HARS protein samples were prepared with final concentration 1 μ M in 96-plates for DSF. All samples performed in 4 replicates. Samples were heated from 25 °C to 96 °C at 1 °C per minute and fluorescence intensity was measured. Standard error of each data point represented by lighter-colored error bars. (G) Melting temperature (T_M) of HARS variants in apo form show reduced stability of V133F, V155G and Y454S. Initial analysis was performed in the Protein Thermal Shift software and data was fit to the Boltzmann equation to estimate the T_M . Bars indicate the mean of 4 replicates \pm the standard error. Significance levels are indicated using asterisks (**** p <0.0001, ** p <0.01, * p <0.05, ns = statistically non-significant).

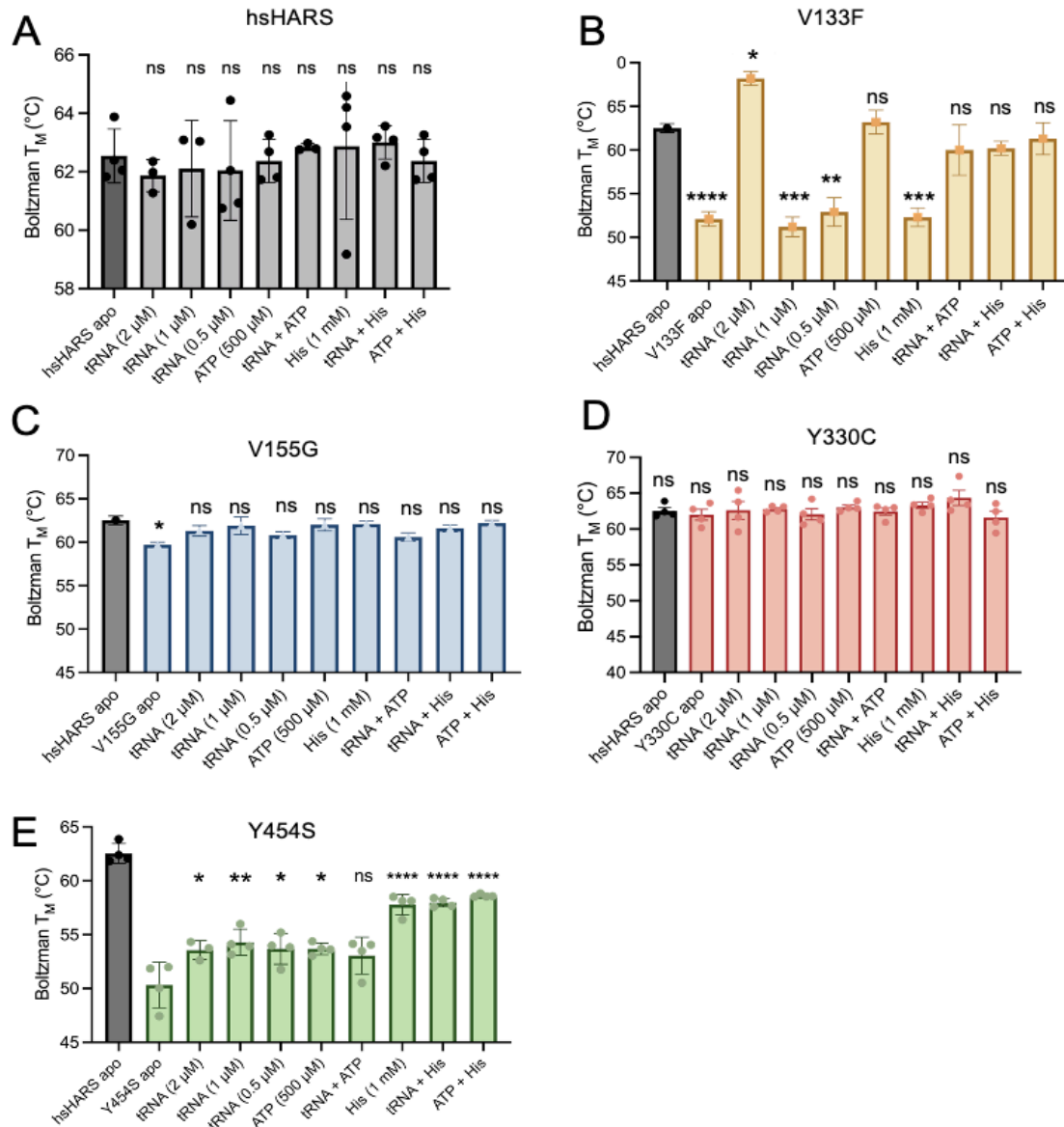


Figure 21. Recombinant protein mutants V133F and V155G lead to reduced protein stability, which can be rescued by substrate supplementation. T_M of (A) hsHARS, (B) V133F, (C) V155G, (D) Y330C, and (E) Y454S variants with substrate supplementation. Protein variants were incubated with either 2 μ M, 1 μ M, or 0.5 μ M of tRNA^{His}, 1 mM histidine or 500 μ M ATP either on their own, in combination with each other, or with 2 μ M tRNA^{His}. (**** p <0.0001, *** p <0.001, ** p <0.01, * p <0.05, ns = statistically non-significant).

3.7 Histidine supplementation rescues HARS V155G and S356N growth defects and prevents accumulation of insoluble proteins

To investigate whether histidine substrate supplementation can rescue the growth defect in the yeast model, we performed growth curve analyses of wild-type hsHARS and mutant HARS under amino acid stress by increasing media concentrations of histidine from 20 mg/L to 200 mg/L (Fig. 22A) or by reducing histidine levels in the growth media (Fig. 22B) to 2 mg/L. Neither high nor low histidine growth conditions had a significant impact on yeast cells expressing wild-type hsHARS (Fig. 22A-C, Table 4).

The four CMT2W associated mutants display two distinct phenotypes in response to the increased histidine concentration in the media. While all CMT2W associated mutants show a significant increase in doubling time by 1.2-1.3-fold compared to wild-type hsHARS under normal SD Leu(-) growth conditions with 20 mg/L histidine (Fig. 16), this growth defect is amplified for the Y330C mutant when supplemented with histidine (Table 4, Fig. 22A,C). Cells expressing HARS Y330C showed an increased doubling time by 1.4-fold compared to normal histidine conditions. For mutants V155G and S356N, on the other hand, histidine supplementation showed a significant rescue effect and doubling times for cells expressing these variants at high histidine conditions were not significantly different from wild-type hsHARS (Table 4, Fig. 22C). Cells expressing HARS V133F were not sensitive to increased histidine concentrations.

We next tested the effect of decreased histidine conditions on growth for the CMT2W associated mutants. Low histidine concentrations had no effect on wild-type or S356N expressing cells, while the three other mutants, V133F, V155G and Y330C showed increased doubling times by ~1.5-fold (Fig. 22C). These results show that histidine supplementation can rescue the growth defect of HARS variants V155G and S356N, while conversely, histidine supplementation is toxic to Y330C expressing cells, suggesting that not all disease-causing HARS alleles will benefit from histidine supplementation.

To assess whether histidine supplementation resolves the accumulation of insoluble proteins in V155G and S356N mutants, we performed sedimentation assays using cells

grown under high histidine and low histidine growth conditions (Fig. 24). Wildtype hsHARS expressing cells showed no change in insoluble protein accumulation (Figs. 22E). For both V155G and S356N mutants, insoluble protein accumulation was rescued to wild-type levels under high histidine conditions, but not low histidine conditions, reflecting the rescued growth phenotype upon histidine supplementation. Interestingly, both increased and decreased histidine led to an increase of insoluble proteins in both V133F and Y330C mutants (Fig. 20E).

We and others show that Y454S reduces thermal stability, and the symptoms of USH3B HARS-related disease are exacerbated during febrile episodes (46). We therefore grew hsHARS and Y454S expressing yeast cells at elevated temperatures of 40 °C, in low and high histidine conditions. Both Y454S and hsHARS carrying cells showed a generally decreased growth at 40 °C (Fig. 23). Increased histidine concentrations in the media did lead to slightly increased lag phase for both hsHARS and Y454S, but no significant increase in doubling time was observed for either strain (Figs. 22D, 23C). On the other hand, decreased histidine availability led to a similar and significant decrease of growth in both strains, indicating that reduced histidine availability is disadvantageous under heat stress conditions (Figs. 22D, 23D). Overall, the Y454S mutation does not significantly increase doubling times compared to wild-type hsHARS at 30 °C or 40 °C and does not lead to protein accumulation in the insoluble protein fraction (Fig. 22D, 18C).

Table 4. Doubling time of yeast grown in high histidine and low histidine SD Leu(-) conditions. (****p<0.0001, ***p<0.001, **p<0.01, *p<0.05, ns = statistically non-significant).

	High His			Low His		
	Doubling time (mins)	Fold change to hsHARS	Significance compared to hsHARS	Low His	Fold change to hsHARS	Significance compared to hsHARS
<i>hsHARS</i>	285 ± 3	-	-	350 ± 13	-	-
	292 ± 3	-	-	340 ± 13	-	-
	285 ± 3	-	-	320 ± 13	-	-
V133F	382 ± 9	1.3	****	610 ± 63	1.7	****
	367 ± 9	1.2	****	470 ± 63	1.4	****
	389 ± 9	1.4	****	600 ± 63	1.9	****
V155G	286 ± 4	1.0	ns	514 ± 4	1.5	***
	296 ± 4	1.0	ns	508 ± 4	1.5	***
	290 ± 4	1.0	ns	518 ± 4	1.6	***
Y330C	390 ± 17	1.4	****	450 ± 15	1.3	**
	420 ± 17	1.4	****	480 ± 15	1.4	**
	430 ± 17	1.5	****	490 ± 15	1.5	**
S356N	300 ± 15	1.0	ns	450 ± 8	1.3	*
	290 ± 15	1.0	ns	435 ± 8	1.3	*
	320 ± 15	1.1	ns	452 ± 8	1.4	*

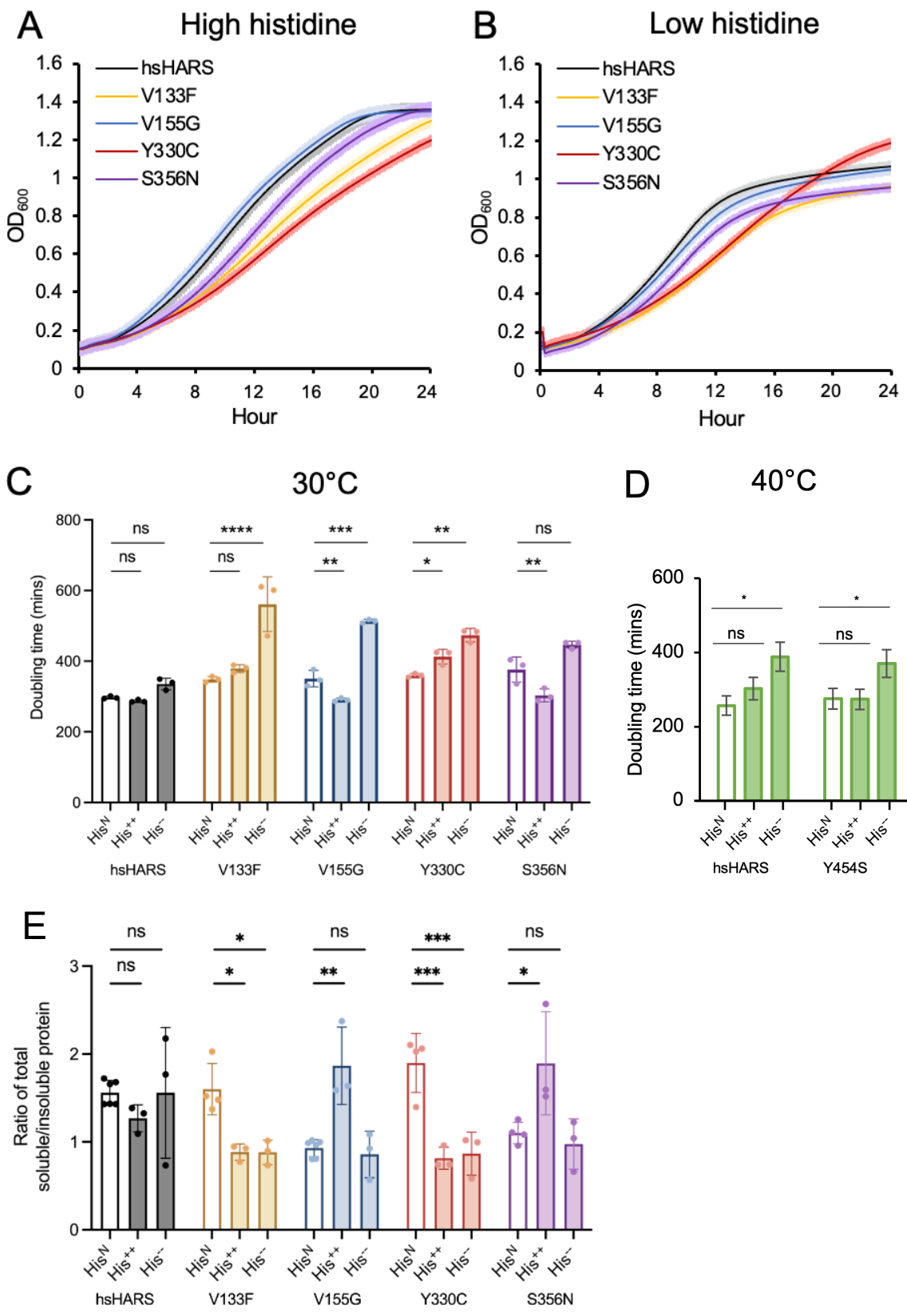


Figure 22. Histidine supplementation rescues V155G and S356N mutants' growth deficiency and protein aggregation. Growth curve of yeast grown in (A) high histidine and (B) low histidine SD Leu(-) media. Yeast cultures were incubated in Synergy-H1 plate reader (BioTek) for 24 hours in 30 °C with 10-min read intervals using 3 biological replicates and 3 technical replicates per biological. For His⁺⁺, histidine was supplemented to a final concentration of (200 mg/L) in SD Leu(-). For His⁻, histidine was reduced to 2 mg/L. Normal SD Leu (-) growth media contains 20 mg/L histidine. One standard deviation of each data point represented by lighter-coloured error bars. Comparison of doubling time in high histidine (His⁺⁺) and low histidine (His⁻) to normal histidine (His^N) conditions for (C) CMT mutants and (D) Y454S mutant. Doubling time obtained by calculating the slope of the exponential phase of the growth curve, and using the equation, doubling time = (log(2))/slope. (E) Ratio of soluble to insoluble protein fraction from a sedimentation assay for hsHARS and CMT mutant expressing cells grown under high and low histidine conditions. First lane (L) is the protein ladder. Equal volumes of whole lysate (W), soluble fraction (S) and insoluble fraction (P) portions extracted from different yeast variants in the sedimentation assay was loaded on to 15% SDS gel in 3 replicates. A lower ratio represents a higher proportion of insoluble fraction compared to soluble fraction. (****p<0.0001, ***p<0.001, **p<0.01, *p<0.05, ns = statistically non-significant).

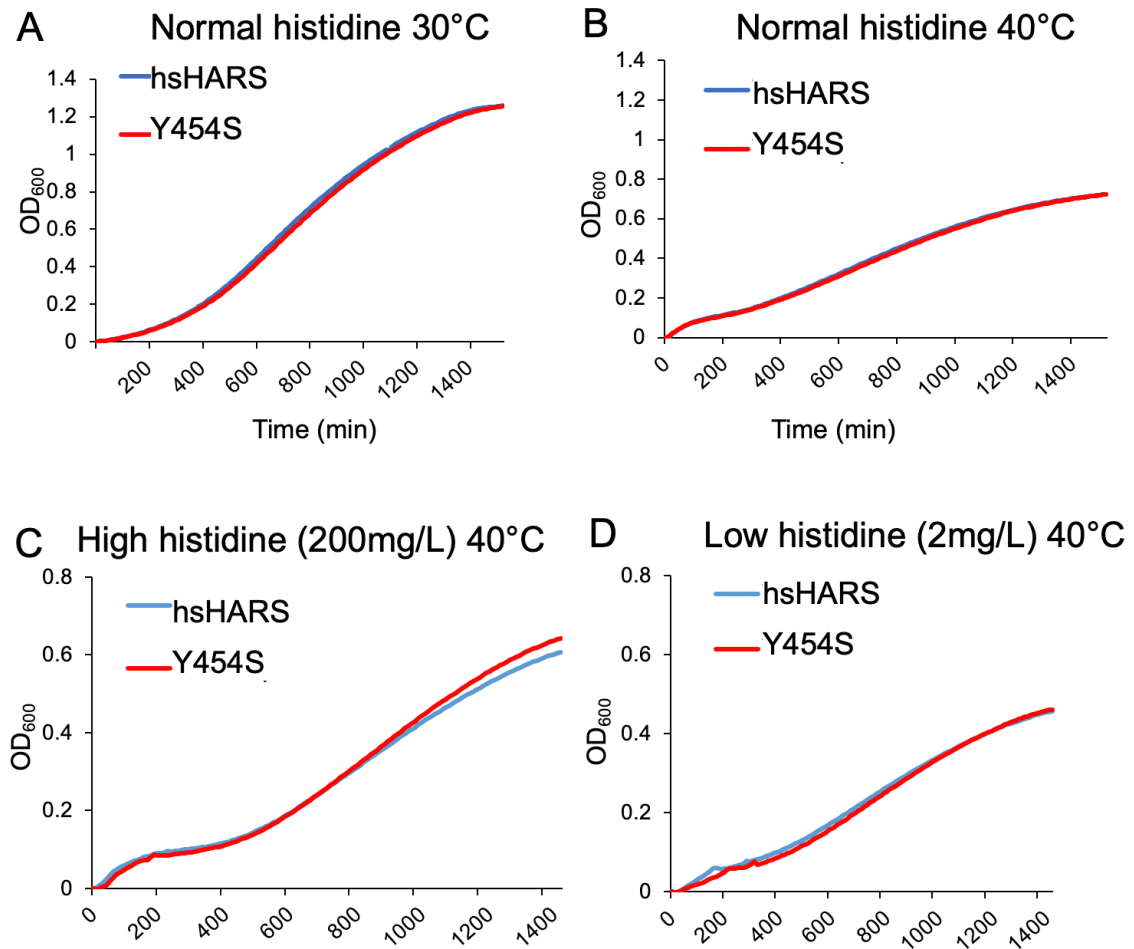


Figure 23. Growth curves of Y454S with temperature and histidine treatment. Y454S mutant was grown in Synergy-H1 plate reader (BioTek) for 24 hours in 30 °C with (A) normal high and (C) high histidine, or in 40 °C with (B) normal or (D) low histidine. For high histidine, histidine was supplemented to a final concentration of (200 mg/L) in SD Leu(-). For low histidine, histidine was reduced to 2 mg/L. Normal growth media SD Leu(-) contains 20 mg/L histidine.

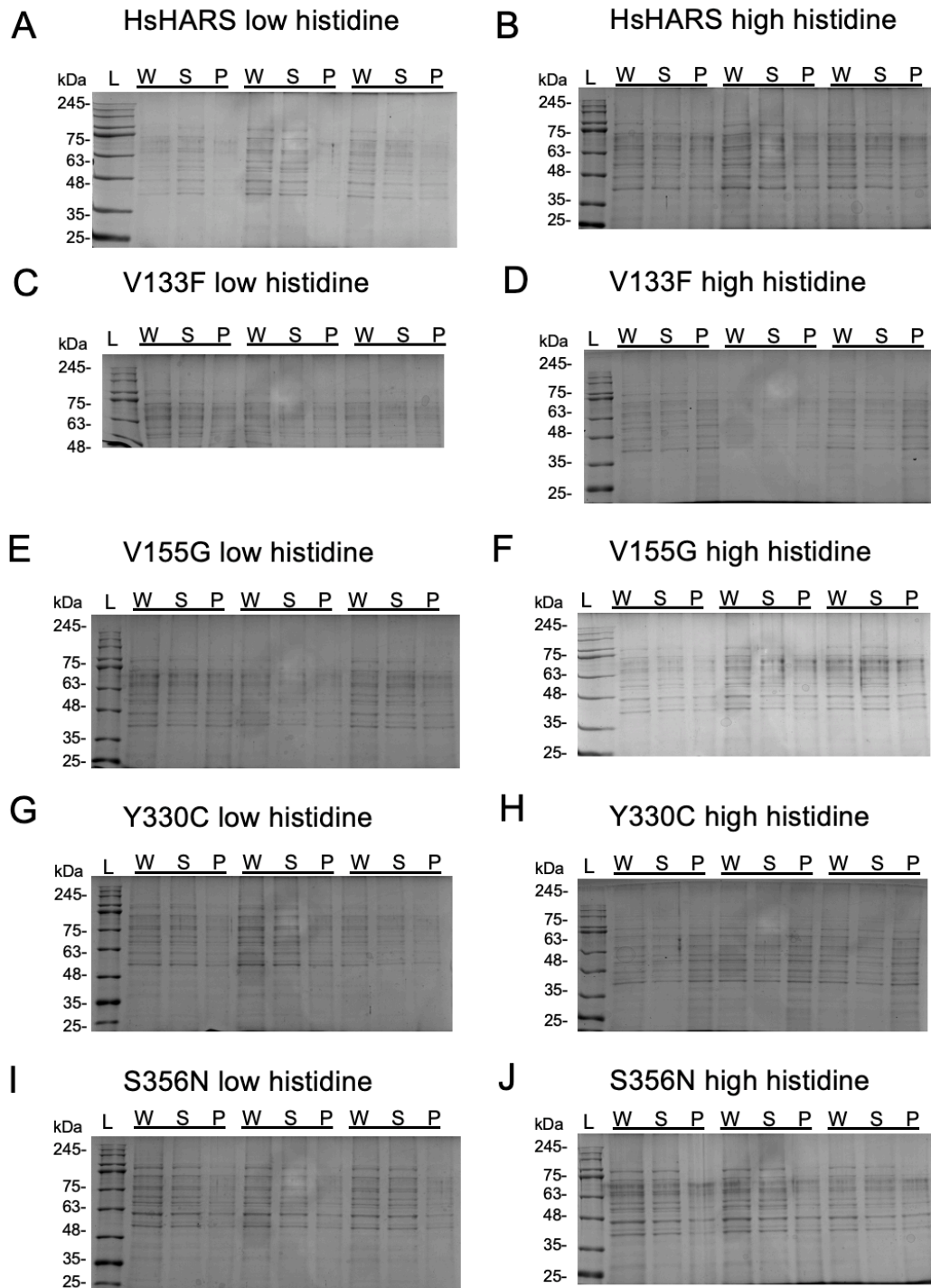
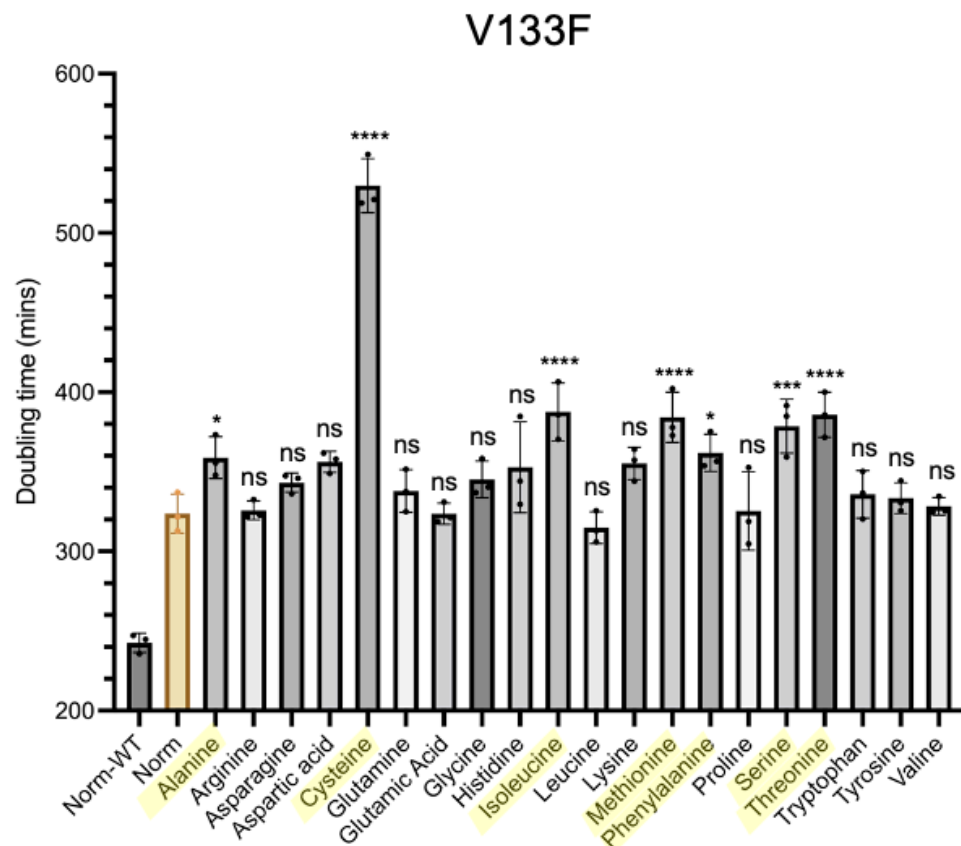
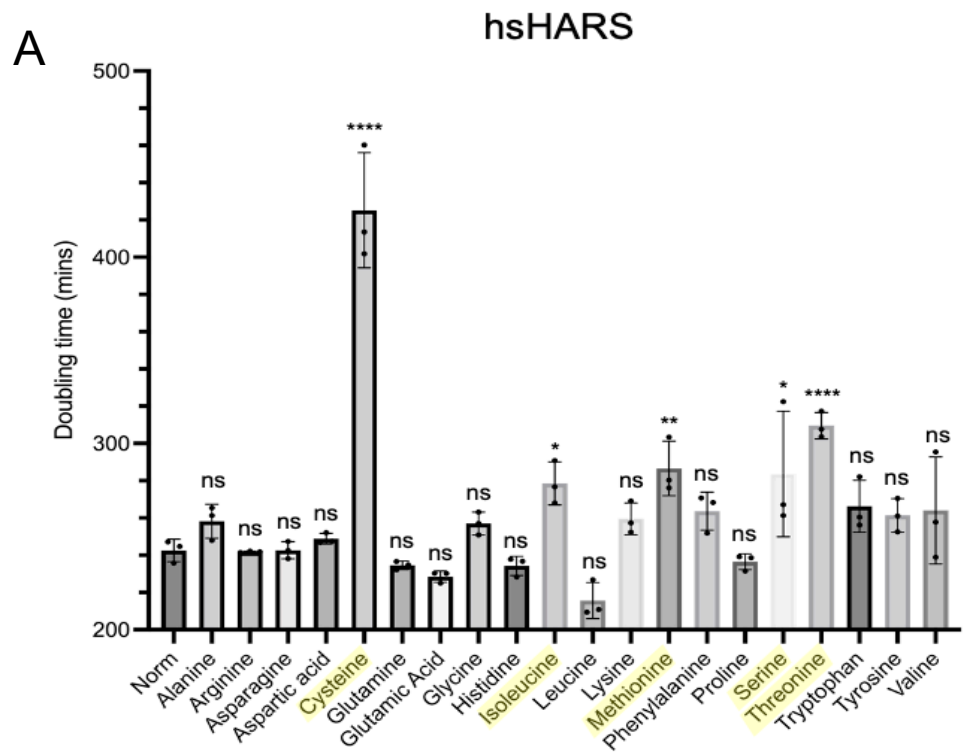
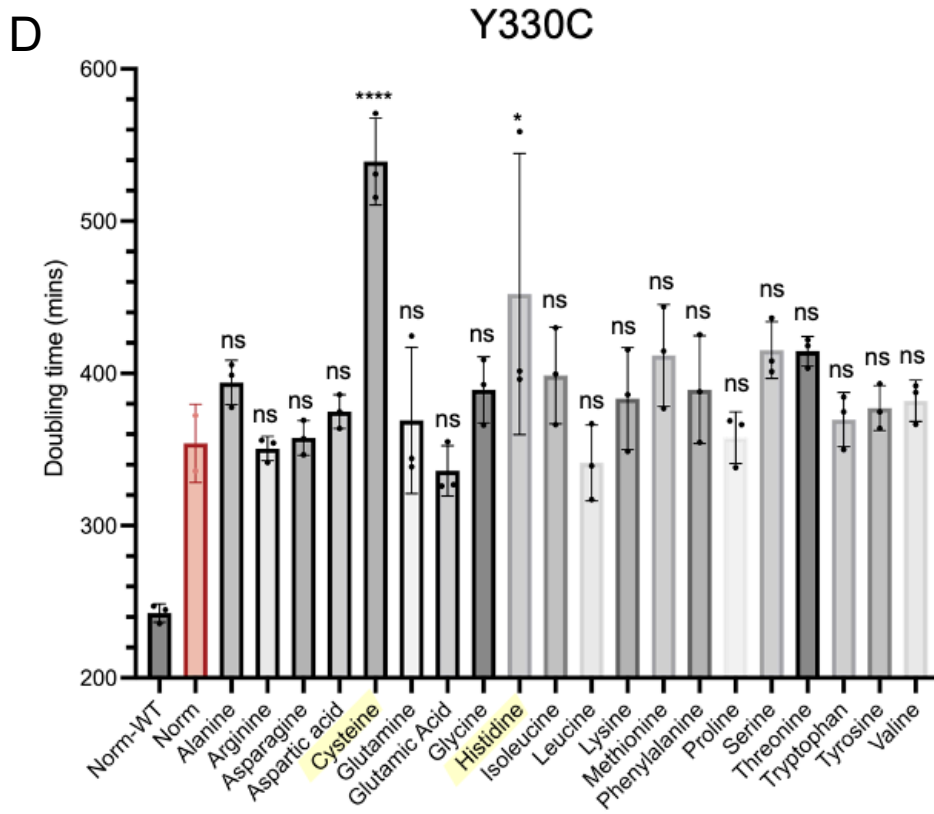
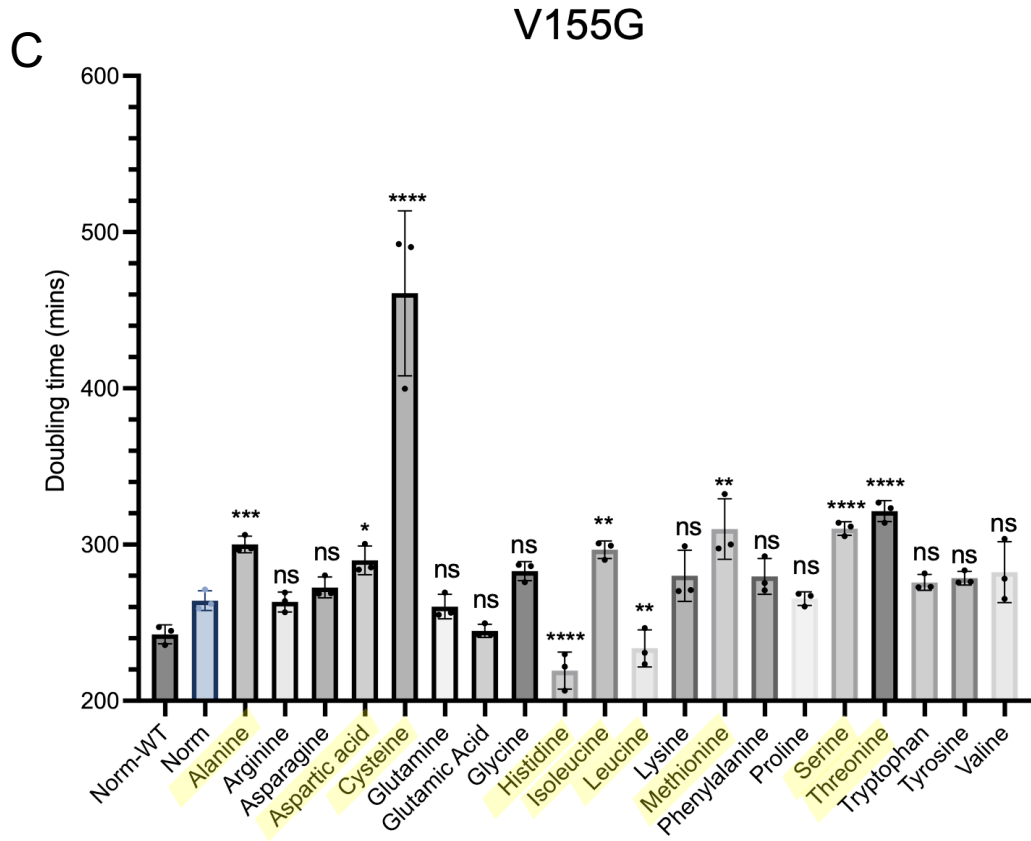


Figure 24. Sedimentation assay gels after histidine treatment. Sedimentation assay gels for hsHARS and CMT-HARS mutants in high or low histidine SD Leu(-) conditions. First lane is the protein ladder (FroggaBio) with labelled molecular weights. Equal volumes of whole lysate (W), soluble fraction (S) and insoluble fraction (P) extracted from different yeast variants in the sedimentation assay was loaded on to 15% SDS gel in 3 replicates. Gels imaged using the Gel Doc XR+ (Biorad). Gels were quantified using ImageJ.

3.8 Growth phenotype characterization under supplementation with all 20 amino acids

To investigate whether any of the remaining proteinogenic amino acids apart from histidine lead to a growth phenotype difference in the CMT-HARS mutants, we performed growth curve analysis while supplementing the growth media with all 20 amino acids separately. If a specific amino acid exacerbates the doubling time of the CMT-HARS mutant, it suggests that HARS could be mis-aminoacylating that particular amino acid leading to mistranslation of that amino acid at histidine codons. In hsHARS, cysteine, isoleucine, methionine, serine and threonine (5 baseline stressors) supplementation led to significantly increased doubling time compared to normal conditions (Fig. 25A). Cysteine is particularly toxic to the yeast cells, leading to 1.7-fold increase in doubling time, consistent with previous findings that extracellular cysteine inhibits yeast cell growth in a dose-dependent manner (81). Leucine had a rescuing effect on all strains, which was expected since the absence of leucine was used in our SD media to select for the p425 plasmids. In the V133F mutant, alanine and phenylalanine also further stressed the cells, along with the 5 baseline stressors (Fig. 25B). In the V155G mutant, alanine and aspartic acid significantly stressed the cells in addition to the 5 baseline stressors (Fig. 25C). Histidine rescued the growth as demonstrated previously. In the Y330C mutant, only cysteine and histidine significantly increased doubling time, and there is no longer a significant difference in doubling time when supplemented with isoleucine, methionine, serine and threonine (Fig. 25D). Finally, for the S356N mutant, a significant increase in doubling time was found in cysteine, isoleucine, methionine, and threonine, while histidine expectedly rescued this mutant's growth (Fig. 25E). Figure 26 shows a heat map visualization of the fold change in doubling times across all amino acid treatments compared to normal growth conditions for all yeast strains. Doubling times are summarized in Appendix 8.





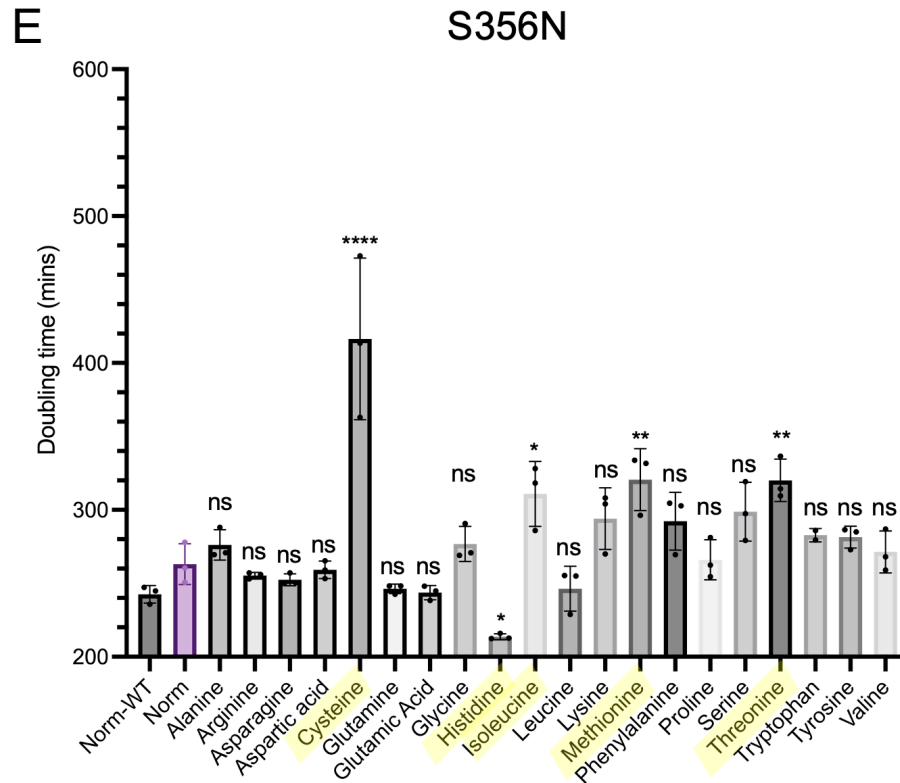


Figure 25. Doubling time of HARS variants supplemented with all 20 amino acids. Growth curves and doubling times were obtained for (A) hsHARS, (B) V133F, (C) V155G, (D) Y330C, and (E) S356N while supplementing with 200 mg/L amino acids. Yellow highlights amino acids that are significantly different from the Norm. Norm-WT is the doubling time of hsHARS in SD Leu(-). Norm is the doubling time for each mutant in SD Leu(-). (**** $p < 0.0001$, *** $p < 0.001$, ** $p < 0.01$, * $p < 0.05$, ns = statistically non-significant).

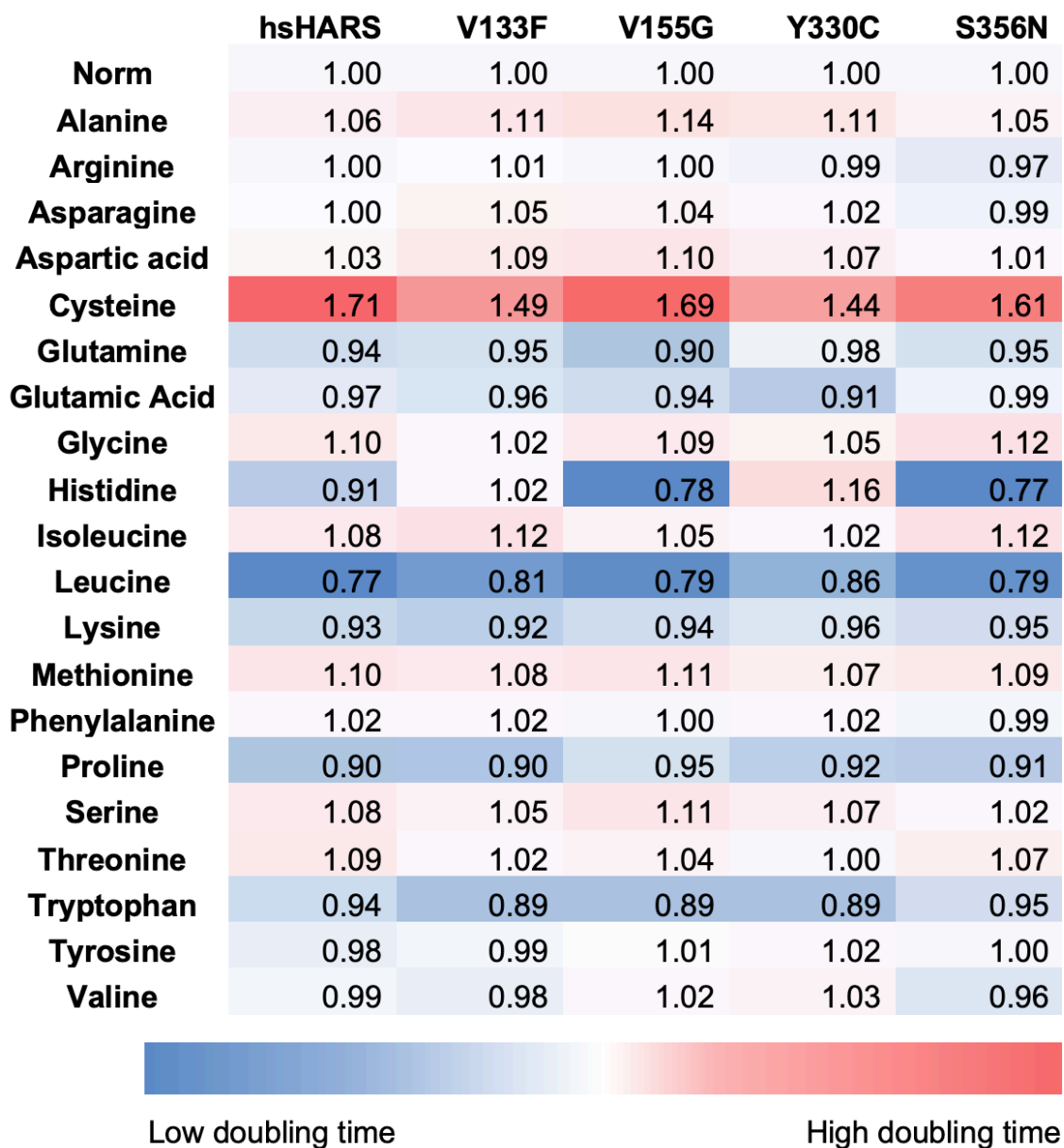


Figure 26. Heat map visualization of fold change of doubling times from amino acids supplementation. Fold change in doubling times comparing amino acid-supplemented conditions to normal SD Leu(-)conditions for hsHARS and CMT-HARS. Blue represents low fold change in doubling time and red represents high fold change in doubling time.

3.9 Growth phenotype characterization under chemical stress

Some major stressors of *S. cerevisiae* and their stress-inducing mechanisms are outlined in Table 3. To investigate whether these chemical stressors will lead to a phenotypic growth difference in the CMT-HARS mutants, growth curves were performed by adding EtOH, AZC, H₂O₂ or hydroxyurea to the growth media and doubling times were calculated (Appendix 9). If a CMT-HARS mutant shows synthetic toxicity towards a particular chemical stressor but the same chemical has no or little effect on hsHARS, it could provide insight on the stress-inducing mechanism of the mutation.

The ratio of doubling time in the chemical stress condition versus doubling time in the normal condition was obtained (Fig. 27). A ratio larger than one means increased doubling time in the stress condition, while higher ratios correspond to more defective growth. All chemical stressors increased the doubling time for hsHARS and CMT-HARS mutants. Interestingly, mutants were either not significantly different or had a lower ratio compared to hsHARS, therefore no synthetic toxicity was observed.

Ethanol induces growth and viability defects on yeast cells (67). Yeast can also induce the production of heat shock proteins to reduce protein aggregation during ethanol stress. Under ethanol stress, growth for V155G and S356N were not as affected as hsHARS, while V133F and Y330C were affected by the same level as hsHARS (Fig. 27A).

Next, I tested the effect of AZC, which competes with its analog proline, causing misincorporation of AZC instead of proline, leading to defective protein production and proteotoxic stress (65). AZC drastically affected all yeast strains by increasing the doubling time around 6-fold (Fig. 27B). Interestingly, V133F and Y330C mutants were not as affected by AZC as hsHARS, while V155G and S356N mutants were affected by the same level as hsHARS.

Next, I tested the yeast strains' response to oxidative stress by exposing cells to H₂O₂. Under H₂O₂ stress, only the Y330C mutant was significantly less affected compared to hsHARS (Fig. 27C).

Finally, I tested the effect of hydroxyurea on the yeast strains. Hydroxyurea is a potent inhibitor of ribonucleotide reductase that catalyzes the formation of deoxyribonucleotides from ribonucleotides, leading to DNA replication arrest (69). Hydroxyurea affected all yeast strains the same as no mutant was particularly sensitive to it compared to hsHARS (Fig. 27D).

Overall, no synthetic toxicity of the tested chemical stressors was observed in combination for any of the HARS mutants, and some mutants exhibited a protective function towards chemical stressors.

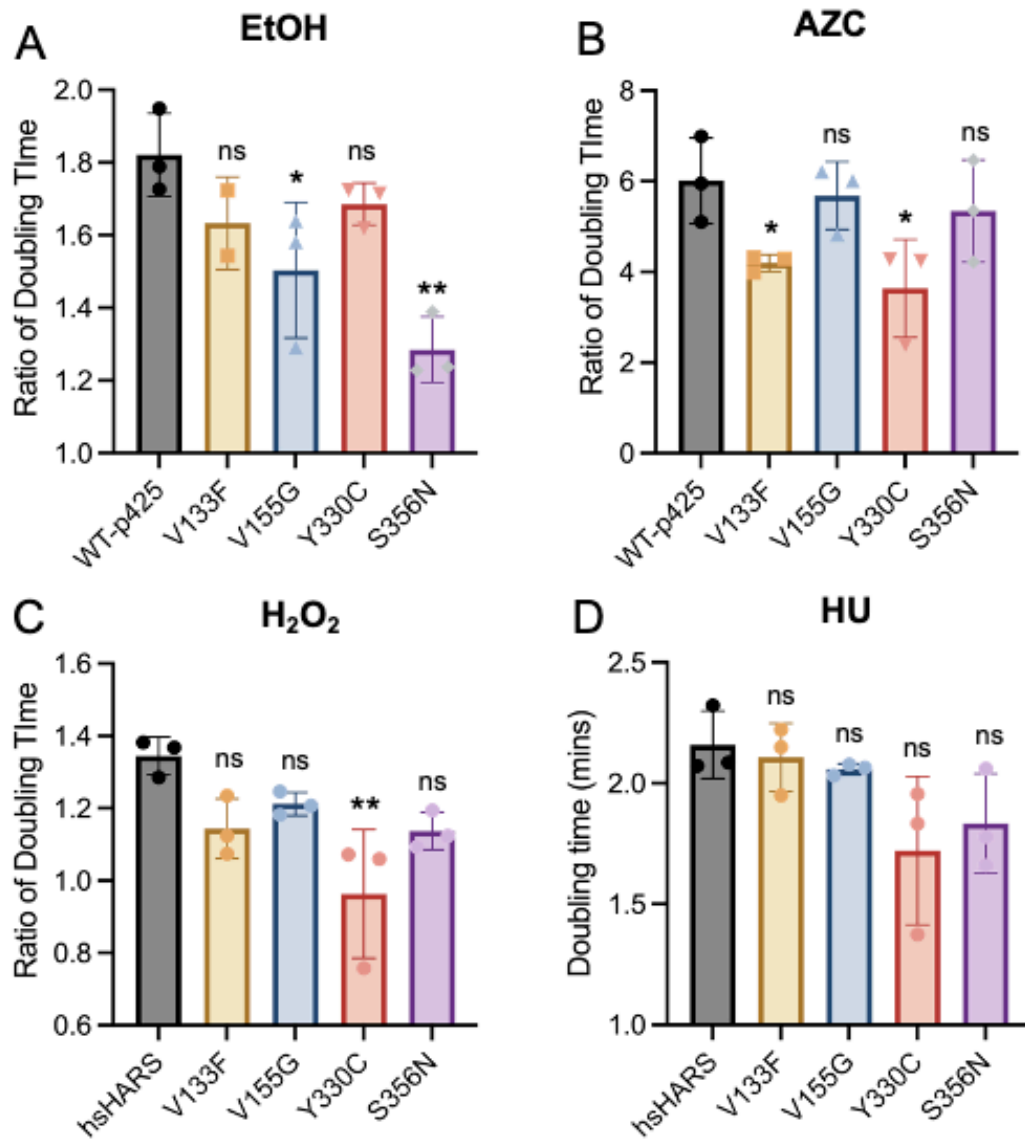


Figure 27. Chemical stress on hsHARS and CMT-HARS. Ratio of doubling time of chemically-supplemented SD Leu (-) growth condition over doubling time of normal SD Leu(-) growth condition is shown for (A) ethanol, (B) AZC, (C) H₂O₂, and (D) hydroxyurea stress. Final concentration for chemical stressors are AZC (0.5 mM), ethanol (4 %), H₂O₂ (100 μM), and hydroxyurea (200 mM). (****p<0.0001, ***p<0.001, **p<0.01, *p<0.05, ns = statistically non-significant).

Chapter 4

4 Discussion

Mutations in ARSs are often associated with diseases of the peripheral nervous system (PNS) (17). Several disease-causing HARS mutants were previously biochemically characterized. Mutations T132I, P134H, D175E, V244C, L305dup and D364Y confer partial or complete loss of function in yeast (40), Y454S confers thermal lability in recombinant protein (43), while T132I, P134H, D175E lead to deficits in structural integrity of the HARS protein (23). In patient derived samples, V133F leads to reduced aminoacylation activity (42) and Y454S leads to reduced histidine incorporation into the proteome (43). Mutations in other ARSs associated with peripheral neuropathy, however, retained wild-type like aminoacylation activity (53,85). It is unclear how and to what extent the loss of aminoacylation or stability in HARS cause diseases of the PNS, and no current cure or disease-specific treatment is available. Nutritional histidine supplementation is currently in a clinical trial for USH3B patients carrying a HARS Y454S mutation (ClinicalTrials.gov Identifier: NCT02924935). Since the impact of individual mutations on HARS function and disease progression are multifaceted and the disease-causing mechanism of each HARS mutant is not well understood, this apparently simple therapy may not work for all mutants.

To investigate the impact of histidine on pathological HARS variants in a cellular context, I designed a *S. cerevisiae* model system for CMT2W to study the impact of pathological HARS mutations on protein stability, the cellular proteome, and cell viability. I phenotypically and biochemically characterized four HARS mutants associated with CMT2W (V133F, V155G, Y330C and S356N), as well as the USH3B associated mutation Y454S. In previous attempts to generate a yeast model system, mutations V155G, Y330C, and S356N failed to complement the deletion of yeast HARS ortholog HTS1 (41). I found that wild-type and mutant hsHARS are all able to complement the deletion of yeast HARS homolog HTS1. In agreement with previous studies, mutant HARS variants were unable to complement cells lacking HTS1 with low copy plasmids, but in higher copy number episomal plasmids, each of the mutant HARS enable cell growth and viability. Thus, while the mutations impact HARS functionality in yeast, sufficient aminoacylation activity is

retained for survival. Although V133F, V155G, Y330C and S356N were all located in the hsHARS active site, the mutants lead to different phenotypic responses in cells. My data suggests that the mutants can be divided into two sub-categories: V133F and Y330C mutations largely display a loss of aminoacylation, affecting cell growth. On the other hand, V155G and S356N mutations exhibit a gain-of-function effect, leading to global accumulation of insoluble proteins.

4.1 HARS V133F and Y330C are loss-of-function mutations

The CMT2W variant V133F was discovered in a single patient (42) and is linked to cognitive deficits and peripheral neuropathy. V133 is strictly conserved in eukaryotes, and the V133F mutant is associated with reduced aminoacylation activity in dermal fibroblasts, but overall protein synthesis and growth remains intact (42). Our data shows that V133F significantly reduced HARS thermal stability, which was rescued by either tRNA or ATP binding, but not histidine. The Y330C mutation is localized opposite to V133F in the active site of HARS, and both amino acids coordinate the R-group of the histidine substrate (Fig. 1B). Y330C was identified in a cohort of patients (41) with autosomal dominant CMT disease. Recombinant Y330C shows reduced aminoacylation activity (41) and expression of Y330C in zebrafish disrupted the structure and function of the peripheral nervous system (45). My data show that the Y330C mutation does not significantly affect thermal stability of recombinant HARS protein, which is in line with a previous observation that HARS Y330C was stably expressed in rat pheochromocytoma cells (PC12) (45). Interestingly, I observed significantly reduced HARS abundance for both V133F and Y330C mutants in yeast cells. It is therefore likely that they lead to a loss-of-function disease phenotype, caused by reduced thermal stability (V133F) or loss of aminoacylation (Y330C).

Recent studies have demonstrated that CMT-HARS mutations impair global protein synthesis in *Drosophila* models (86), and exert toxic effects in the neurons by activating the integrated stress response (ISR) (45,87). ISR is the restoration of cellular homeostasis in eukaryotes in response to diverse stress signals. Four major stress signals activate four discrete kinases, all of which phosphorylate eukaryotic translation initiation factor 2 (eIF2 α) to initiate translation of ISR-specific mRNAs (88). The activation of ISR can be caused by mutations in ARS, as previously shown for the CMT-associated glycyl-tRNA

synthetase mutation C201R. Here, the mutant GARS enzyme binds tRNA^{Gly} but fails to release it, depleting the cellular tRNA^{Gly} pool, causing ribosome stalling on glycine codons and activating the ISR (87). Additionally, GARS deficiency activates ISR through the general control nonderepressible 2 (GCN2) regulator, which responds to ribosome stalling (89). Our data and published literature indicate that HARS V133F and Y330C mutants lead to reduced HARS stability and aminoacylation of tRNA^{His}, likely causing the accumulation of uncharged tRNA^{His} in the cells. The small valine to bulky phenylalanine (V133F) substitution in the active site near the histidine aromatic group leads to a drastic reduction of the active site binding pocket (Fig 1B), and likely leads to significantly reduced binding of histidine. The highly conserved aromatic tyrosine to small non-polar cysteine mutation (Y330C) disrupts amino acid binding, as Y330 is thought to lead to stabilization upon histidine binding (22). Elevated histidine concentrations are toxic to cells carrying these mutations, indicating increasing histidine does not rescue the phenotype by increasing His-tRNA^{His} formation. The toxicity may be due to mutant Y330C HARS misaminoacylating histidine onto non-cognate tRNAs leading to toxic mistranslation, but the exact mechanism remains unclear. I show that reduced histidine availability amplifies the mutant phenotype, likely leading to further decreased aminoacylation of tRNA^{His}. Uncharged tRNA in turn leads to growth arrest by inhibiting the initiation of protein synthesis in both human cells and yeast (90,91). Based on my data and these studies, it is likely that HARS V133F and Y330C mutants may also activate the ISR (Fig 28), which will be tested in future work.

I show that histidine supplementation or limitation in V133F and Y330C mutants does not rescue cell viability, but conversely, significantly reduced cell viability and increased doubling time. The role of elevated histidine in aggravating HARS deficiency remains to be elucidated, but for now excludes histidine supplementation as a potential treatment for patients with V133F and Y330C mutations. Balancing histidine requirements in Y330C or V133F mutation carrying CMT2W patients is therefore crucial to minimize the phenotypic effects of these pathogenetic HARS mutations.

4.2 HARS V155G and S356N disease variants de-regulate protein synthesis

Two HARS mutations, V155G and S356N were associated with autosomal dominant CMT disease with both enzymes displaying compromised aminoacylation activity *in vitro* (41). While our purified recombinant HARS S356N quickly aggregated, a previous study showed no significant reduction in thermal stability (41). Similarly, V155G was only slightly reduced in stability, and was rescued by histidine addition. Similar to studies in rat cells (45), I found HARS V155G is stably expressed in yeast. The V155G mutation was also studied in zebrafish, where V155G expression disrupts structure and function of the peripheral nervous system. My data shows that cells expressing either V155G or S356N showed reduced growth compared to wild-type expressing cells. Interestingly, I observed a significant increase in accumulation of insoluble proteins for both mutants, which indicates global protein misfolding and a significant impact of these HARS variants on protein homeostasis and translational fidelity. The global protein misfolding that I observed could be the cause for increased phosphorylation of eIF2 α , a marker of the integrated stress response that was observed in HARS V155G overexpressing PC12 cells (92).

A study on Threonyl-tRNA synthetase (TARS) mutants with reduced activity showed an increase in insoluble proteins, similar to our observations in cells expressing the HARS mutants. Accumulation of unfolded proteins leads to the activation of protein kinase RNA-like endoplasmic reticulum kinase (PERK) in mammalian cells, which in turn phosphorylates eIF2 α (Fig. 28). EIF2 α initiates production of activating transcription factor 4 (ATF4), which controls transcription of genes involved in protein degradation, translation, and autophagy (93). Our data indicate that HARS mutations V155G and S356N lead to the same kind of global response in the insoluble proteome. It is possible that the HARS mutants will cause endoplasmic reticulum (ER) stress, another one of the four major stress signals that induce ISR through the activation of PERK and will be investigated in mammalian cells in the future (Fig. 28) (94).

4.3 Rescuing HARS deficient V155G and S356N with histidine

There is currently no cure for CMT2W, yet histidine supplementation is a promising avenue for treatment of HARS-associated diseases. Excitingly, our data show both V155G and S356N leading to a growth defect likely caused by insoluble protein accumulation in yeast that can be rescued to wild-type levels by histidine supplementation. The mutations V155G and S356N are localized near the alpha carbon of the histidine substrate in the HARS active site (Fig. 8). Mutation of valine to the smaller glycine (V155G) may reduce histidylating activity or potentially amino acid specificity by increasing the size of the amino acid binding site. In S356N, substitution of the small serine to the larger asparagine may impact the amino acid binding site conformation, but S356N has no effect on histidine binding (9). Our data show that a high copy plasmid is required to complement the yeast deletion strain with HARS mutants, yet wild-type hsHARS is sufficiently active to complement using a low copy plasmid, indicating reduced aminoacylation activity of the mutants. It is also possible that both mutations cause a loss of specificity, leading to mistranslation of other amino acids in response to improper folding. Such mistranslation leads to global impaired translational fidelity, production of mutated and misfolded proteins, and finally unfolded protein accumulation. The observed restoration of growth, and restoration of the proteome upon histidine supplementation shows that increased histidine outcompetes other amino acids in the active site of the mutant HARS proteins, leading to restored translational fidelity. In agreement with this data, low histidine concentrations increase the toxicity of V155G, perhaps as a result of mistranslation. These data indicate that V155G and S356N mutants lead to global mistranslation, which can be remedied by histidine supplementation.

4.4 HARS Y454S associated with USH3B is rescued by histidine *in vitro*

A HARS c.1361A>C mutant was first detected in USH3B patients from the Old Amish Order in Lancaster County in Pennsylvania and a separate patient in Ontario (46). Subsequent biochemical experiments revealed no significant loss of aminoacylation, tRNA^{His} binding, or dimerization of Y454S HARS. This HARS variant showed similar expression levels in fibroblast cells and similar intracellular localization compared to wild-type HARS (43,46). The pathogenicity of HARS Y454S is likely due to decreased thermal stability. A previous study showed that Y454S patient-derived fibroblast cells grown at elevated temperatures showed reduced protein synthesis compared to those of WT cells (43). Interestingly, I found that yeast cells expressing HARS Y454S did not show reduced growth compared to cells expressing wild-type hsHARS. As previously shown (43) and confirmed by our data, the Y454S mutant is less thermally stable than wild-type human HARS. I showed that the thermal instability of Y454S can be restored to almost wild-type levels by the addition of histidine, which provides a simple mechanism of action that supports histidine supplementation in USH3B patients. Consistent with the lack of a phenotype in yeast, no increase in protein misfolding was observed due to the Y454S mutation, and no significant growth defects were observed compared to cells expressing wild-type hsHARS under normal or conditions of histidine stress or deprivation.

The Y454S mutation is in the tRNA binding domain, at the catalytic domain interface. Y454S likely disrupts hydrogen bonding with catalytic domain residue E439, which may be the cause for the observed thermal instability. Rather than a loss of aminoacylation activity or histidine specificity, the HARS Y454S mutation may cause USH3B because of its thermal instability. The resulting loss of function and thermal instability can be rescued by histidine addition to facilitate efficient tRNA^{His} aminoacylation.

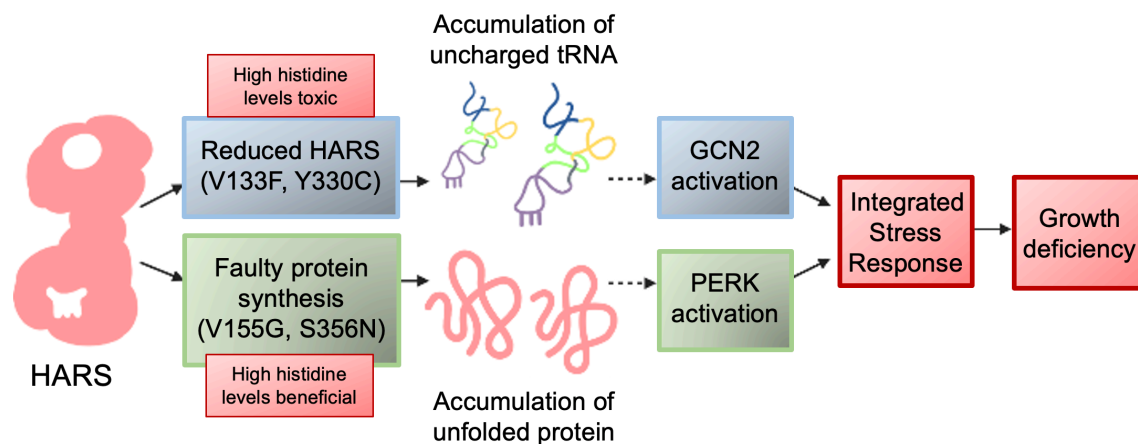


Figure 28. CMT2W associated mutations have different phenotypes. Mutants V133F and Y330C lead to reduced aminoacylation and accumulation of uncharged tRNA. Uncharged tRNAs activate GCN1 and the integrated stress response leading to growth deficiency. Histidine supplementation amplified the phenotype. Mutants V155G and S356N lead to reduced amino acid specificity, causing the accumulation of insoluble proteins. PERK activation triggers the integrated stress response, leading to growth deficiency. Histidine supplementation rescued this phenotype.

4.5 Chemical stress shows no synthetic toxicity

Chemical stressors ethanol, AZC, H₂O₂ and hydroxyurea did not lead to synthetic toxicity of the yeast strains, and interestingly impacted the growth of certain mutants significantly less than hsHARS. Ethanol stress affected the V155G and S356N mutations significantly less compared to hsHARS or the remaining mutants. The yeast cellular response to ethanol stress is the activation of heat shock proteins to suppress protein aggregation (67). It can be speculated that V155G and S356N mutants already have activated heat shock response as they already experience protein aggregation, therefore additional ethanol does not have much of an effect on them compared to the other mutants. However, future studies regarding heat shock proteins are necessary to validate this hypothesis. AZC is a non-proteinogenic competitive analog of proline, and therefore the incorporation of AZC in the proteome leads to mistranslation and proteotoxic stress (65). AZC affected the V133F and Y330C mutants significantly less compared to

hsHARS but not mutants V155G and S356N. It is possible that the V155G and S356N mutants already experience substantial mistranslation, so additional stress does not have as much of an effect on these mutants. Additionally, I speculate that the loss of function effects of V133F and Y330C prepared these mutants for reduced or slower rate of translation, therefore they are more equipped to handle AZC stress. Additional data are needed to elucidate the mechanism behind these speculations. Hydrogen peroxide is a reactive oxygen species that damages proteins and leads to ER stress (68). Y330C mutant was significantly less affected by H₂O₂, perhaps again due to the overlapping activation of stress response pathways. Further studies are necessary to evaluate the impact of peroxide stress on these mutants. Finally, hydroxyurea had no effect on the yeast strains, therefore the CMT-HARS mutants are likely not experiencing stress related to DNA replication (69).

4.6 CMT-HARS mutants are more sensitive to certain amino acid stress

Growth curve analysis performed under amino acid stress identifies certain amino acids that exacerbate the mutants' growth compared to hsHARS, and certain amino acids that rescue the mutant's growth compared to hsHARS (Table 5). Many amino acids had no effect on the growth phenotypes. As before, we show that histidine rescues V155G and S356N, but it exacerbates the effect of Y330C compared to hsHARS. Other amino acids listed shed light on potential codons of mistranslation, however further mass spectrometry data are necessary to validate mistranslation.

Table 5. Summary of effect of amino acid stress on CMT-HARS mutants.

	Exacerbate	Rescue or increased resistance to stress compared to hsHARS
V133F	Alanine Phenylalanine	N/A
V155G	Alanine Aspartic acid	Histidine Leucine
Y330C	Histidine	Isoleucine Methionine Serine Threonine
S356N	N/A	Histidine Serine

Chapter 5

5 Conclusions

5.1 Significance

The data are directly relevant to on-going clinical trials. Currently, L-histidine oral nutritional supplement to treat HARS deficiency in children with homozygous Y454S mutation is an approved clinical trial (NCT02924935) in phase 3. I developed a novel yeast model of CMT disease, which provided a rapid screening approach to evaluate human disease-causing HARS variants and determine the cellular and molecular consequences of histidine supplementation. This study demonstrates that histidine supplementation can rescue the growth deficiency in HARS with V155G and S356N mutations, further supporting histidine supplementation as an avenue of treatment for these particular HARS variants. On the other hand, Y330C displayed synthetic toxicity with histidine, excluding histidine supplementation as a treatment. Amino acid supplementation should therefore only be considered after careful examination of biochemical, cellular and organismal effects dependent on the disease-causing allele.

5.2 Future work

Future work involves the investigation of cellular pathways responsible for the growth phenotypes of the CMT-HARS mutants. To test whether the integrated stress response is activated in the CMT-HARS mutants, future work should see whether eIF2 α is activated by phosphorylation. To show if there is an accumulation of uncharged tRNA in the V133F and Y330C cells, acid gel northern blot can be performed to detect tRNA expression. To prove that mistranslation is occurring in the V155G and S356N mutants, mass spectroscopy can be performed by purifying YFP from the yeast cells and detecting misincorporation of amino acids at histidine codons or histidine in other amino acid codons. Furthermore, since tRNA^{His}_{Micro} was able to rescue the instability of HARS protein *in vitro*, future work can generate a system to overexpress tRNA_{His} *in vivo* in the yeast HARS disease model to see if there are any rescuing effects. Additionally, other CMT-associated HARS mutants can be tested in our yeast model to determine if they behave similarly to the mutants screened in this study. Finally, to validate the

significance of the current findings in the context of humans, histidine treatments and sedimentation assays can be performed in USH3B and CMT2W patient samples.

References

1. Crick, F. (1970) Central dogma of molecular biology. *Nature*, **227**, 561-563.
2. Clancy, S. (2008) DNA Transcription. *Nature Education*, **1**, 41.
3. Clancy, S. and Brown, W. (2008) Translation: DNA to mRNA to Protein. *Nature Education*, **1**, 101.
4. Ibba, M. and Soll, D. (2000) Aminoacyl-tRNA synthesis. *Annu Rev Biochem*, **69**, 617-650.
5. Kwon, N.H., Fox, P.L. and Kim, S. (2019) Aminoacyl-tRNA synthetases as therapeutic targets. *Nat Rev Drug Discov*, **18**, 629-650.
6. Turner, R.J., Lovato, M. and Schimmel, P. (2000) One of two genes encoding glycyl-tRNA synthetase in *Saccharomyces cerevisiae* provides mitochondrial and cytoplasmic functions. *J Biol Chem*, **275**, 27681-27688.
7. Tolkunova, E., Park, H., Xia, J., King, M.P. and Davidson, E. (2000) The human lysyl-tRNA synthetase gene encodes both the cytoplasmic and mitochondrial enzymes by means of an unusual alternative splicing of the primary transcript. *J Biol Chem*, **275**, 35063-35069.
8. Chang, C.Y., Chien, C.I., Chang, C.P., Lin, B.C. and Wang, C.C. (2016) A WHEP Domain Regulates the Dynamic Structure and Activity of *Caenorhabditis elegans* Glycyl-tRNA Synthetase. *J Biol Chem*, **291**, 16567-16575.
9. Nathanson, L. and Deutscher, M.P. (2000) Active aminoacyl-tRNA synthetases are present in nuclei as a high molecular weight multienzyme complex. *J Biol Chem*, **275**, 31559-31562.
10. Giege, R., Sissler, M. and Florentz, C. (1998) Universal rules and idiosyncratic features in tRNA identity. *Nucleic Acids Res*, **26**, 5017-5035.
11. Gile, G.H., Moog, D., Slamovits, C.H., Maier, U.G. and Archibald, J.M. (2015) Dual Organellar Targeting of Aminoacyl-tRNA Synthetases in Diatoms and Cryptophytes. *Genome Biol Evol*, **7**, 1728-1742.
12. Lant, J.T., Berg, M.D., Heinemann, I.U., Brandl, C.J. and O'Donoghue, P. (2019) Pathways to disease from natural variations in human cytoplasmic tRNAs. *J Biol Chem*, **294**, 5294-5308.
13. Guo, R.T., Chong, Y.E., Guo, M. and Yang, X.L. (2009) Crystal structures and biochemical analyses suggest a unique mechanism and role for human glycyl-tRNA synthetase in Ap4A homeostasis. *J Biol Chem*, **284**, 28968-28976.

14. Wakasugi, K., Slike, B.M., Hood, J., Ewalt, K.L., Cheresch, D.A. and Schimmel, P. (2002) Induction of angiogenesis by a fragment of human tyrosyl-tRNA synthetase. *J Biol Chem*, **277**, 20124-20126.
15. Kwon, N.H., Kang, T., Lee, J.Y., Kim, H.H., Kim, H.R., Hong, J., Oh, Y.S., Han, J.M., Ku, M.J., Lee, S.Y. *et al.* (2011) Dual role of methionyl-tRNA synthetase in the regulation of translation and tumor suppressor activity of aminoacyl-tRNA synthetase-interacting multifunctional protein-3. *Proc Natl Acad Sci U S A*, **108**, 19635-19640.
16. Howard, O.M., Dong, H.F., Yang, D., Raben, N., Nagaraju, K., Rosen, A., Casciola-Rosen, L., Hartlein, M., Kron, M., Yang, D. *et al.* (2002) Histidyl-tRNA synthetase and asparaginyl-tRNA synthetase, autoantigens in myositis, activate chemokine receptors on T lymphocytes and immature dendritic cells. *J Exp Med*, **196**, 781-791.
17. Boczonadi, V., Jennings, M.J. and Horvath, R. (2018) The role of tRNA synthetases in neurological and neuromuscular disorders. *FEBS Lett*, **592**, 703-717.
18. Grice, S.J., Sleigh, J.N., Motley, W.W., Liu, J.L., Burgess, R.W., Talbot, K. and Cader, M.Z. (2015) Dominant, toxic gain-of-function mutations in gars lead to non-cell autonomous neuropathology. *Hum Mol Genet*, **24**, 4397-4406.
19. Ognjenovic, J. and Simonovic, M. (2018) Human aminoacyl-tRNA synthetases in diseases of the nervous system. *RNA Biol*, **15**, 623-634.
20. Wasmuth, J.J. and Carlock, L.R. (1986) Chromosomal localization of human gene for histidyl-tRNA synthetase: clustering of genes encoding aminoacyl-tRNA synthetases on human chromosome 5. *Somat Cell Mol Genet*, **12**, 513-517.
21. Perona, J.J. and Gruic-Sovulj, I. (2014) Synthetic and editing mechanisms of aminoacyl-tRNA synthetases. *Top Curr Chem*, **344**, 1-41.
22. Koh, C.Y., Wetzel, A.B., de van der Schueren, W.J. and Hol, W.G. (2014) Comparison of histidine recognition in human and trypanosomatid histidyl-tRNA synthetases. *Biochimie*, **106**, 111-120.
23. Blocquel, D., Sun, L., Matuszek, Z., Li, S., Weber, T., Kuhle, B., Kooi, G., Wei, N., Baets, J., Pan, T. *et al.* (2019) CMT disease severity correlates with mutation-induced open conformation of histidyl-tRNA synthetase, not aminoacylation loss, in patient cells. *Proc Natl Acad Sci U S A*, **116**, 19440-19448.
24. Tian, Q., Wang, C., Liu, Y. and Xie, W. (2015) Structural basis for recognition of G-1-containing tRNA by histidyl-tRNA synthetase. *Nucleic Acids Res*, **43**, 2980-2990.

25. Qiu, X., Janson, C.A., Blackburn, M.N., Chhohan, I.K., Hibbs, M. and Abdel-Meguid, S.S. (1999) Cooperative structural dynamics and a novel fidelity mechanism in histidyl-tRNA synthetases. *Biochemistry*, **38**, 12296-12304.
26. Rubio Gomez, M.A. and Ibba, M. (2020) Aminoacyl-tRNA synthetases. *RNA*, **26**, 910-936.
27. Arnez, J.G., Augustine, J.G., Moras, D. and Francklyn, C.S. (1997) The first step of aminoacylation at the atomic level in histidyl-tRNA synthetase. *Proc Natl Acad Sci U S A*, **94**, 7144-7149.
28. Arnez, J.G., Harris, D.C., Mitschler, A., Rees, B., Francklyn, C.S. and Moras, D. (1995) Crystal structure of histidyl-tRNA synthetase from *Escherichia coli* complexed with histidyl-adenylate. *EMBO J*, **14**, 4143-4155.
29. de Poupplana, L.R. and Kaguni, L.S. (2020) *Biology of Aminoacyl-tRNA Synthetases*. Elsevier Science.
30. Liu, H. and Gaudl, J.W. (2008) Substrate-assisted catalysis in the aminoacyl transfer mechanism of histidyl-tRNA synthetase: a density functional theory study. *J Phys Chem B*, **112**, 16874-16882.
31. Nameki, N., Asahara, H., Shimizu, M., Okada, N. and Himeno, H. (1995) Identity elements of *Saccharomyces cerevisiae* tRNA(His). *Nucleic Acids Res*, **23**, 389-394.
32. Heinemann, I.U., Nakamura, A., O'Donoghue, P., Eiler, D. and Soll, D. (2012) tRNA^{His}-guanylyltransferase establishes tRNA^{His} identity. *Nucleic Acids Res*, **40**, 333-344.
33. Rudinger, J., Florentz, C. and Giege, R. (1994) Histidylation by yeast HisRS of tRNA or tRNA-like structure relies on residues -1 and 73 but is dependent on the RNA context. *Nucleic Acids Res*, **22**, 5031-5037.
34. Himeno, H., Hasegawa, T., Ueda, T., Watanabe, K., Miura, K. and Shimizu, M. (1989) Role of the extra G-C pair at the end of the acceptor stem of tRNA(His) in aminoacylation. *Nucleic Acids Res*, **17**, 7855-7863.
35. Hawko, S.A. and Francklyn, C.S. (2001) Covariation of a specificity-determining structural motif in an aminoacyl-tRNA synthetase and a tRNA identity element. *Biochemistry*, **40**, 1930-1936.
36. Guth, E.C. and Francklyn, C.S. (2007) Kinetic discrimination of tRNA identity by the conserved motif 2 loop of a class II aminoacyl-tRNA synthetase. *Mol Cell*, **25**, 531-542.

37. Guth, E., Farris, M., Bovee, M. and Francklyn, C.S. (2009) Asymmetric amino acid activation by class II histidyl-tRNA synthetase from *Escherichia coli*. *J Biol Chem*, **284**, 20753-20762.
38. Guth, E., Connolly, S.H., Bovee, M. and Francklyn, C.S. (2005) A substrate-assisted concerted mechanism for aminoacylation by a class II aminoacyl-tRNA synthetase. *Biochemistry*, **44**, 3785-3794.
39. Vester, A., Velez-Ruiz, G., McLaughlin, H.M., Program, N.C.S., Lupski, J.R., Talbot, K., Vance, J.M., Zuchner, S., Roda, R.H., Fischbeck, K.H. *et al.* (2013) A loss-of-function variant in the human histidyl-tRNA synthetase (HARS) gene is neurotoxic in vivo. *Hum Mutat*, **34**, 191-199.
40. Safka Brozkova, D., Deconinck, T., Griffin, L.B., Ferbert, A., Haberlova, J., Mazanec, R., Lassuthova, P., Roth, C., Pilunthanakul, T., Rautenstrauss, B. *et al.* (2015) Loss of function mutations in HARS cause a spectrum of inherited peripheral neuropathies. *Brain*, **138**, 2161-2172.
41. Abbott, J.A., Meyer-Schuman, R., Lupo, V., Feely, S., Mademan, I., Oprescu, S.N., Griffin, L.B., Alberti, M.A., Casanovas, C., Aharoni, S. *et al.* (2018) Substrate interaction defects in histidyl-tRNA synthetase linked to dominant axonal peripheral neuropathy. *Hum Mutat*, **39**, 415-432.
42. Royer-Bertrand, B., Tsouni, P., Mullen, P., Campos Xavier, B., Mittaz Crettol, L., Lobrinus, A.J., Ghika, J., Baumgartner, M.R., Rivolta, C., Superti-Furga, A. *et al.* (2019) Peripheral neuropathy and cognitive impairment associated with a novel monoallelic HARS variant. *Ann Clin Transl Neurol*, **6**, 1072-1080.
43. Abbott, J.A., Guth, E., Kim, C., Regan, C., Siu, V.M., Rugar, C.A., Demeler, B., Francklyn, C.S. and Robey-Bond, S.M. (2017) The Usher Syndrome Type IIIB Histidyl-tRNA Synthetase Mutation Confers Temperature Sensitivity. *Biochemistry*, **56**, 3619-3631.
44. Pierce, S.B., Chisholm, K.M., Lynch, E.D., Lee, M.K., Walsh, T., Opitz, J.M., Li, W., Klevit, R.E. and King, M.C. (2011) Mutations in mitochondrial histidyl tRNA synthetase HARS2 cause ovarian dysgenesis and sensorineural hearing loss of Perrault syndrome. *Proc Natl Acad Sci U S A*, **108**, 6543-6548.
45. Mullen, P., Abbott, J.A., Wellman, T., Aktar, M., Fjeld, C., Demeler, B., Ebert, A.M. and Francklyn, C.S. (2021) Neuropathy-associated histidyl-tRNA synthetase variants attenuate protein synthesis in vitro and disrupt axon outgrowth in developing zebrafish. *FEBS J*, **288**, 142-159.
46. Puffenberger, E.G., Jinks, R.N., Sougnez, C., Cibulskis, K., Willert, R.A., Achilly, N.P., Cassidy, R.P., Fiorentini, C.J., Heiken, K.F., Lawrence, J.J. *et al.* (2012) Genetic mapping and exome sequencing identify variants associated with five novel diseases. *PLoS One*, **7**, e28936.

47. Boerkoel, C.F., Takashima, H., Garcia, C.A., Olney, R.K., Johnson, J., Berry, K., Russo, P., Kennedy, S., Teebi, A.S., Scavina, M. *et al.* (2002) Charcot-Marie-Tooth disease and related neuropathies: mutation distribution and genotype-phenotype correlation. *Ann Neurol*, **51**, 190-201.
48. Theadom, A., Roxburgh, R., MacAulay, E., O'Grady, G., Burns, J., Parmar, P., Jones, K., Rodrigues, M. and Impact, C.M.T.R.G. (2019) Prevalence of Charcot-Marie-Tooth disease across the lifespan: a population-based epidemiological study. *BMJ Open*, **9**, e029240.
49. Carter, G.T., Weiss, M.D., Han, J.J., Chance, P.F. and England, J.D. (2008) Charcot-Marie-Tooth disease. *Curr Treat Options Neurol*, **10**, 94-102.
50. Higuchi, Y. and Takashima, H. (2022) Clinical genetics of Charcot-Marie-Tooth disease. *J Hum Genet*.
51. Pareyson, D. and Marchesi, C. (2009) Diagnosis, natural history, and management of Charcot-Marie-Tooth disease. *Lancet Neurol*, **8**, 654-667.
52. Szigeti, K. and Lupski, J.R. (2009) Charcot-Marie-Tooth disease. *Eur J Hum Genet*, **17**, 703-710.
53. Jordanova, A., Irobi, J., Thomas, F.P., Van Dijck, P., Meerschaert, K., Dewil, M., Dierick, I., Jacobs, A., De Vriendt, E., Guerguelcheva, V. *et al.* (2006) Disrupted function and axonal distribution of mutant tyrosyl-tRNA synthetase in dominant intermediate Charcot-Marie-Tooth neuropathy. *Nat Genet*, **38**, 197-202.
54. Latour, P., Thauvin-Robinet, C., Baudalet-Mery, C., Soichot, P., Cusin, V., Faivre, L., Locatelli, M.C., Mayencon, M., Sarcey, A., Broussolle, E. *et al.* (2010) A major determinant for binding and aminoacylation of tRNA(Ala) in cytoplasmic Alanine-tRNA synthetase is mutated in dominant axonal Charcot-Marie-Tooth disease. *Am J Hum Genet*, **86**, 77-82.
55. Gonzalez, M., McLaughlin, H., Houlden, H., Guo, M., Yo-Tsen, L., Hadjivassiliou, M., Speziani, F., Yang, X.L., Antonellis, A., Reilly, M.M. *et al.* (2013) Exome sequencing identifies a significant variant in methionyl-tRNA synthetase (MARS) in a family with late-onset CMT2. *J Neurol Neurosurg Psychiatry*, **84**, 1247-1249.
56. Antonellis, A., Ellsworth, R.E., Sambuughin, N., Puls, I., Abel, A., Lee-Lin, S.Q., Jordanova, A., Kremensky, I., Christodoulou, K., Middleton, L.T. *et al.* (2003) Glycyl tRNA synthetase mutations in Charcot-Marie-Tooth disease type 2D and distal spinal muscular atrophy type V. *Am J Hum Genet*, **72**, 1293-1299.
57. Waldron, A., Wilcox, C., Francklyn, C. and Ebert, A. (2019) Knock-Down of Histidyl-tRNA Synthetase Causes Cell Cycle Arrest and Apoptosis of Neuronal Progenitor Cells in vivo. *Front Cell Dev Biol*, **7**, 67.

58. Hooykaas, P.J., den Dulk-Ras, A., Bundock, P., Soltani, J., van Attikum, H. and van Heusden, G.P. (2006) Yeast (*Saccharomyces cerevisiae*). *Methods Mol Biol*, **344**, 465-473.
59. Liti, G. (2015) The fascinating and secret wild life of the budding yeast *S. cerevisiae*. *Elife*, **4**.
60. Goffeau, A., Barrell, B.G., Bussey, H., Davis, R.W., Dujon, B., Feldmann, H., Galibert, F., Hoheisel, J.D., Jacq, C., Johnston, M. *et al.* (1996) Life with 6000 genes. *Science (New York, N.Y.)*, **274**, 546, 563-547.
61. Botstein, D. and Fink, G.R. (1988) Yeast: an experimental organism for modern biology. *Science (New York, N.Y.)*, **240**, 1439-1443.
62. Duina, A.A., Miller, M.E. and Keeney, J.B. (2014) Budding yeast for budding geneticists: a primer on the *Saccharomyces cerevisiae* model system. *Genetics*, **197**, 33-48.
63. Nislow, C., Wong, L.H., Lee, A.H. and Giaever, G. (2016) Functional Profiling Using the *Saccharomyces* Genome Deletion Project Collections. *Cold Spring Harb Protoc*, **2016**.
64. Hamza, A., Tammpere, E., Kofoed, M., Keong, C., Chiang, J., Giaever, G., Nislow, C. and Hieter, P. (2015) Complementation of Yeast Genes with Human Genes as an Experimental Platform for Functional Testing of Human Genetic Variants. *Genetics*, **201**, 1263-1274.
65. Berg, M.D., Zhu, Y., Isaacson, J., Genereaux, J., Loll-Krippleber, R., Brown, G.W. and Brandl, C.J. (2020) Chemical-Genetic Interactions with the Proline Analog L-Azetidine-2-Carboxylic Acid in *Saccharomyces cerevisiae*. *G3 (Bethesda)*, **10**, 4335-4345.
66. Bandara, A., Fraser, S., Chambers, P.J. and Stanley, G.A. (2009) Trehalose promotes the survival of *Saccharomyces cerevisiae* during lethal ethanol stress, but does not influence growth under sublethal ethanol stress. *FEMS Yeast Res*, **9**, 1208-1216.
67. Alexandre, H., Ansanay-Galeote, V., Dequin, S. and Blondin, B. (2001) Global gene expression during short-term ethanol stress in *Saccharomyces cerevisiae*. *FEBS Lett*, **498**, 98-103.
68. Collinson, L.P. and Dawes, I.W. (1992) Inducibility of the response of yeast cells to peroxide stress. *J Gen Microbiol*, **138**, 329-335.
69. Koc, A., Wheeler, L.J., Mathews, C.K. and Merrill, G.F. (2004) Hydroxyurea arrests DNA replication by a mechanism that preserves basal dNTP pools. *J Biol Chem*, **279**, 223-230.

70. Seiler, C.Y., Park, J.G., Sharma, A., Hunter, P., Surapaneni, P., Sedillo, C., Field, J., Algar, R., Price, A., Steel, J. *et al.* (2014) DNASU plasmid and PSI:Biological-Materials repositories: resources to accelerate biological research. *Nucleic Acids Res*, **42**, D1253-1260.
71. Katzen, F. (2007) Gateway((R)) recombinational cloning: a biological operating system. *Expert Opin Drug Discov*, **2**, 571-589.
72. Edelheit, O., Hanukoglu, A. and Hanukoglu, I. (2009) Simple and efficient site-directed mutagenesis using two single-primer reactions in parallel to generate mutants for protein structure-function studies. *BMC Biotechnol*, **9**, 61.
73. Baudin, A., Ozier-Kalogeropoulos, O., Denouel, A., Lacroute, F. and Cullin, C. (1993) A simple and efficient method for direct gene deletion in *Saccharomyces cerevisiae*. *Nucleic Acids Res*, **21**, 3329-3330.
74. Morin, A., Moores, A.W. and Sacher, M. (2009) Dissection of *Saccharomyces cerevisiae* asci. *J Vis Exp*.
75. Gietz, R.D. and Woods, R.A. (2006) Yeast transformation by the LiAc/SS Carrier DNA/PEG method. *Methods Mol Biol*, **313**, 107-120.
76. Fan, L. and Xiao, W. (2021) Study Essential Gene Functions by Plasmid Shuffling. *Methods Mol Biol*, **2196**, 53-62.
77. Petropavlovskiy, A.A., Tauro, M.G., Lajoie, P. and Duennwald, M.L. (2020) A Quantitative Imaging-Based Protocol for Yeast Growth and Survival on Agar Plates. *STAR Protoc*, **1**, 100182.
78. Shiber, A., Breuer, W., Brandeis, M. and Ravid, T. (2013) Ubiquitin conjugation triggers misfolded protein sequestration into quality control foci when Hsp70 chaperone levels are limiting. *Mol Biol Cell*, **24**, 2076-2087.
79. Sambrook, J. and Russell, D.W. (2006) SDS-Polyacrylamide Gel Electrophoresis of Proteins. *CSH Protoc*, **2006**.
80. Rosen, A.E., Brooks, B.S., Guth, E., Francklyn, C.S. and Musier-Forsyth, K. (2006) Evolutionary conservation of a functionally important backbone phosphate group critical for aminoacylation of histidine tRNAs. *RNA*, **12**, 1315-1322.
81. Soto, C. and Pritzkow, S. (2018) Protein misfolding, aggregation, and conformational strains in neurodegenerative diseases. *Nat Neurosci*, **21**, 1332-1340.
82. Rozik, P., Szabla, R., Lant, J.T., Kiri, R., Wright, D.E., Junop, M. and O'Donoghue, P. (2022) A novel fluorescent reporter sensitive to serine misincorporation. *RNA Biol*, **19**, 221-233.

83. Francklyn, C. and Schimmel, P. (1990) Enzymatic aminoacylation of an eight-base-pair microhelix with histidine. *Proc Natl Acad Sci U S A*, **87**, 8655-8659.
84. Francklyn, C., Shi, J.P. and Schimmel, P. (1992) Overlapping nucleotide determinants for specific aminoacylation of RNA microhelices. *Science*, **255**, 1121-1125.
85. Froelich, C.A. and First, E.A. (2011) Dominant Intermediate Charcot-Marie-Tooth disorder is not due to a catalytic defect in tyrosyl-tRNA synthetase. *Biochemistry*, **50**, 7132-7145.
86. Niehues, S., Bussmann, J., Steffes, G., Erdmann, I., Kohrer, C., Sun, L., Wagner, M., Schafer, K., Wang, G., Koerdt, S.N. *et al.* (2015) Impaired protein translation in *Drosophila* models for Charcot-Marie-Tooth neuropathy caused by mutant tRNA synthetases. *Nat Commun*, **6**, 7520.
87. Zuko, A., Mallik, M., Thompson, R., Spaulding, E.L., Wienand, A.R., Been, M., Tadenev, A.L.D., van Bakel, N., Sijlmans, C., Santos, L.A. *et al.* (2021) tRNA overexpression rescues peripheral neuropathy caused by mutations in tRNA synthetase. *Science*, **373**, 1161-1166.
88. Pakos-Zebrucka, K., Koryga, I., Mnich, K., Ljubic, M., Samali, A. and Gorman, A.M. (2016) The integrated stress response. *EMBO Rep*, **17**, 1374-1395.
89. Spaulding, E.L., Hines, T.J., Bais, P., Tadenev, A.L.D., Schneider, R., Jewett, D., Pattavina, B., Pratt, S.L., Morelli, K.H., Stum, M.G. *et al.* (2021) The integrated stress response contributes to tRNA synthetase-associated peripheral neuropathy. *Science*, **373**, 1156-1161.
90. Vaughan, M.H. and Hansen, B.S. (1973) Control of initiation of protein synthesis in human cells. Evidence for a role of uncharged transfer ribonucleic acid. *J Biol Chem*, **248**, 7087-7096.
91. Gu, W., Hurto, R.L., Hopper, A.K., Grayhack, E.J. and Phizicky, E.M. (2005) Depletion of *Saccharomyces cerevisiae* tRNA(His) guanylyltransferase Thg1p leads to uncharged tRNA^{His} with additional m(5)C. *Mol Cell Biol*, **25**, 8191-8201.
92. Bond, S., Lopez-Lloreda, C., Gannon, P.J., Akay-Espinoza, C. and Jordan-Sciutto, K.L. (2020) The Integrated Stress Response and Phosphorylated Eukaryotic Initiation Factor 2alpha in Neurodegeneration. *J Neuropathol Exp Neurol*, **79**, 123-143.
93. Lounsbury, K.M. and Francklyn, C.S. (2016) Aminoacyl-Transfer RNA Synthetases: Connecting Nutrient Status to Angiogenesis Through the Unfolded Protein Response. *Arterioscler Thromb Vasc Biol*, **36**, 582-583.

94. Walter, P. and Ron, D. (2011) The unfolded protein response: from stress pathway to homeostatic regulation. *Science*, **334**, 1081-1086.

Appendices

Appendix 1. Plasmid used in this study.

Plasmids	Vector Backbone	Promoter	Replicon	Marker	Plasmid type
HTS1-p426	pRS426	GPD	2 micron - Yeast Episomal plasmids (Yep)	URA3, ampR	Destination vector for native protein expression
hsHARS-p426					
Y454S-HARS-p426					
hsHARS-p426-YFP					Destination vector for fusion protein expression
Y454S-HARS-p426- YFP					
HTS1-p425	pRS425	GPD	2 micron - Yeast Episomdeal plasmids (Yep)	LEU2, ampR	Destination vector for native protein expression
hsHARS-p425					
Y454S-HARS-p425					
hsHARS-p425-YFP					Destination vector for fusion protein expression
V133F-HARS-p425- YFP					
V155G-HARS-p425- YFP					
Y330C-HARS-p425- YFP					
S356N-HARS-p425- YFP					
HTS1-p415	pRS415	GPD	CEN6 - yeast centromere plasmid (YCp)	LEU2, ampR	Destination vector for native protein expression

Appendix 2. Primers used in this study.

Primer ID	Oligonucleotide Sequence (5'-3')	Primer Direction for gene amplification	Purpose of use
HARS_H_F	GGGGACAAGTTTGTACAAAAAAGCA GGCTCCATGGCAGAGCGTGCGGCG	Forward	Gateway cloning PCR to insert HARS into the system
HARS_H_stop_R	GGGGACCACTTTGTACAAGAAAGCT GGGTCTCAGCAGATGCAGAGGGGCT	Reverse	
HARS_H_nonstop_R	GGGGACCACTTTGTACAAGAAAGCT GGGTcGCAGATGCAGAGGGGCT	Reverse	
HARS_QKCHNG_c.136 1C>A F	GCTACTGAACCAGTTACAGTACTGTG AGGAGGCAGGCATCC	Forward	Quick change PCR: from Y454S to hsHARS
HARS_QKCHNG_c.136 1C>A R	GGATGCCTGCCTCCTCACAGTACTGT AACTGGTTCAGTAGC	Reverse	
HARS_QKCHNG_c.136 1A>C F	GCTACTGAACCAGTTACAGTCCTGTG AGGAGGCAGGCATCC	Forward	Quick change PCR: from hsHARS to Y454S-HARS
HARS_QKCHNG_c.136 1A>C R	GGATGCCTGCCTCCTCACAGGACTGT AACTGGTTCAGTAGC	Reverse	
HARS_QKCHNG_c.397 G>T F	CCTTCGCTATGACCTCACTTTTCCTTT TGCTCGGTATTT	Forward	Quick change PCR: from hsHARS to V133F HARS
HARS_QKCHNG_c.397 G>T R	AAATACCGAGCAAAGGAAAAGTGA GGTCATAGCGAAGG	Reverse	
HARS_QKCHNG_c.464 T>G F	CGCTACCACATAGCAAAGGGATATC GGCGGGATAACCCA	Forward	Quick change PCR: from hsHARS to V155G HARS
HARS_QKCHNG_c.464 T>G R	TGGGTTATCCCGCCGATATCCCTTTG CTATGTGGTAGCG	Reverse	
HARS_QKCHNG_c.989 A>G F	CTTGCTCGAGGGCTGGATTGCTACAC TGGGGTGATCTAT	Forward	Quick change PCR: from hsHARS to Y330C HARS
HARS_QKCHNG_c.989 A>G R	ATAGATCACCCAGTGTAGCAATCC AGCCCTCGAGCAAG	Reverse	
HARS_QKCHNG_c.106 7G>A F	CTGGGTGTGGGCAATGTGGCTGCTG GA	Forward	Quick change PCR: from hsHARS to S356N HARS
HARS_QKCHNG_c.106 7G>A R	TCCAGCAGCCACATTGCCACACCCCA G	Reverse	

pDONR201_F	TCGCGTTAACGCTAGCATGGATCTC	Forward	Sequencing any gene in a pDONR201 vector
pDONR201_R	GTAACATCAGAGATTTTGAGACAC	Reverse	
GPD-F	CGGTAGGTATTGATTGTAATTCTG	Forward	Sequencing any gene in p426, p425, p415 vectors
pBluescript KS_R	CTCGAGGTCGACGGTATCG	Reverse	
HARS_seq_F1	CGATACCGGGAATTCTACCA	Forward	Sequencing HARS to confirm mutagenesis
HARS_seq_F2	AGGCAGTGCTGCTACAGACC	Forward	
HARS_seq_F3	CCCAAGGGCACAAGAGACTA	Forward	Sequencing HARS to confirm mutagenesis
HARS_seq_F4	GCTGCTCCAGGATCCTAAACT	Forward	Sequencing HARS to confirm mutagenesis
HARS_F3	CTCAGAACTGTGGGATGCTG	Forward	Sequencing upstream of HARS
HARS_R1	TGAAGCAACGGATGATTACG	Reverse	Sequencing downstream of HARS
YFP_F1	CGACCACTACCAGCAGAACA	Forward	To confirm YFP is on plasmid
HTS1_F	ATCTTCCAAATCGCTGGTGT	Forward	Sequencing <i>hts1</i>
HTS1_R	CGATAGTGACACCACCATGC	Reverse	

Appendix 3. Melting temperatures (T_M) for wildtype hsHARS with and without substrate addition as determined by differential scanning fluorimetry

hsHARS	T_M
T_M of apoenzyme:	62.5 ± 0.5
T_M with tRNA ^{His} (2 μ M)	60.5 ± 1.4
T_M with tRNA ^{His} (1 μ M)	61.2 ± 1.1
T_M with tRNA ^{His} (0.5 μ M)	62.0 ± 0.9
T_M with ATP (0.5 mM)	62.4 ± 0.4
T_M with His (1 mM)	62.9 ± 1.3
T_M with tRNA ^{His} (2 μ M) and ATP (0.5 mM)	61.2 ± 1.7
T_M with tRNA ^{His} (2 μ M) and His (1 mM)	63.0 ± 0.3
T_M with ATP (0.5 mM) and His (1 mM)	63.7 ± 0.6

Appendix 4. Melting temperatures (T_M) for HARS Y330C with and without substrate addition as determined by differential scanning fluorimetry

Y330C	T_M	Fold Change to hsHARS	Significance vs. matching hsHARS condition	Significance vs. hsHARS
T_M of apoenzyme:	61.9 ± 0.7	0.99	n.s.	n.s.
T_M with tRNA ^{His} (2 μ M)	62.6 ± 1.2	1.04	n.s.	n.s.
T_M with tRNA ^{His} (1 μ M)	62.7 ± 0.2	1.03	n.s.	n.s.
T_M with tRNA ^{His} (0.5 μ M)	62 ± 0.7	1.00	n.s.	n.s.
T_M with ATP (0.5 mM)	63 ± 0.3	1.01	n.s.	n.s.
T_M with His (1 mM)	63.3 ± 0.4	1.01	n.s.	n.s.
T_M with tRNA ^{His} (2 μ M) and ATP (0.5 mM)	62.4 ± 0.5	1.02	n.s.	n.s.
T_M with tRNA ^{His} (2 μ M) and His (1 mM)	64.3 ± 1	1.02	n.s.	n.s.
T_M with ATP (0.5 mM) and His (1 mM)	61.6 ± 0.8	0.97	n.s.	n.s.

Appendix 5. Melting temperatures (T_M) for HARS Y454S with and without substrate addition as determined by differential scanning fluorimetry

Y454S	T_M	Fold Change to hsHARS	Significance vs. matching hsHARS condition	Significance vs. hsHARS
T_M of apo enzyme	50.3 ± 1	0.80	$p < 0.0001$	<0.0001
T_M with tRNA ^{His} (2 μ M)	53.5 ± 0.5	0.89	$p < 0.0001$	<0.0001
T_M with tRNA ^{His} (1 μ M)	54.2 ± 0.6	0.89	$p < 0.0001$	<0.0001
T_M tRNA ^{His} (0.5 μ M)	53.6 ± 0.7	0.87	$p < 0.0001$	<0.0001
T_M with ATP (0.5 mM)	53.6 ± 0.2	0.86	$p < 0.0001$	<0.0001
T_M with His (1 mM)	57.7 ± 0.4	0.92	$p < 0.0001$	<0.0001
T_M with tRNA ^{His} (2 μ M) and ATP (0.5 mM)	53 ± 0.8	0.87	$p < 0.0001$	0.0002
T_M with tRNA ^{His} (2 μ M) and His (1 mM)	57.9 ± 0.2	0.92	$p < 0.0001$	0.0003
T_M with ATP (0.5 mM) and His (1 mM)	58.6 ± 0	0.92	$p < 0.0001$	0.0022

Appendix 6. Melting temperatures (T_M) for HARS V133F with and without substrate addition as determined by differential scanning fluorimetry

V133F	T_M	Fold Change to hsHARS	Significance vs. matching hsHARS condition	Significance vs. hsHARS Apo form
T_M of apoenzyme:	52.1 ± 0.83	0.84	<0.0001	0.0007
T_M with tRNA ^{His} (2 μ M)	68.2 ± 0.80	1.10	<0.0001	0.0466
T_M with tRNA ^{His} (1 μ M)	51.2 ± 1.13	0.82	<0.0001	0.0003
T_M with tRNA ^{His} (0.5 μ M)	52.9 ± 1.65	0.85	<0.0001	0.0017
T_M with ATP (0.5 mM)	63.2 ± 1.38	1.01	n.s.	ns
T_M with His (1 mM)	52.3 ± 1.07	0.84	<0.0001	0.0009
T_M with tRNA ^{His} (2 μ M) and ATP (0.5 mM)	60.0 ± 2.89	0.97	ns	ns
T_M with tRNA ^{His} (2 μ M) and His (1 mM)	60.2 ± 0.80	0.97	ns	ns
T_M with ATP (0.5 mM) and His (1 mM)	61.3 ± 1.84	0.99	ns	ns

Appendix 7. Melting temperatures (T_M) for HARS V155G with and without substrate addition as determined by differential scanning fluorimetry

V155G	T_M	Fold Change to hsHARS	Significance vs. matching hsHARS condition	Significance vs. hsHARS Apo form
T_M of apoenzyme:	59.7 ± 0.3	0.96	$p = 0.0279$	$p = 0.00279$
T_M with tRNA ^{His} (2 μ M)	61.3 ± 0.6	1.01	n.s.	n.s.
T_M with tRNA ^{His} (1 μ M)	61.9 ± 0.2	1.01	n.s.	n.s.
T_M with tRNA ^{His} (0.5 μ M)	60.8 ± 0.4	0.98	n.s.	n.s.
T_M with ATP (0.5 mM)	62 ± 0.7	0.99	n.s.	n.s.
T_M with His (1 mM)	62.1 ± 0.3	0.99	n.s.	n.s.
T_M with tRNA ^{His} (2 μ M) and ATP (0.5 mM)	60.6 ± 0.5	0.99	n.s.	n.s.
T_M with tRNA ^{His} (2 μ M) and His (1 mM)	61.6 ± 0.4	0.98	n.s.	n.s.
T_M with ATP (0.5 mM) and His (1 mM)	62.2 ± 0.3	0.98	n.s.	n.s.

Appendix 8. Doubling time (min) \pm standard deviation of yeast strains grown in the presence of amino acid supplementation.

	hsHARS	V133F	V155G	Y330C	S356N
Norm	243 \pm 5	324 \pm 10	264 \pm 5	354 \pm 15	263 \pm 11
Alanine	258 \pm 7	359 \pm 11	300 \pm 4	394 \pm 12	276 \pm 8
Arginine	242 \pm 1	326 \pm 5	263 \pm 5	351 \pm 6	255 \pm 2
Asparagine	243 \pm 4	343 \pm 5	273 \pm 5	358 \pm 9	252 \pm 3
Aspartic acid	249 \pm 2	356 \pm 5	290 \pm 7	375 \pm 9	259 \pm 5
Cysteine	425 \pm 25	530 \pm 14	491 \pm 1	539 \pm 23	416 \pm 45
Glutamine	235 \pm 2	338 \pm 11	260 \pm 6	369 \pm 39	246 \pm 3
Glutamic Acid	228 \pm 2	324 \pm 5	245 \pm 3	336 \pm 13	244 \pm 4
Glycine	257 \pm 5	345 \pm 9	283 \pm 5	389 \pm 17	277 \pm 10
Histidine	234 \pm 4	353 \pm 23	219 \pm 10	452 \pm 75	214 \pm 2
Isoleucine	279 \pm 9	388 \pm 15	297 \pm 5	399 \pm 26	311 \pm 18
Leucine	216 \pm 8	315 \pm 8	234 \pm 10	341 \pm 20	246 \pm 12
Lysine	260 \pm 7	355 \pm 8	280 \pm 13	383 \pm 27	294 \pm 17
Methionine	287 \pm 12	384 \pm 13	310 \pm 16	412 \pm 27	321 \pm 17
Phenylalanine	264 \pm 8	362 \pm 9	280 \pm 9	389 \pm 29	292 \pm 16
Proline	236 \pm 3	325 \pm 20	265 \pm 4	358 \pm 14	266 \pm 11
Serine	284 \pm 27	379 \pm 14	310 \pm 4	415 \pm 15	299 \pm 16
Threonine	310 \pm 6	386 \pm 11	321 \pm 5	415 \pm 8	320 \pm 12
Tryptophan	266 \pm 11	336 \pm 12	276 \pm 4	370 \pm 14	283 \pm 3
Tyrosine	261 \pm 7	333 \pm 8	278 \pm 4	377 \pm 12	281 \pm 6
Valine	264 \pm 23	328 \pm 5	282 \pm 16	382 \pm 11	271 \pm 11

Appendix 9. Doubling time (min) \pm *standard deviation* of yeast strains grown in the presence of chemical stressors.

	hsHARS	V133F	V155G	Y330C	S356N
EtOH	542 \pm 26	576 \pm 25	525 \pm 33	607 \pm 11	481 \pm 12
AZC	1460 \pm 199	1358 \pm 23	1497 \pm 136	1382 \pm 191	1521 \pm 305
H₂O₂	451 \pm 27	676 \pm 16	566 \pm 25	698 \pm 13	561 \pm 12
HU	523 \pm 17	856 \pm 34	673 \pm 31	860 \pm 24	721 \pm 81

Curriculum Vitae

Name: Yi Qiu

Post-secondary Education and Degrees:

University of Western Ontario
M.Sc. Candidate
Schulich Medicine and Dentistry
London, Ontario, Canada
2021-2022
Supervisor: Ilka U. Heinemann

University of Western Ontario
B.Sc. Honors Specialization in Medical Cell Biology
Schulich Medicine and Dentistry
London, Ontario, Canada
2017-2021

Honors and Awards:

Western Graduate Research Scholarship (WGRC)
University of Western Ontario
2021-2022

Dean's Honor List
University of Western Ontario
2018-2021

The Western Scholarship of Excellence
University of Western Ontario
2017

Related Work Experience

Teaching Assistant
University of Western Ontario
2022

Research Assistant
Department of Pediatric Epilepsy
Victoria Hospital & Children Hospital
London, ON
2020-2021

Research Assistant
Department of Pediatric Nephrology
Victoria Hospital & Children Hospital
London, ON
2018-2020

Posters and Presentations

Histidine supplementation can escalate or rescue HARS deficiency in a Charcot Marie Tooth Disease model
28th tRNA Conference
Ohio State University, Columbus, Ohio
2022

Characterization of disease-causing HARS mutations
Harold Stewards Research Showcase, Department of Biochemistry
University of Western Ontario
2022

Characterization of disease-causing HARS mutations
Graduate Student Seminars, Department of Biochemistry
University of Western Ontario, London, ON
2022

Adolescent and caregiver attitudes towards telemedicine use in pediatric nephrology.
Great Lakes Pediatric Research Day
Michigan State University, Detroit, MI, USA
2020

Publications

Qiu, Y., Kenana, R., Beharry, A., Hsu, S. Y., Siu, V. M., Duennwald, M., Heinemann, I. U. (2022) Histidine supplementation can escalate or rescue HARS deficiency in a Charco Marie Tooth Disease model. Under Review.

Qiu, Y., Coulson, S., McIntyre, C.W., Wile, B. and Filler, G. (2021) Adolescent and caregiver attitudes towards telemedicine use in pediatric nephrology. BMC Health Serv Res, 21, 537

Filler, G., **Qiu, Y.**, Kaskel, F. and McIntyre, C.W. (2021) Principles responsible for trace element concentrations in chronic kidney disease. Clinical nephrology, 96, 1-16.